

Impact of Charge Carrier Density and Trap States on the Open Circuit Voltage and the Polaron Recombination in Organic Solar Cells

Dissertation zur Erlangung des
naturwissenschaftlichen Doktorgrades
der Julius-Maximilians-Universität Würzburg



vorgelegt von

Daniel Rauh

aus Werneck

Würzburg 2013

Eingereicht am 05.02.2013
bei der Fakultät für Physik und Astronomie

1. Gutachter: Prof. Dr. Vladimir Dyakonov
2. Gutachter: Prof. Dr. Hartmut Buhmann
3. Gutachter:
der Dissertation.

1. Prüfer: Prof. Dr. Vladimir Dyakonov
2. Prüfer: Prof. Dr. Hartmut Buhmann
3. Prüfer: Prof. Dr. Wolfgang Kinzel
im Promotionskolloquium.

Tag des Promotionskolloquiums: 11.12.2013

Doktorurkunde ausgehändigt am:

Contents

1. Introduction	1
2. Bulk Heterojunction Solar Cells	5
2.1. Organic Semiconductors	5
2.2. Operating Principles	6
2.2.1. Fundamentals	6
2.2.2. Recombination Processes	13
2.2.3. The Open Circuit Voltage	16
2.3. Determination of Power Conversion Efficiency	21
3. Experimental	25
3.1. Charge Extraction Measurements	25
3.2. Sample Preparation	32
3.3. Materials	34
4. Relation of Open Circuit Voltage to Charge Carrier Density in Organic Bulk Hetero- junction Solar Cells	39
4.1. Introduction	39
4.2. Experimental	40
4.3. Results and Discussion	40
4.4. Conclusion	46
5. Charge Density Dependent Nongeminate Recombination in Organic Bulk Hetero- junction Solar Cells	47
5.1. Introduction	47
5.2. Experimental	48
5.3. Theory	49
5.4. Results and Discussion	51
5.4.1. Results	51
5.4.2. Discussion	54
5.5. Conclusion	57
6. Influence of Trap States on the Open Circuit Voltage and the Recombination Dy- namics in Organic Solar Cells	59
6.1. Influence of Oxygen Exposure on the Open Circuit Voltage and Recombination Dynamics in P3HT:PC ₆₁ BM	59
6.1.1. Introduction	59
6.1.2. Experimental	59

Contents

6.1.3. Results and Discussion	60
6.2. Influence of Extrinsic Trap States on the Performance of Organic Solar Cells . .	71
6.2.1. Introduction	71
6.2.2. Experimental	71
6.2.3. Results and Discussion	71
6.3. Conclusion	77
7. S-shaped IV-Characteristics as Result of a Reduced Surface Recombination Velocity and its Influence on the Open Circuit Voltage	79
7.1. Introduction	79
7.2. Experimental	79
7.3. Results and Discussion	80
7.4. Conclusion	87
8. Summary	89
9. Zusammenfassung	93
A. List of Abbreviations	107
B. List of Symbols	111
C. Acknowledgement	117

1. Introduction

At the 30th of June, 2011, the German Bundestag voted to accept a change in the atomic energy act, resulting in a stop of all German nuclear power plants until 2022. The impact of this decision becomes obvious when one takes into account that nuclear power provided 108 billion kWh of electrical energy in 2011, which is 17.6 % of the gross electric power generation in Germany, and 39 % of the base load power supply [46]. To provide a stable electricity supply the capacities have to be replaced by other types of energy generation since the tendency of the total electrical energy consumption did not significantly decrease in the last years. As nuclear power has a relative low carbon dioxide emission per kWh, the power stations that will replace these nuclear power plants have to be low CO₂ emissive, too, in order to not further accelerate the climate change. This excludes conventional energy sources like coal or gas as long as no working carbon capture and storage methods are developed, to reduce CO₂ emission. All these points lead inevitably to the expansion of the so-called renewable energy, with the most important types for electricity production being water, wind, sun and biomass beside others.

The expansion of the usage of water power is limited, at least in Germany, since most interesting spots are already occupied and the fabrication of new plants is not easy because it often has a high impact on nature and countryside. In the case of the usage of biomass, the limitation could be given by an ethnic conflict: how much of the limited area can we supply for production of biomass instead of food. Nevertheless, those two types are important for the future energy mix because they are base loadable instead of sun and wind energy, where energy storage systems and smarter electricity grids have to be designed before they can be connected to the grid in great number. Wind energy is the renewable energy with the highest actual percentage at all being 7.6 % of the German gross electric power generation 2011 [46], with growing tendency and the potential to even reach 25 % in 2025 [45]. These values are already impressive, nevertheless the fraction in the gross electric power generation (3.1 %) is still low, which is why electric energy from the sun with its high potential is also an important candidate for near future clean energy generation. This gets obvious by just taking into account that the sun delivers around 1.08×10^{18} kWh per year to the earth, which is 7000 times the global primary energy consumption [86]. Up to now the market for photovoltaics is dominated by conventional silicon solar cells (SC) (crystalline and amorphous) with only a small but growing fraction of thin film solar cells (CIS, CIGS, CdTe). The reason why photovoltaics are not more important at present are the relative high costs of the produced energy in comparison with other technologies and the commercialization is highly depending on governmental subsidies. This disadvantage of inorganic solar cells can be the starting point for new photovoltaic concepts like dye sensitized solar cells (DSSC) or organic solar cells (OSC) (small molecules or polymeric) that can be processed from solution or by evaporation in a roll-to-roll process which promises to have a high throughput and low cost. Up to now the efficiencies are still too low to compete with inorganic solar cells, 11.9 % for DSSC and 11.1 % for OSC in lab scale with growing tendency [38], anyhow the chance for commercialization is present especially because of their other beneficial

properties like being lightweight or the ability to produce the cells in various colors. To further increase the performance of those solar cells, more investigations about the working principles and the testing of new materials are inevitable.

In this thesis the focus is set on one special type of organic solar cell concepts, the so-called organic bulk heterojunction (BHJ) solar cells. In the second chapter, a brief overview is given what organic semiconductors are and of which materials organic BHJ SCs consist of. Then the general working principles of organic BHJ SCs starting from the absorption of light to the final extraction of the generated charge carriers at the electrodes into the external circuit is explained. Afterwards the correct measurement of the three important characteristics determining the performance of the SC, the open circuit voltage V_{oc} , the short circuit current density j_{sc} and the fill factor FF is presented. The performance is not only influenced by external parameters like light intensity or temperature, but also by microscopic properties, where one of the most important is the recombination of generated charge carriers within the active layer of the SC, which was investigated in this thesis under open circuit conditions. Therefore, the different recombination mechanisms as well as V_{oc} are discussed in more detail in separate subchapters.

After the theory part, chapter 3 will be more technical. First the charge extraction (CE) experiment, which is not a common technique, is introduced as this measurement provides the basis of many investigations described in the experimental results chapters later on. The measurement principle, the used setup and important points that have to be considered when evaluating the CE signals will be explained. Up to that point, the working principles and the measurement technique is presented, but one important part is missing: the object under investigation itself. Therefore, a short prescription of how the standard solar cell preparation takes place is given. The chapter is closed by a detailed description of the specific single materials used in the framework of the thesis.

In chapter 4 the first experimental results are presented. Here the relation of the open circuit voltage to the charge carrier density n under open circuit conditions in the active layer of BHJ SC is discussed. Therefore, V_{oc} and n were measured under different light intensities and temperatures in standard P3HT¹:PC₆₁BM² solar cells. Additionally, the influence of non-ohmic contacts as well as an electron acceptor with different LUMO³ energy level were investigated.

Chapter 5 focuses on recombination of charge carriers, which is an intensively discussed topic in organic photovoltaics. By determination of the charge carrier density under open circuit and short circuit conditions in combination with j_{sc} and V_{oc} it was shown that the recombination rate can not be explained by known recombination paths alone but an additional effect has to be taken into account to explain the experimental results. This recombination mechanism is based on the existence of trap states, which is an inherent property of organic semiconductors. The measurements confirming the extended theory were not only performed for the standard material system but also on a material system which shows the highest efficiency of all commercially available materials.

Whereas in chapter 5 only intrinsic trap states caused by e.g. disorder of the organic semiconductors were investigated, in chapter 6 additional extrinsic trap states were introduced into the active material system. This was done by controlled oxygen exposure of the active material as well as the incorporation of small amounts of an additional material into the absorber layer. By

¹poly(3-hexylthiophene-2,5-diyl)

²[6,6]-phenyl C61 butyric acid methyl ester

³Lowest Unoccupied Molecular Orbital

performing various measurement techniques for characterization of the solar cells a qualitative dependence of the recombination rate, the dominant recombination process and the overall solar cell efficiency on the amount of extrinsic trap states could be established.

Chapter 7 differs from the other experimental chapters 4-6, as here the focus is not set on V_{oc} , n and recombination processes. An effect is discussed that can take place in organic photovoltaics (OPV), when the electrode and the active material do not fit together energetically as perfectly as in the material systems presented in the foregoing chapters. In special cases the current voltage characteristics under illumination do not show the typical behavior, but an s-shape, which significantly reduces the solar cell efficiency, especially at higher illumination levels. In this work, such s-shaped solar cells could be reproducibly fabricated, characterized and the physical background of the s-shape could be identified.

The results of the complete thesis are summarized in chapter 8 and chapter 9. The list of used abbreviations and symbols can be found in appendix A and B.

2. Bulk Heterojunction Solar Cells

This chapter is a brief introduction into the physics of organic solar cells. At first, the term "organic" is described and why these materials can act as semiconductors. The second part will go directly in media res summarizing the fundamental physical processes occurring in organic solar cells, describing their operation principles and showing their limitations. The recombination of charge carriers, that is the annihilation of two oppositely charged charge carriers, and one of the important parameters determining the efficiency of a SC – the open circuit voltage is discussed in more details. Finally, it is explained how to measure the efficiency of a working solar cell correctly and why it is more difficult than just to use a solar simulator and measure a current–voltage curve.

2.1. Organic Semiconductors

Organic matter is commonly known as material that is produced by living organisms or decay products of those. In chemistry and physics another definition is used: Organic materials are carbon-based compounds, hydrocarbons, and their derivatives. In the field of organic photovoltaics, small molecules (e.g. fullerenes) and polymers are used. The large number of different organic materials and their properties have their origin in the special electronic configuration of the carbon, namely $[\text{He}] 2s^2 2p^2$. This configuration is the basis of the ability of carbon to hybridize to special orbitals. In materials used for organic electronics the sp^2 orbitals are essential. In this case one $2s$ electron and two $2p$ electrons form three sp^2 orbitals, oriented 120° relative to each other, forming σ -bonds and hence the planar sigma framework of the molecule. The residual electron occupies the p_z orbital perpendicular to the molecular plane in which the σ -bonds lie.

The crossover from an isolated carbon atom via a small molecule to a polymer formed with many carbon atoms and the accompanying evolution of the electronic properties is shown schematically in Fig. 2.1. In a single carbon atom the electron in the p_z orbital (π) has one specific energy. When a second carbon atom is added to build a covalent σ -bond to the first atom, the p_z energy level splits into two molecular orbitals. The one that lies lower in energy is populated by both π electrons, which form the binding π -bond, and is called HOMO (Highest Occupied Molecular Orbital). The unpopulated one is called LUMO, which has an antibinding character. Adding more carbon atoms to the carbon chain leads to additional splitting until the energy states can be seen as continuous and a π -band is formed in which the π electrons are delocalized over the whole carbon chain. In such a system no band gap would exist and the material would have metal rather than semiconductor properties. The reason for the opening of the band gap is the Peierls distortion, which is that the atomic positions are not perfectly ordered as in a crystal but rather oscillate in space.

Organic semiconductors as commonly used for bulk heterojunction solar cells exhibit band gaps in the range of 1–3 eV and mobilities in the range of 10^{-5} – 10^{-3} $\text{cm}^2/(\text{Vs})$ [64, 115].

2. Bulk Heterojunction Solar Cells

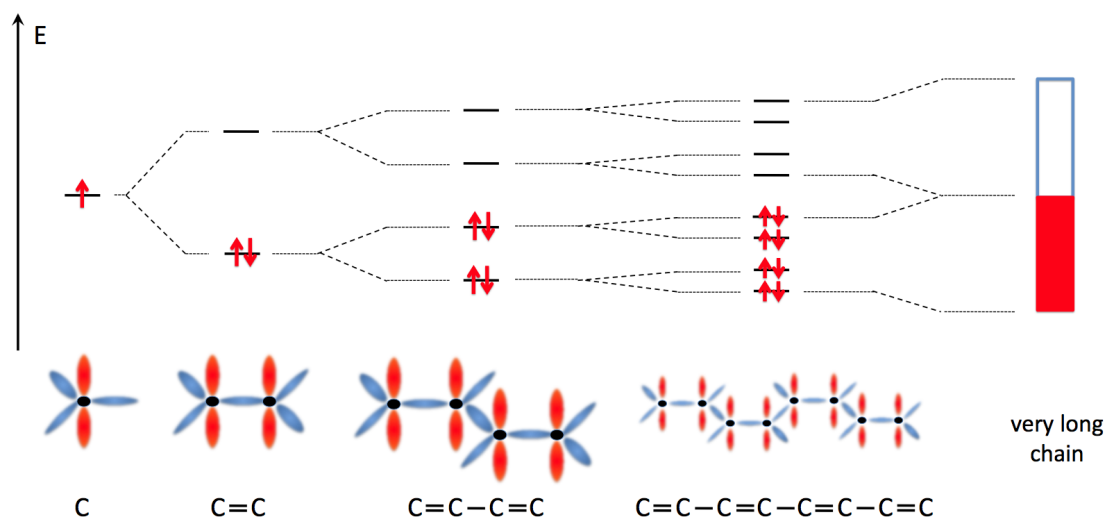


Figure 2.1.: Evolution of the electronic levels from a single carbon atom to a very long conjugated carbon chain resulting in energy band, which is the basis of organic semiconductors. In this case the material would show metallic character, the reason for the molecule to be a semiconductor is the Peierls distortion which causes the opening of a band gap (not shown). (After [4])

Details about the specific organic semiconductors used in this thesis are given in section 3.3.

2.2. Operating Principles

2.2.1. Fundamentals

The motivation to build solar cells is to convert photon energy into electric energy. In the case of SC using organic semiconductors as photo active layer the fundamental processes for the energy conversion differ from the commonly known inorganic semiconductor solar cells such as silicon SC. In Fig. 2.2 the main fundamental steps that have to take place for a working solar cell are illustrated and can be summed up as:

- (I) Photon Absorption and Exciton Generation
- (II) Exciton Diffusion and Dissociation to Polaron Pairs
- (III) Polaron Pair Dissociation
- (IV) Charge Carrier Transport to the Electrodes
- (V) Charge Carrier Extraction at the Respective Electrodes

In the following all steps concerning the device operation and their influence on the solar cell behavior are discussed in detail. Since in this work polymeric organic bulk heterojunction solar cells were investigated, the main focus is set on this type, whereas the differences to other OSCs types, like e.g. planar heterojunction solar cells consisting of small molecules will be referred to in special cases. Many high quality overview articles about the fundamentals of

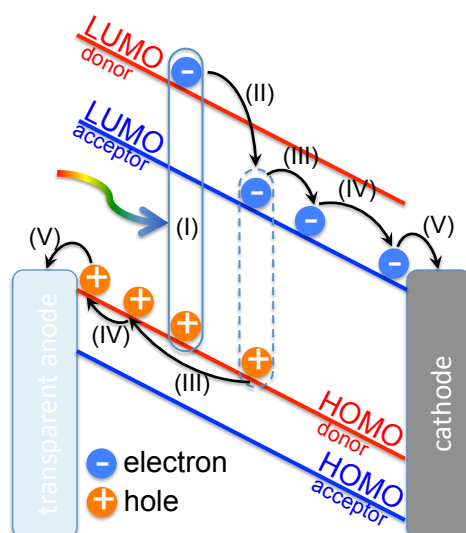


Figure 2.2.: Energetic scheme to describe the fundamental steps occurring in a working solar cell, starting from the absorption of a photon (I) to the final extraction of free charge carriers (V). The intermediate steps are: exciton diffusion and dissociation (II), polaron pair dissociation (III) and charge transport (IV). Details about all processes are given in the text.

OSC were published for example by Deibel *et al.* [26] and Bredas *et al.* [18], for more detail it is recommended to have a closer look at these.

(I) Photon Absorption and Exciton Generation

The first step to create electrical energy from photons is their absorption. In organic materials the absorption band is intense because of the overlap between the wave functions of the electronic ground state and the lowest excited state [18]. The large extinction coefficient in the range of 10^{-5} cm^{-1} ensures that film thicknesses of only 80 to several hundred nm are sufficient to absorb most of the incident photons in the material.

If a photon is absorbed, an electron from the HOMO will be excited into the LUMO. Together with the remaining hole on the HOMO the electron on the LUMO forms instantly an excited singlet exciton which exhibits a high binding energy and is therefore called a Frenkel exciton. Because of the strong electron–vibration coupling in π -conjugated systems the excitation relaxes into the lowest excited state S_1 , whereby this thermalization process is a first energy loss. The reason for the high binding energy of the S_1 is the small relative dielectric constant ϵ_r of organic molecules or polymers in the range of 3–4. Assuming a distance of 1 nm between hole and electron together with $\epsilon_r = 3$ would result in a rough estimation of the binding energy E_B of around 0.5 eV. In regioregular P3HT, E_B was determined to be 0.7 eV by a combination of (inverse) photoemission spectroscopy, absorption and external quantum efficiency measurements [27]. This strongly bound exciton can not be dissociated into free charge carriers by thermal energy ($\sim 25 \text{ meV}$ at room temperature) and will decay radiatively within its lifetime ($\tau = 400 \text{ ps}$ for P3HT [97]) which can be detected by photoluminescence (PL) measurements. To dissociate the exciton effectively, a second material with a higher electron affinity (imply-

2. Bulk Heterojunction Solar Cells

ing a lower LUMO level) acting as electron acceptor has to be introduced. In this work the used electron donating materials (from now on called donors) are polymers but also the use of small molecules as donors is possible. The electron accepting materials (acceptors) used here are fullerene derivatives. In this definition of donors and acceptors, the exciton generation takes place in the donor material, which is not generally the case. Even if in the commonly used donor-acceptor (DA) systems most of the photons are absorbed by the donor material, also excitons in the acceptor can be generated. However, since most fullerene acceptors exhibit only low absorption coefficients this process is less probable, but many efforts are made to develop polymeric acceptors to increase the absorption width of the complete system.

(II) Exciton Diffusion and Dissociation to Polaron Pairs

In organic photovoltaics two different device configurations are often used: the bilayer and the bulk heterojunction solar cell. In a bilayer solar cell an acceptor layer is applied on top of a donor layer and in a bulk heterojunction solar cell the donor and acceptor are mixed within one single layer. Both approaches yield advantages and disadvantages but have in common that the exciton has to reach the DA interface within its diffusion length L_D to get dissociated. In bilayer solar cells the DA interface is planar and therefore smaller than in BHJ solar cells and only excitons generated in the volume within the distance of the exciton diffusion length to this interface can be separated. In contrast, in BHJ cells the area of the interface is large because of the fine intermixing of donor and acceptor. This disadvantage of bilayer SC can be compensated by higher diffusion lengths of the excitons, since in this approach the donor consists almost always on evaporated small molecules, which are highly ordered yielding reported diffusion lengths of e.g. 62 nm in Cu-phthalocyanine [106]. L_D values in polymeric systems are smaller, likely caused by the higher disorder. For example in P3HT, values of 2.6 to 8.5 nm [57, 69, 97] have been reported. The diffusion of the exciton itself is often described by a Förster resonant energy-transfer.

If the exciton, e.g. located on the donor, reaches the donor–acceptor interface, the electron is transferred from the donor to the acceptor. This process appears to be very efficient since it takes place on the fs time scale and is therefore much faster than any other competing process as for instance the before described exciton lifetime which is in the range of ns. In P3HT:PC₆₁BM blend charge separation times <120 fs have been reported [48]. After the splitting of the exciton the electron on the acceptor and the hole on the polymer may still be Coulomb bound and have to be further dissociated. This state is called polaron pair or charge transfer (CT) state in literature.

In recent publications by Banerji et al. [5, 6] it was claimed that the above stated process of photoinduced charge separation after diffusion of excitons to the DA interface is not consistent with the measured time scale of exciton formation and migration and the ultrafast photoinduced electron transfer time. It was shown that the exciton migration is too slow to explain the measured electron transfer rate. Therefore they propose, that “the excitation (from a π - π interband transition) reaches the polymer:fullerene interface for charge separation before it becomes spatially self-localized and bound within an exciton” [5]. In this picture the exciton diffusion and binding energy become irrelevant to the charge transfer. The measurements on P3HT:PC₆₁BM

and PCDTBT¹:PC₇₁BM² blends show that even in these well investigated systems it is not clearly understood how exciton formation and dissociation work.

Concerning excitons a second loss mechanism beside the exciton recombination has to be mentioned. In molecules with heavy atoms or spherical shape, as for instance in fullerenes, an intersystem crossing from a singlet exciton to a triplet exciton is allowed. If the intersystem crossing is faster than the charge transfer, a triplet exciton can be formed which decays by phosphorescence and the excitation is lost for the photocurrent. Another possibility to create an undesired triplet is by an electron back transfer from the CT state to the triplet state, if the triplet state lies lower in energy than the CT state, which was already observed experimentally [65].

(III) Polaron Pair Dissociation

After dissociation of the exciton, the resulting bound polaron pair has to be further separated to gain free charge carriers which can contribute to the photocurrent. Beside many models, the most used one to describe this process is the Onsager–Braun theory. Already 1934 Onsager calculated the dissociation probability for an ion pair with a primary distance with the help of an external field [82]. Braun expanded the theory to the dissociation of polaron pairs in DA systems and included their finite lifetime [17]. Fig. 2.3 visualizes this process. k_d is the dissociation rate of bound polaron pairs into free charge carriers, k_f is the rate given for the competing process of the polaron pair decay back into the ground state. The dissociation probability P can then be calculated by

$$P(T, F) = \frac{k_d(F, T)}{k_d(F, T) + k_f} \quad , \quad (2.1)$$

where $k_d(F, T)$ is a complex term dependent on the temperature T as well as the electric field F . The free charge carriers can now be transported to the respective electrodes leading to the desired photocurrent or meet again and recombine to polaron pairs with the rate k_r .



Figure 2.3.: Schematic description of the possible processes determining the dissociation probability P of polaron pairs (see Eq. (2.1)). The desired dissociation takes place with the dissociation rate k_d . These free charge carriers can recombine again with a certain rate k_r into the bound polaron pair state, which can once more be dissolved or decays with the rate k_f .

¹Poly[[9-(1-octylonyl)-9H-carbazole-2,7-diyl]-2,5-thiophenediyl-2,1,3-benzothiadiazole-4,7-diyl-2,5-thiophenediyl]

²[6,6]-phenyl C71 butyric acid methyl ester

2. Bulk Heterojunction Solar Cells

An often addressed issue is the question of the driving force leading to the polaron generation which was investigated by Ohkita *et al.* [81] for eight different polymers. As result it was shown that the generation of long-living polarons, which was measured by transient absorption, depends exponentially on the free energy difference for charge separation ΔG . In a simple picture ΔG is the offset between the LUMO levels of donor and acceptor ($\Delta G = E_{LUMO_{donor}} - E_{LUMO_{acceptor}}$). This finding has a high impact for the optimization of solar cells because a high ΔG , which is preferable for the photocurrent generation, always limits the open circuit voltage that is among other things given by the effective band gap $E_g (=E_{HOMO_{donor}} - E_{LUMO_{acceptor}})$.

(IV) Charge Transport

After the polaron pairs are dissociated into free charge carriers, these have to move to the respective electrodes. For organic semiconductors several theories about charge transport exist which can mainly be classified in two different mechanisms. One is the description by a hopping transport in a percolating network and the other is a band like transport in the presence of trap states. Both theories will be briefly explained in the following, for more details review articles specified for charge transport are recommended [26, 103, 108].

The principle of the hopping transport mechanism is shown in Fig. 2.4, where the transport is achieved by a hopping of charge carriers from one localized state to another. Localized states in disordered organic materials occur from the lack of high range order in contrast to inorganic semiconductor crystals where a band structure is formed leading to a delocalization over the whole crystal. Even one single long polymer chain consists of many different localized states which are extended in space over several monomers. This is called conjugation length, which is typically around 20 monomers long, for example in PPV¹ 9-12 nm [85]. The energy levels of the localized states are distributed in a density of states (DOS) which is assumed to have an exponential or a Gaussian shape. For polymers a Gaussian shape is often used, explained by randomly distributed conjugation lengths forming one localized state or polarization effects between neighboring polymers. The hopping process itself is a statistic process, given by the rate W_{ij} with which a charge carrier located in state i with energy ϵ_i hops into a state j with energy ϵ_j . There exist many expressions for W_{ij} where the most popular is known as Miller–Abrahams equation [76]

$$W_{ij} = v_0 \exp(-2\gamma_0 |R_{ij}|) \begin{cases} \exp\left(-\frac{(\epsilon_j - \epsilon_i)}{k_B T}\right) & \epsilon_j > \epsilon_i \\ 1 & \text{otherwise} \end{cases} \quad (2.2)$$

v_0 is the phonon vibration frequency, also often called the "attempt to escape frequency" and k_B the Boltzmann constant. The first exponential factor $\exp(-2\gamma_0 |R_{ij}|)$ describes the tunneling of charge carriers to overcome the spatial distance R_{ij} between site i and j . γ_0 is the inverse localization radius given by the overlap integral of the wavefunctions of both states. The second factor describes the process of overcoming the energetic distance. In the case of a hop into a higher energy state a phonon has to be absorbed and the hopping probability is handicapped which is taken into account by a Boltzmann factor. For a hop into deeper lying energy states it is assumed that a phonon can always be emitted. It is obvious from Eq. (2.2) that hopping into deeper states is always more probable as into higher states, assuming the spatial distance

¹poly(p-phenylenevinylene)

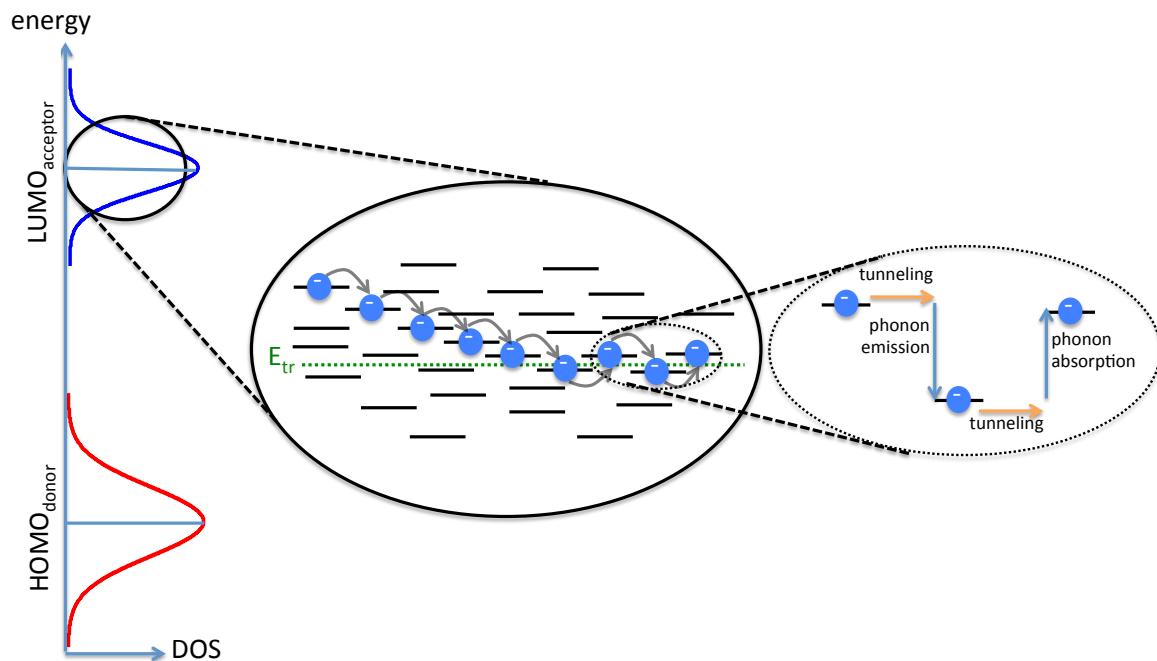


Figure 2.4.: Schematic description of the microscopic hopping transport in disordered organic semiconductors in the case of electrons. The electrons are randomly generated (by light or injection) in the electron density of states (stated as LUMO_{acceptor}), that consist of many localized states that are distributed in space and in a gaussian manner in energy forming the Gaussian density of states (DOS). As given by the Miller–Abrahams equation (Eq. (2.2)), downhops in energy are more probable resulting first of all in a thermalization of the electrons until most lower lying energy states are occupied. Then the equilibrium charge transport takes place around a specific energy – called transport energy – by downhops and uphops. To fulfill the energy conservation, a phonon has to be rather emitted (downhop) or absorbed (uphop), the spatial distance is overcome by tunneling.

2. Bulk Heterojunction Solar Cells

R_{ij} is equal. This leads to an effect that is called relaxation. When a free polaron is formed after dissociation of a polaron pair or by injection into the device via contacts, these are located in most cases in relative high lying states (in terms of energy). Therefore, they will first of all perform a number of downhops until they arrive at energies where charge carriers, that are already relaxed, occupy most sites. For a further transport uphops have to be executed as well as downhops. The energy where the probability for hops (downwards and upwards) is maximized is called transport energy E_{tr} . This is one definition of the transport energy and can differ in details from other reported models.

The second way to interpret the charge transport in a disordered system is the trap controlled band transport adopted from amorphous inorganic semiconductors - often referred to as multiple trapping and release model (MTR). The principle of the model is depicted in Fig. 2.5 and can be summarized as follows: Above a certain energy — in inorganic semiconductors named mobility

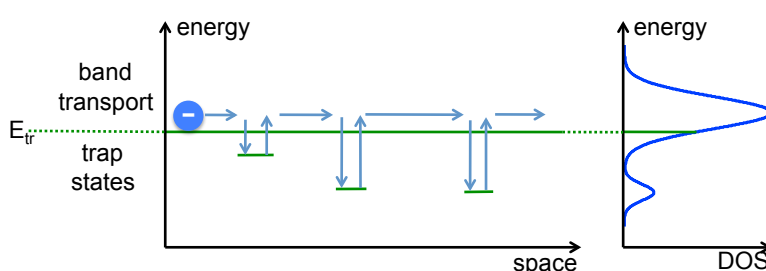


Figure 2.5.: Scheme of the charge transport by the multiple trapping and release model. Above the transport energy E_{tr} the electrons are described by band transport. All states below this energy act as trap states, where the electrons are captured for a certain time until they are released to take place in the transport again. In this model it gets clear that not only trap states inside the band gap (as schematically illustrated by the smaller Gaussian DOS on the right side) are defined as traps but also these states in the DOS, that are below E_{tr} .

edge, here transport energy — the charge carriers move quasi-freely in a band like in crystalline semiconductors. The transport is hindered by unoccupied states below E_{tr} in which charge carriers can be trapped. These trapped polarons can be detrapped after a certain time, depending on the depth of the trap state, and participate in the transport again until they are retrapped.

Both presented models are microscopic models. In measurements only macroscopic physical values are accessible. The most important physical value concerning charge transport is the mobility μ which is defined as proportionality factor between the drift velocity v_d and the electric field F :

$$v_d = \mu F \quad (2.3)$$

In organic solar cells the mobility has to fulfill two major requirements: Firstly, the mobilities of electrons in the acceptor phase μ_n and holes in the donor phase μ_p need to be balanced. Otherwise a space charge would form up limiting the solar cell performance. Secondly, the mobility values have to be in a special range. At a first glance one might think that higher mobilities would lead to a more efficient charge extraction and therefore a better performance of the solar cell. Nevertheless, if the mobility is too high, the fast charge extraction leads to a low charge carrier density in the device decreasing the open circuit voltage. More details

about the open circuit voltage will be given in section 2.2.3. Macroscopic simulations using typical P3HT:PC₆₁BM parameters with balanced mobilities varied from 10⁻¹⁴ to 10⁶ m²/Vs showed that the best solar cells would be obtained for mobilities of 10⁻⁶ m²/Vs [30]. In real P3HT:PC₆₁BM devices, a balanced transport is e.g. achieved in an annealed sample with a donor:acceptor weight ratio of 1:1 yielding mobilities of 10⁻⁸ m²/Vs [9].

The mobility itself is dependent on a number of parameters. The most intuitive is the dependence on the temperature that can be explained best by the above introduced microscopic models. At lower temperatures the probability to perform a hop into a higher lying state decreases which directly lowers the mobility. Also the disorder influences the mobility in that way that a higher disorder means lower mobility. The disorder can be parametrized for instance by the width of the Gaussian DOS σ in the Gaussian disorder model (GDM). Monte-Carlo simulations using the GDM and Eq. (2.2) gave [8]

$$\mu(T, \sigma, F) \propto \exp \left[- \left(\frac{2\sigma}{3k_B T} \right)^2 \right] \sqrt{F} \quad , \quad (2.4)$$

which includes even a square root dependence on the electric field. Additionally, the charge carrier density in the device can have an impact on the mobility which will be discussed in more detail in chapter 5.

During the transport of the polarons to the respective electrodes recombination can take place, that has a high impact on the functionality of organic solar cells. If a free polaron meets a free polaron of opposite charge, they can annihilate and will be lost for the photocurrent. This process is named bimolecular recombination and will be explained in more detail in section 2.2.2.

(V) Charge Extraction

Finally, after the charge carriers have been transported to the electrodes, they have to leave the device via the contacts to the external circuit to generate power. Therefore, the contacts have to be chosen carefully, otherwise two main problems can occur:

If the charge carriers can only be extracted with a lower rate than they are generated, they will accumulate at the contact and form a space charge. This would result in an s-shaped current–voltage (IV) behavior and low solar cell efficiencies as often reported in literature. In the framework of this thesis solar cells with adjustable s-shaped IV-characteristics could be fabricated. These cells could be modeled using the parameter of a finite surface recombination velocity by Wagenpfahl *et al.* [117].

The second problem is the extraction of charge carriers at the wrong electrode, meaning electrons (holes) at the anode (cathode) which are then lost for the photocurrent. This effect was recently investigated by Monte Carlo simulations [105], where the importance of selective electrodes was highlighted. Selective electrodes can experimentally be achieved by (electron / hole) blocking layers between the active material and the respective electrode.

2.2.2. Recombination Processes

Already mentioned in section 2.2.1, several loss mechanisms occur in working OSC devices. Fig.2.6 illustrates the main recombination processes in inorganic semiconductors: band-to-band

2. Bulk Heterojunction Solar Cells

and trap assisted recombination as well as recombination via interface states. In the band-to-band recombination the free electron in the conduction band (CB) drops back into the valence band (VB), annihilating the electron hole pair. Energy conservation is fulfilled by either emission of a photon or by energy transfer to another electron in the CB (named Auger recombination). In the trap-assisted recombination an electron (hole) is firstly captured by a trap state in the band gap of the semiconductor, in the second step a hole (electron) is captured in the same already occupied trap state leading to recombination of both charge carriers. This mechanism is called Shockley-Read-Hall (SRH) recombination. At the interface of two materials, which can stand for semiconductor–semiconductor as well as semiconductor–metal interfaces, additional energy states can be formed inside the band gap over which the recombination can occur in successive small steps.

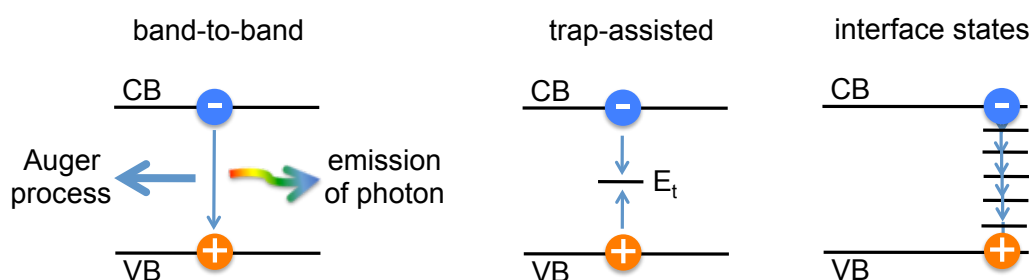


Figure 2.6.: Illustration of the recombination mechanisms known from inorganic semiconductors: In the case of band-to-band recombination (left) a free electron in the conduction band (CB) directly recombines with a hole in the valence band (VB). In this case two different processes can occur to fulfill the energy conservation, by emission of a photon or by transferring the energy to a second electron. The latter is a three particle process and known in literature as Auger recombination. Trap-assisted recombination (middle) occurs, when trap states are located in the band gap. This mechanism is often described by Shockley–Read–Hall recombination and tends to be the dominant recombination mechanism in inorganic semiconductors. Recombination over interface states (right) that form at the interface (grains, metal–semiconductor) is the third important mechanism.

Whereas in inorganic crystalline semiconductors the recombination mechanisms are well understood and it is known that SRH recombination is the dominating process, for organic BHJ solar cells things are more complicated. The reason therefore is the phase separation of donor and acceptor that implies that free electrons and free holes can only meet at the DA interface. If two free polarons of opposite charge - not originating from the same exciton - meet and recombine, this process is called nongeminate bimolecular recombination. Recombination of polarons which originate from the same exciton is called geminate and appears to be a monomolecular process. This process was already described above in the framework of polaron pair dissociation and is illustrated in Fig. 2.3 with the rate k_r . *Monomolecular* means that the recombination rate is directly proportional to the charge carrier density, whereas bimolecular stands for a process where the recombination rate is proportional to the square of the charge carrier density.

Many work was carried out to find the dominating recombination process in organic BHJ SC. Until now, the discussions about this topic are still controversial. Many authors explain their

results by bimolecular recombination, whereas others state the main recombination process is monomolecular, where SRH as well as recombination over interface states is mentioned. The reason for this different opinions could lie in the various measurement conditions that are applied, i.e. temperature, light illumination level, open circuit or short circuit conditions, equilibrium or only quasi-equilibrium, different material systems, purity of the materials and so forth.

In general, without knowing the exact physical mechanism, the influence of recombination gets obvious mathematically by looking at the continuity equation

$$\frac{dn}{dt} = -\frac{1}{q} \frac{dj_n}{dx} + G - R \quad , \quad (2.5)$$

where q is the elementary charge, dn/dt is the time derivative of the charge carrier density, dj_n/dx the spatial derivative of the current density, G the generation rate and R the recombination rate of charge carriers. In steady-state dn/dt is zero and the rate of extraction of photogenerated charge carriers, which is defined by dj_n/dx and represents the photocurrent, is directly related to the $G - R$. For $R = 0$, the current density would be

$$j = GqL \quad , \quad (2.6)$$

where L is the thickness of the active layer in which the charge carriers are generated. If recombination takes place the current density decreases inevitably.

The recombination rate can be given by the empirical equation

$$R = k_\lambda n^{\lambda+1} \quad , \quad (2.7)$$

where k_λ is a constant recombination prefactor and $\lambda + 1$ is the recombination order. Assuming only monomolecular recombination would result in a recombination order of one and one obtains:

$$R = k_r n \quad , \quad (2.8)$$

where k_r is the monomolecular recombination rate. Bimolecular recombination with a recombination order of two is often described as Langevin recombination [59]. Despite the theory having been developed for ions finding each other by brownian motion in a diluted electrolyte, it has been applied to organic solar cells. The recombination rate is given as

$$R = \gamma(np - n_i^2) \approx \gamma n^2 \quad , \quad (2.9)$$

where γ is the Langevin recombination prefactor, n and p are the electron and hole density, respectively. n_i is the intrinsic charge carrier density which is very low because it is very unlikely to thermally activate charge carriers over a band gap of ~ 1 eV, therefore n_i can be neglected. Since the dissociation of an exciton always results in one hole and one electron, it can also be assumed that $n = p$. The recombination prefactor itself is defined by:

$$\gamma = \frac{q}{\epsilon} (\mu_n + \mu_p) \quad , \quad (2.10)$$

with ϵ the absolute permittivity of the active layer, μ_n and μ_p the mobility of electrons and holes, respectively. The mobility takes into account that the limiting process in bimolecular

2. Bulk Heterojunction Solar Cells

recombination is not the recombination of the two free charge carriers itself but the finding of those.

Evaluation of experimental data of OSCs using Langevin theory (Eq. 2.9) showed that the theory overestimates the recombination rate by several orders of magnitude [25, 49]. This can be taken into account by implementing a reduction factor ζ . The discrepancy between Langevin theory and experiment was explained by different approaches. Koster *et al.* [56] argued that not the fastest charge carriers dominate the recombination rate like in Eq. (2.10) but the slowest ($\gamma_K = (q/\epsilon)\min(\mu_n, \mu_p)$). Another explanation is given by Adriaenssens *et al.* [1]. They claim that potential fluctuations in the semiconductor lead to an thermally activated recombination resulting in a reduced recombination prefactor $\gamma_A = \gamma \exp(\Delta E/(k_B T))$, where ΔE is activation energy. Both approaches can explain a reduced Langevin recombination, unfortunately they can not reproduce the temperature behavior correctly. To solve this problem Deibel *et al.* [31] gave another quite simple explanation. In experiments the extracted charge carrier density $n_{extr} = n = p$ is the average density over the whole active area. This does not take into account the spatial gradient of the electron density $n(x)$ and the hole density $p(x)$ that results from asymmetric contacts. The parameter x is the position in an one dimensional model, where position $x = 0$ is the anode and $x = L$ the cathode. For example, the density of electrons at the anode $n(0)$ is orders of magnitudes lower than at the cathode $n(L)$. This results in the recombination prefactor

$$\gamma_D = \gamma \frac{\frac{1}{L} \int_0^L n(x)p(x)dx}{\overline{n(x)} \cdot \overline{p(x)}} \quad , \quad (2.11)$$

where the denominator is the spatial average of the charge carrier density and corresponds to measured values from charge extraction experiments. This model can describe the temperature behavior of the recombination prefactor correctly, nevertheless it needs a second factor that is temperature independent to describe the absolute values which has to be investigated further.

Beside monomolecular ($\lambda + 1 = 1$) and bimolecular ($\lambda + 1 = 2$) recombination, several publications reported recombination orders even higher than two [35, 50, 73, 98, 100]. The reason for this is still not understood and will be discussed in more detail in the experimental chapter 5.

2.2.3. The Open Circuit Voltage

The open circuit voltage V_{oc} is one of the key parameters of solar cells which directly influences their efficiency. Therefore, it is important to know the limitations and dependencies of V_{oc} in order to optimize the solar cell. Beside this, there is a second aspect making the open circuit voltage interesting to investigate. As can be seen from Eq. (2.5), under open circuit conditions at steady state, i.e. $dj/dx = 0$ and $dn/dt = 0$, the generation rate equals the recombination rate, making this distinguished point in the IV-curve dedicated for recombination investigations.

For the sake of simplicity it is started again with the inorganic p-n junction solar cell where the IV-curve in forward bias is given by the ideal Shockley equation

$$j = j_0 \left[\exp\left(\frac{V}{n_{id} k_B T}\right) - 1 \right] - j_{ph} \quad , \quad (2.12)$$

where j_0 is the dark saturation current density, V the applied voltage, n_{id} the ideality factor and j_{ph} the (voltage independent) photocurrent density. From Eq. (2.12) it is easy to find a first

expression for the open circuit voltage:

$$V_{oc} = \frac{n_{id}k_B T}{q} \ln \left(\frac{j_{ph}}{j_0} \right) \quad (2.13)$$

Unfortunately, Eq. (2.12) is, as the name says, only valid for an idealized system. In a real device a parallel R_p and serial R_s resistance influences the IV-behavior, leading to the not ideal Shockley equation:

$$j = j_0 \left[\exp \left(\frac{(V - jR_s)}{n_{id}k_B T} \right) - 1 \right] - \frac{V - jR_s}{R_p} - j_{ph} \quad (2.14)$$

Fig. 2.7(a) displays the dark IV-curve of an organic solar cell using P3HT:PC₆₁BM as active material together with a fit using Eq. (2.14) ($j_{ph} = 0$). Since both curves show a very good accordance it can be stated that the Shockley equation can be applied also to organic solar cells even if the equation was derived for inorganic p-n junctions, at least for $j_{ph} = 0$.

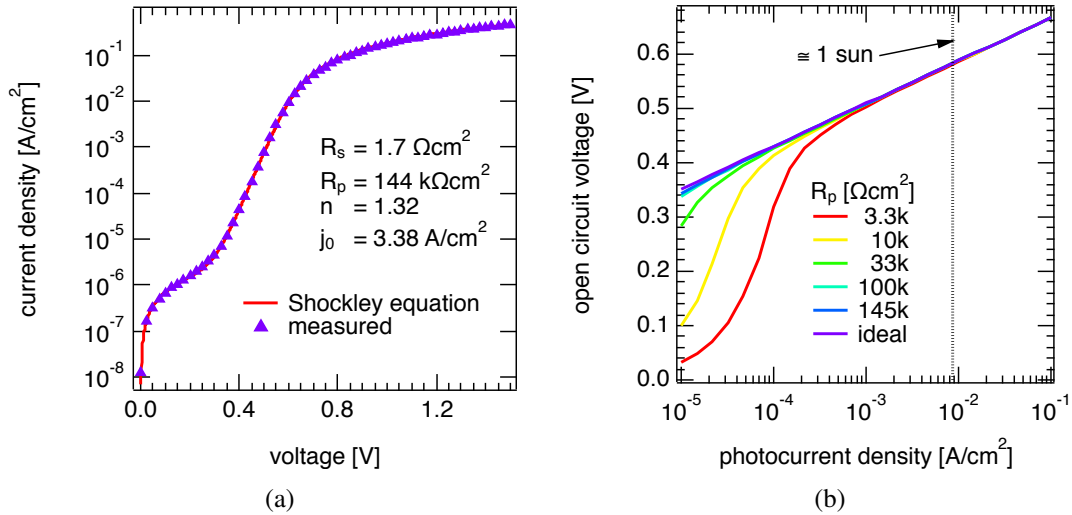


Figure 2.7.: (a) IV-characteristic of a P3HT:PC₆₁BM solar cell in the dark together with a fit according to Eq. (2.14). The fitting parameters are shown in the inset. (b) Influence of the parallel resistance on the open circuit voltage derived for different j_{ph} using Eq. (2.14). n , j_0 and R_s are the values from the dark IV-curve.

The question arises if Eq. (2.14) is still valid for $j_{ph} \neq 0$ since in organic solar cells the photocurrent density is not voltage independent as in inorganic solar cells. Additionally, the physical meaning for R_s and R_p is not understood until now. Nevertheless, Eq. (2.14) enables us to focus on a problem which can occur when investigating the open circuit voltage. If the parallel resistance is too low, meaning a not sufficiently blocking diode, the measured open circuit voltage is lower than it would be in an ideal solar cell with $R_p = \infty$, making it more complicated to interpret the dependence of V_{oc} on, for example, the charge carrier density as shown in chapter 4. The effect of a too low R_p is even increased for lower photocurrent densities (see Fig. 2.7(b)). The dependence of V_{oc} on R_s is negligible.

2. Bulk Heterojunction Solar Cells

Since the validity of the Shockley equation is not proven for OSC, Koster *et al.* suggested an alternative approach for V_{oc} [55]. Describing the semiconductors as effective medium with the $LUMO$ of the acceptor ($LUMO_{acceptor}$) as conduction band and the $HOMO$ of the donor $HOMO_{donor}$ as valence band they introduced the quasi Fermi levels of electrons ϕ_n as

$$n = n_i \exp \frac{q(V - \phi_n)}{k_B T} \quad (2.15)$$

The same applies to holes with density p and the quasi Fermi level ϕ_p . From a drift–diffusion model and the additional assumptions that the generation and (Langevin) recombination of charge carriers takes place completely via charge transfer states, (see section 2.2.2) they found the following expression for V_{oc} .

$$V_{oc} = \frac{E_g}{q} - \frac{k_B T}{q} \ln \left(\frac{(1-P)\gamma N_c^2}{PG} \right) \quad (2.16)$$

where E_g is the effective band gap ($= |E_{HOMO_{donor}} - E_{LUMO_{acceptor}}|$), P is the dissociation probability of polaron pairs and G the generation rate of these. N_c is the effective density of states ($N_c^2 = N_e N_h$, N_e : electron density of states, N_h : hole density of states). Using the continuity equation in a different form than Eq. (2.5) [54]

$$\frac{1}{q} \frac{d}{dx} j_n(x) = PG - (1 - PR) \quad (2.17)$$

where the left side is zero under open circuit conditions, in combination with Eq. (2.9) results in

$$V_{oc} = \frac{E_g}{q} - \frac{k_B T}{q} \ln \left(\frac{N_c^2}{np} \right) \quad (2.18)$$

This simple dependence of V_{oc} on the charge carrier density was investigated in the framework of this thesis experimentally, where the results for different organic BHJ solar cell configurations are discussed in chapter 4. Eq. (2.18) was also derived by Cheyns *et al.* [20] for bilayer solar cells in an analytical approach starting from

$$qV_{oc} = |E_{HOMO_{donor}} - E_{LUMO_{acceptor}}| + BB_{donor} + BB_{acceptor} - \phi_n - \phi_p \quad (2.19)$$

In this calculation the band bending of the electrostatic potential ($BB_{acceptor}$, BB_{donor}) as well as injection barriers of the contacts (ϕ_n , ϕ_p) were taken into account. For bulk heterojunction devices as investigated here, it was found that Eq. (2.18) is only valid for negligible injection barriers. The dependence of V_{oc} on different injection barriers was firstly investigated experimentally by Mihailetschi *et al.* [74] where they used cathode materials with different work functions. For non-ohmic contacts, i.e. large injection barriers, they found that V_{oc} is controlled by the work function difference of both electrodes in accordance to the metal–insulator–metal (MIM) model [67], whereas for ohmic contacts the open circuit voltage is governed by the effective band gap as described by the above mentioned equations. This was previously experimentally observed by Brabec *et al.* [15], where different acceptors with varying electron affinities (i.e. LUMO levels) were fabricated with the aim to investigate the influence on V_{oc} . For devices using PC₆₁BM as acceptor it was shown by comparing the V_{oc} versus the oxidation

level (i.e. HOMO level) of the donor taken from various material systems that the open circuit voltage follows the simple relation $V_{oc} \approx E_g/q - 0.3$ V [94].

The main question is, which mechanisms exactly limits the open circuit voltage and if it is possible to eliminate or at least minimize these? In a thermodynamic approach, again for p-n junction solar cells, Shockley and Queisser determined the efficiency limit for a given band gap by a detailed balance approach, the famous Shockley–Queisser limit. In the framework of this calculation they showed that V_{oc} is limited by recombination which they divided into two parts: radiative and non-radiative recombination. For organic solar cells Vandewal *et al.* [114] could isolate the different recombination processes from each other and quantify their influences. Therefore, they started with Eq. (2.13) and related j_0 to electro-optical properties [88]

$$j_0 = \frac{q}{EQE_{EL}} \int EQE_{PV}(E) \phi_{BB}^T dE \quad , \quad (2.20)$$

where EQE_{EL} is the external quantum efficiency of the electroluminescence (EL), i.e. the ratio between the number of emitted photons originating from radiative recombination to the number of injected charges. $EQE_{PV}(E)$ is the photovoltaic external quantum efficiency, meaning the number of extracted charges divided by the number of incident photons, which is dependent on the energy of the incident photon E . ϕ_{BB}^T is the black body radiation at a temperature T , which has a strong decrease with increasing energy at NIR-VIS at room temperature. Therefore, the integral in Eq. (2.20) is mainly determined by the low energy range of the EQE_{PV} , which was shown to be a direct CT state absorption by highly sensitive Fourier–transform photocurrent spectroscopy [113]. Using the spectral lineshape of the CT state absorption according to Marcus theory [37, 72] for the calculation of the spectral shape of EQE_{PV} in the CT absorption range one can calculate Eq. (2.20) in a new form which results finally in an expression for V_{oc} , where the losses can be parted in those occurring from radiative (ΔV_{rad}) and non radiative recombination (ΔV_{nonrad}):

$$V_{oc} = \frac{E_{CT}}{q} + \underbrace{\frac{k_B T}{q} \ln \left(\frac{J_{sc} h^3 c^2}{f q 2\pi (E_{CT} - \lambda_0)} \right)}_{\Delta V_{rad}} + \underbrace{\frac{k_B T}{q} \ln(EQE_{EL})}_{\Delta V_{nonrad}} \quad . \quad (2.21)$$

E_{CT} is the energy of the charge transfer state and can be set equal to E_g , λ_0 is the reorganization energy as defined from Marcus theory and f is a factor describing the interaction between donor and acceptor. h is Planck’s constant and c the speed of light in vacuum. For different material systems they could extract the parameters directly from EQE and EL measurements or the respective fits of the data and quantify ΔV_{rad} as well as ΔV_{nonrad} . In a P3HT:PC₆₁BM device they calculated for example $\Delta V_{rad} = 0.11$ V and $\Delta V_{nonrad} = 0.42$ V. The overall loss is more than the predicted 0.3 V from Scharber *et al.* [94], nevertheless Eq. (2.21) correctly predicts the light intensity and temperature dependence of V_{oc} . In their conclusion Vandewal *et al.* [114] noted that the radiative losses are unavoidable, but the reduction of non-radiative decay paths are important for the development of BHJ solar cells. Unfortunately, no practical details how this can be achieved were proposed.

In recent works by Blakesley *et al.* [11, 12], the dependence of the open circuit voltage on the disorder of the device was discussed for two different density of states models: a Gaussian

2. Bulk Heterojunction Solar Cells

and an exponential distribution. In the case of the Gaussian DOS

$$g_{h/e}(E) = \frac{N_{h/e}}{\sigma\sqrt{2\pi}} \exp \left[-\frac{(\pm E \mp E_{HOMO_{donor}/LUMO_{acceptor}})^2}{2\sigma^2} \right], \quad (2.22)$$

with width σ , they calculated an expression similar to Eq. (2.18), in which only the band gap E_g is reduced by $\sigma^2/(k_B T)$ to a new effective band gap $E_{g,eff}$

$$V_{oc} = \frac{1}{q} \underbrace{\left(|E_{HOMO_{donor}} - E_{LUMO_{acceptor}}| - \frac{\sigma^2}{k_B T} \right)}_{E_{g,eff}} + \frac{k_B T}{q} \ln \left(\frac{G}{\gamma N_h N_e} \right). \quad (2.23)$$

This result can be explained by the relaxation of charge carriers in the DOS (see Fig. 2.4). In a DOS with higher σ the charge carriers can relax into deeper states, therefore the oppositely charged charge carriers get in average closer together in energy, leading to a smaller $E_{g,eff}$. Taking an exponential distribution of the DOS

$$g_{h/e}(E) = \frac{N_{t,h/e}}{E_0} \exp \left[\frac{\pm(E - E_{HOMO_{donor}/LUMO_{acceptor}})}{E_0} \right] \quad (2.24)$$

under assumption of $E_0 \gg k_B T$ leads to

$$V_{oc} = \frac{E_g}{q} + n_{id} \frac{k_B T}{q} \ln \left(\frac{G}{\gamma N_{t,h} N_{t,e}} \right), \quad (2.25)$$

where the ideality factor n_{id} (in this case $n_{id} = E_0/(k_B T)$) is an additional factor reducing V_{oc} . $N_{t,h/e}$ is the exponential density of states of holes/electrons. In both cases only bimolecular Langevin recombination of free charge carriers is assumed.

To take also into account a recombination process of trapped charge carriers n_t with free (conductive) charge carriers n_c ($n = n_c + n_t$) Blakesley *et al.* used the MTR model (see Fig. 2.5) [12]. The open circuit voltage in this case is determined by the effective density N of free charge carriers at energy $E_{HOMO_{donor}}/E_{LUMO_{acceptor}}$ and the exponential tail of trap states with density N_t and the characteristic energy E_0 .

$$V_{oc} = \frac{E_g}{q} + n_{id} \frac{k_B T}{q} \ln \left(\frac{G}{\gamma N_t N} \right). \quad (2.26)$$

n_{id} is in this case given by $n_{id} = 2/(1 + (k_B T)/E_0)$.

At last the influence of contacts has to be mentioned. As stated above, injection barriers can have a significant impact on the open circuit voltage, but also the effect of the surface recombination velocity has to be taken into account. The surface recombination velocity S itself is a parameter describing the charge transfer from the blend to the metal contact and is defined as proportionality factor between the current through the interface J and the surface charge carrier density n : $J = qS(n - n_{th})$. n_{th} is the thermally activated charge carrier density that can be calculated by thermionic emission theory. In a solar cell four different surface recombination velocities can be defined for the metal-organic interfaces, concerning the contact (anode/cathode) in combination with the charge carrier specimen (electrons/holes). It was recently shown by Wagenpfahl *et al.* [117] that a reduced S can cause a reduction of the open circuit voltage. Details about this effect will be given in chapter 7.

2.3. Determination of Power Conversion Efficiency

Despite the legitimate interest in all the fundamental physical processes taking place in OSCs, as described in Section 2.2.1, the most important parameter of a solar cell from a practical point of view is the efficiency η . It is defined by the ratio of maximal electrical energy taken from the cell P_{max} to the incident light power P_L :

$$\eta = \frac{P_{max}}{P_L} \quad (2.27)$$

P_{max} can be determined from the current–voltage characteristics of the illuminated solar cell, which is exemplarily shown in Fig. 2.8 for a PTB7¹:PC₇₁BM solar cell together with the power–voltage (PV) graph. At zero voltage the solar cell delivers the maximal current in the 4th

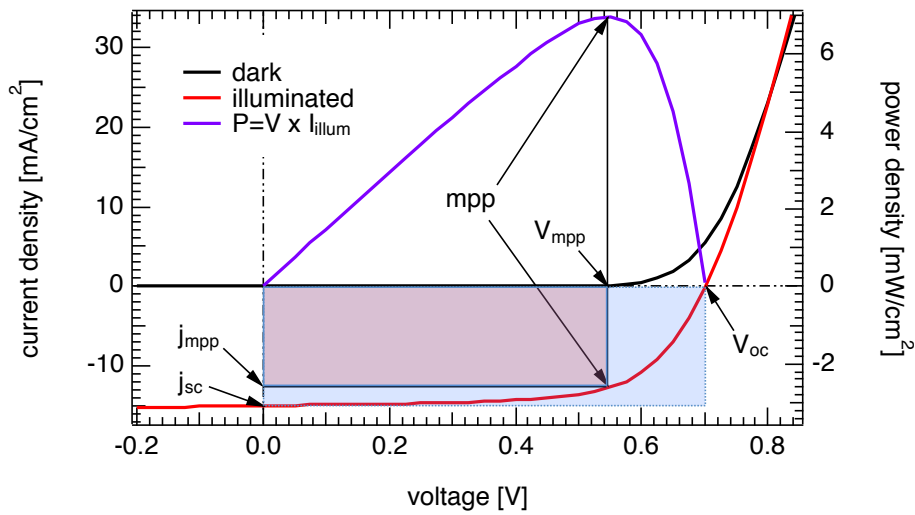


Figure 2.8.: IV-curve of a PTB7:PC₇₁BM solar cell in the dark and under illumination as well as PV-curve to illustrate the solar cell parameters short circuit current density j_{sc} , open circuit voltage V_{oc} and fill factor FF . The FF is given by the ratio of $V_{mpp} \times j_{mpp}$ (red square) to $V_{oc} \times j_{sc}$ (blue square), where V_{mpp} and j_{mpp} are the voltage and current density at the maximum power point mpp .

quadrant, called the short circuit current I_{sc} , nevertheless the supplied power is zero. Increasing the voltage leads to an increase of the power that can be extracted from the cell until a maximum P_{max} is reached at V_{mpp} . This point is named maximum power point (mpp), the corresponding current is I_{mpp} . Further increase of the voltage leads to a reduction of the extracted power until it drops again to zero when the current gets zero. The voltage at this point is called the open circuit voltage V_{oc} as discussed above. The third important parameter beside V_{oc} and I_{sc} is the fill factor FF which is defined as

$$FF = \frac{I_{mpp} V_{mpp}}{I_{sc} V_{oc}} \quad (2.28)$$

¹Poly[[4,8-bis[(2-ethylhexyl)oxy]benzo[1,2-b:4,5-b']dithiophene-2,6-diyl][3-fluoro-2-[(2-ethylhexyl)carbonyl]thieno[3,4-b]thiophenediyl]]

2. Bulk Heterojunction Solar Cells

and describes the "squareness" of the diode in the 4th quadrant. The efficiency can now be calculated by

$$\eta = \frac{I_{mpp}V_{mpp}}{P_L} = \frac{I_{sc}V_{oc}FF}{P_L} \quad (2.29)$$

To account for different active areas A generating I_{sc} , it is common to use the short circuit current density $j_{sc} = I_{sc}/A$. In this case the absolute light power P_L has to be replaced in Eq. (2.29) by the light power density $\Phi_L = P_L/A$.

Making it possible to compare the efficiencies of different research groups it is important to define standard testing conditions (STC) under which the IV-characteristics are measured. These STC are defined by the International Electrochemical Commission in the norm IEC60904-4 and are listed in Table 2.1.

criteria	value
temperature	25 °
irradiation power density	100 mW/cm ²
irradiation spectra	AM1.5g after ASTM G173-03

Table 2.1.: The standard testing conditions as defined by the International Electrochemical Commission.

In the used setup no temperature controlling was possible which implies that all cells were measured at room temperature. The most probable reason for wrong determination of the efficiency is the AM1.5g (ASTM G173-03) standard illumination spectra, which cannot be exactly reproduced by commercial solar simulators. Fig. 2.9 displays the spectra of the used commercial solar simulator using AM1.5g filters together with the AM1.5g spectra for comparison. One can see a spectral mismatch that has to be taken into account for every measurement. This can be achieved by two different methods, which ensure that the solar simulator can be considered as equivalent to 100 mW/cm² of AM1.5g: the direct and indirect method.

The more simple method is the indirect method. Here we only need to measure the external quantum efficiency EQE over the whole wavelength range in which the solar cells absorbs and calculate the theoretical short circuit density j_{sc} under any desired spectrum, in our case the AM1.5g spectrum ($\Phi_{AM1.5g}$), by

$$j_{sc,AM1.5g} = \frac{q}{hc} \int_0^{\infty} \lambda \Phi_{AM1.5g}(\lambda) EQE(\lambda) d\lambda \quad , \quad (2.30)$$

where λ is the wavelength. To calibrate the solar simulator one has only to change the light intensity of the solar simulator until the measured short circuit current density matches the determined $j_{sc,AM1.5g}$. It has to be noted that the EQE has to be measured under bias light in the range of 1 sun to take into account recombination effects at short circuit conditions. For optimized solar cells, e.g. P3HT:PC₆₁BM, the recombination effects at short circuit are negligibly small and Eq. (2.30) can be used even for EQEs measured without bias light illumination.

The more complex method is the direct method. Here the EQE of the solar cell that has to be tested (EQE_{tc}) as well as from a calibrated reference cell (EQE_{rc}) has to be known together

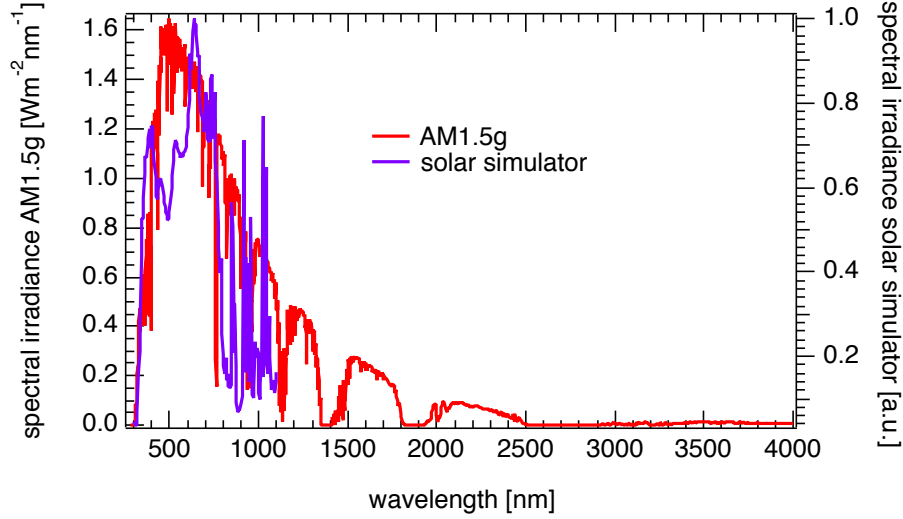


Figure 2.9.: AM1.5g solar spectrum in comparison to the spectrum of the solar simulator measured with a calibrated spectrometer (*getSpec 2048*) ranging from 300–1100 nm. The discrepancy elucidates the importance of a correct calibration of the solar simulator.

with the spectrum of the solar simulator Φ_{ss} . With all these data one can calculate the mismatch factor M by

$$M = \frac{\int_0^\infty \lambda \Phi_{AM1.5g}(\lambda) EQE_{rc}(\lambda) d\lambda}{\int_0^\infty \lambda \Phi_{ss}(\lambda) EQE_{rc}(\lambda) d\lambda} \frac{\int_0^\infty \lambda \Phi_{ss}(\lambda) EQE_{tc}(\lambda) d\lambda}{\int_0^\infty \lambda \Phi_{AM1.5g}(\lambda) EQE_{tc}(\lambda) d\lambda} \quad (2.31)$$

To calibrate the solar simulator, the short circuit current $I_{sc,rc,ss}$ of the reference cell under the solar simulator has to be adjusted to

$$I_{sc,rc,ss} = \frac{I_{sc,rc,AM1.5g}}{M}, \quad (2.32)$$

where $I_{sc,rc,AM1.5g}$ is the short circuit current of the reference cell under AM1.5g spectrum. The advantage of this method is that only the spectral shape of the EQE is important, not the absolute values, which allows to use EQE measurements without bias light even for solar cells, in which recombination does affect the short circuit current.

3. Experimental

In this section the experimental technique mainly used in this thesis — a charge extraction method — will be introduced. Also, the standard sample preparation, starting from the ITO¹ coated glass substrate and the raw materials to the final solar cell will be presented as well as a short description of the used materials.

3.1. Charge Extraction Measurements

To determine the charge carrier density at open circuit conditions a charge extraction (CE) method was used. Its working principle is depicted in Fig. 3.1, the scheme of the setup is shown in Fig. 3.2.

Before the charge extraction measurement can be performed, the open circuit voltage of the solar cell under a specific illumination level has to be determined. Therefore, the solar cell is illuminated constantly by a high power light emitting diode (LED) with 10 W electrical power (*Seoul P7 Emitter*) and the current–voltage characteristics are measured using a *Keithley 2602* source–measure unit.

The actual charge extraction measurement consists of two different time periods. In the first, the LED is on and charge carriers are generated in the solar cell. At the same time a double pulse generator (*Agilent 81150A*) applies the previously measured V_{oc} to the solar cell. In steady state conditions no current flows in the external circuit and all generated charge carriers recombine ($G = R$). At t_0 the LED is switched off by shorting the constant current source (*Keithley 2602*) with a high power transistor triggered by the double pulse generator. To synchronize the turning off of the LED with the short-circuiting of the solar cell ($V=0$ V) one has to take into account the transistor switching time of 215 ns. The resulting current is preamplified by a *FEMTO DHPCA-100* current-voltage amplifier before the signal is detected with an *Agilent DSO 90254A* digital storage oscilloscope. To obtain the extracted charge Q_{extr} one has to integrate the current signal $I(t)$ over time,

$$Q_{extr} = \int_{t_0}^{\infty} I(t) dt \quad . \quad (3.1)$$

In reality, it is not possible to integrate to infinity but to a specific time t_{end} where $I(t_{end})$ is approximately zero and no difference to the signal noise can be detected, where t_{end} depends on the material system and the temperature. As Q_{extr} is dependent on the volume V_s of the solar cell, it is preferable to calculate the extracted charge carrier density $n_{extr}=Q_{extr}/(V_sq)$, where the volume V_s is given by the area of the active layer A and its thickness d . The active layer area is defined as the overlap of both electrodes and was determined with an optical microscope (*Carl Zeiss Axiotech vario 25 HD*), the thickness was measured with a mechanical profilometer (*Veeco Dektak 150*). To calculate the real amount of photogenerated charge carriers in the device at V_{oc} ,

¹indium tin oxide

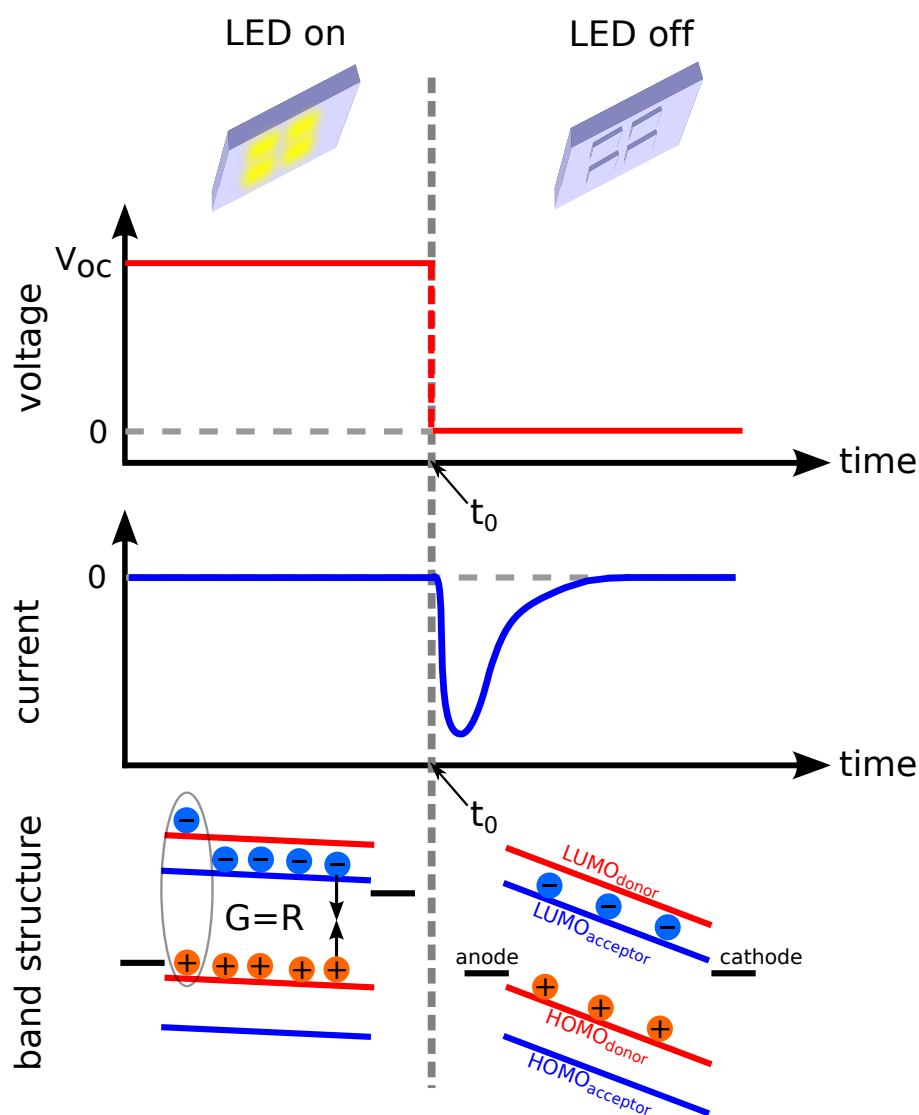


Figure 3.1.: Scheme of working principle of the charge extraction measurement. On the left side of the scheme ($t < t_0$) the LED is on and generates continuously charge carriers in the solar cell. Additionally, a specific voltage, the open circuit voltage V_{oc} , corresponding to the light intensity is applied to the solar cell. In steady state this leads to $I=0$ A implying that all generated charge carriers recombine in the device. At t_0 the LED is switched off and the solar cell is short-circuited ($V=0$ V) resulting in a current, which gives, when integrated over time, the number of extracted charges.

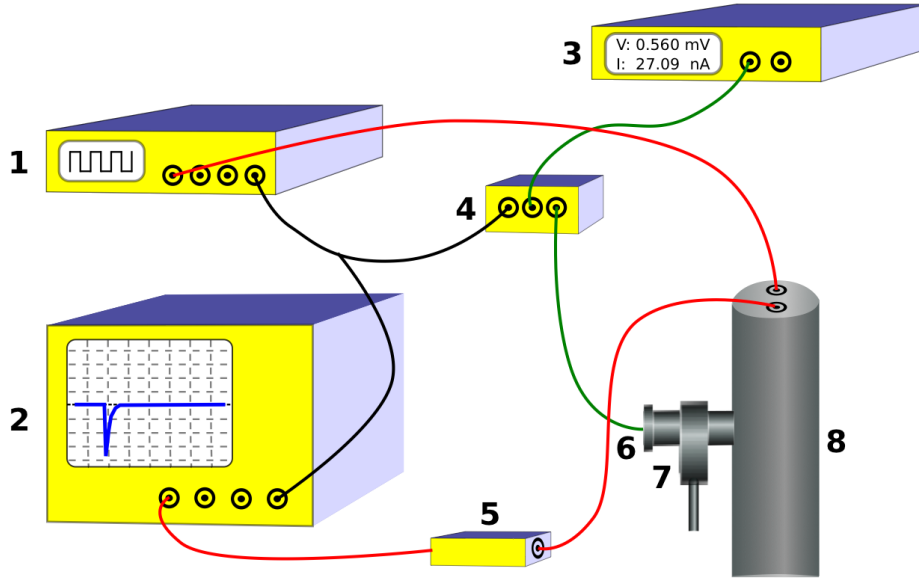


Figure 3.2.: Setup used for charge extraction measurements. **1:** double pulse generator for applying V_{oc} and the triggering of the the LED and the oscilloscope **2:** oscilloscope to record the extraction signal **3:** constant current source for LED **4:** transistor to switch the LED on or off **5:** current voltage preamplifier **6:** LED **7:** six position filter wheel **8:** cryostat containing the solar cell.

one has to bear in mind two additional effects which will be discussed in more detail below: capacitance effects and recombination of charge carriers during the extraction.

By varying the illumination intensity and temperature of the solar cell, it was possible to influence V_{oc} and the corresponding charge carrier density. To control the temperature, all charge extraction measurements were performed in a closed cycle cryostat (*Janis CCS 550*) with He as contact gas. Inside the cryostat the temperature was checked with two sensors and two heaters working against the permanent cooling of the compressor. One heater-sensor pair was located near the device, the other near the coldhead, both were controlled by a *Lakeshore 332* cryogenic temperature controller.

The calibration of the light intensity is a complicated issue since the LED provides a heavily mismatched spectrum to the AM1.5g spectrum ranging only from 400 to 700 nm, with a sharp peak in the blue at 450 nm, resulting in a cold white color with a correlated temperature color of 6300 K. With respect to this high spectral mismatch, the light intensity was defined as $P_L=1$ sun when the solar cell supplies the same short circuit current as obtained from the efficiency determination under the mismatch corrected spectra delivered by a solar simulator. To illuminate the test cell with lower light intensities it is necessary to correlate the constant current driving the LED I_{LED} with the supplied light intensity P_x . The calibration was performed with a silicon solar cell (*Hamamatsu S1133*) which exhibits a linear response of the short circuit current $I_{sc,S1133}$ on the incident light intensity P_x . The measured $I_{sc,S1133}(I_{LED})$ dependence together with $P_x \propto I_{sc,S1133}^x$ ($x=1$) results in $P_x(I_{LED})$. Using the fixed current defining $P_L=1$ sun now allows to illuminate the test solar cell with various intensities in fractions of suns. To reach low

3. Experimental

intensities it is not possible to just reduce the current to any desired I_{LED} because at low currents the LED starts to jitter. Therefore, neutral density filters (*Thorlabs ND*) in a six position filter wheel (*Thorlabs FW102C*) were used to reduce the light intensity. This complicates the calibration because the given values of the optical densities of the filters are only mean values over a special wavelength range and their transmission is again wavelength dependent. Therefore, it is not correct to supply for instance a special I_{LED} to illuminate the cell with $P_L=1$ sun and to use filter with an optical density of 1 and define the light intensity on the solar cell as $P_L=0.1$ sun. To calibrate the light intensity as exactly as possible, the following procedure was performed for every solar cell before it was measured:

1. Find I_{LED} to match the short circuit current I_{sc} of the cell to the measured value under the calibrated solar simulator without using a neutral density filter and define the light intensity as $P_L=1$ sun.
2. Calculate I_{LED} that is necessary to obtain $P_L=0.3$ suns from the calibration curve
3. Measure I_{sc} under $P_L=0.3$ suns
4. Turn the filter wheel to the position with the next lowest optical density
5. Find I_{LED} to match the short circuit current I_{sc} of the cell to the measured value under $P_L=0.3$ sun, to get a calibration for this filter
6. Calculate I_{LED} necessary for $P_L=0.3 \times 0.3$ suns
7. Repeat steps 3. to 6. to get a $P_L(I_{LED})$ calibration for every single filter position.

After this more technical part of the section, the focus will now be set on the two physical effects which have to be taken into account when calculating the (real) charge carrier density stored in the device at open circuit conditions in steady state: the above mentioned capacitance effect and the recombination of charge carriers during the extraction.

Capacitance Effect

A solar cell can not only be considered as a diode but also as a parallel-plate capacitor with the two electrodes as plates and the active material as dielectric. Since the relative dielectric constant ($\epsilon_r \sim 3-4$) of organic materials is small and the active material is thin ($d \sim 100-300$ nm), the capacitance C of the device is relatively high and can be calculated by

$$C = \epsilon_r \epsilon_0 \frac{A}{d} \quad . \quad (3.2)$$

Before the solar cell is short circuited in the charge extraction measurement it can be described as a loaded capacitor where the charge stored on the plates Q_{plates} is given by C and the applied V_{oc} ,

$$Q_{plates} = C \cdot V_{oc} \quad . \quad (3.3)$$

This charge contributes additively to the charge extraction signal when the capacitor is discharged at t_0 and must therefore be subtracted from Q_{extr} . In principle it is possible to calculate $Q_{plates} = \epsilon_r \epsilon_0 \frac{A}{d} V_{oc}$ using literature values of ϵ_r and the measured A and d , but all these values

can be imprecise and for some material systems no literature values of ϵ_r are available. Fortunately, the above described setup allows to measure the capacitance. This can be achieved by performing a charge extraction measurement by applying a small voltage in reverse bias ($V_{appl} < 0$ V) in the dark without using a LED. At t_0 the solar cell is short-circuited ($V=0$ V). The obtained signals for different voltages ranging from $V_{appl} = -0.05$ to -0.25 V can be seen in Fig. 3.3(a).

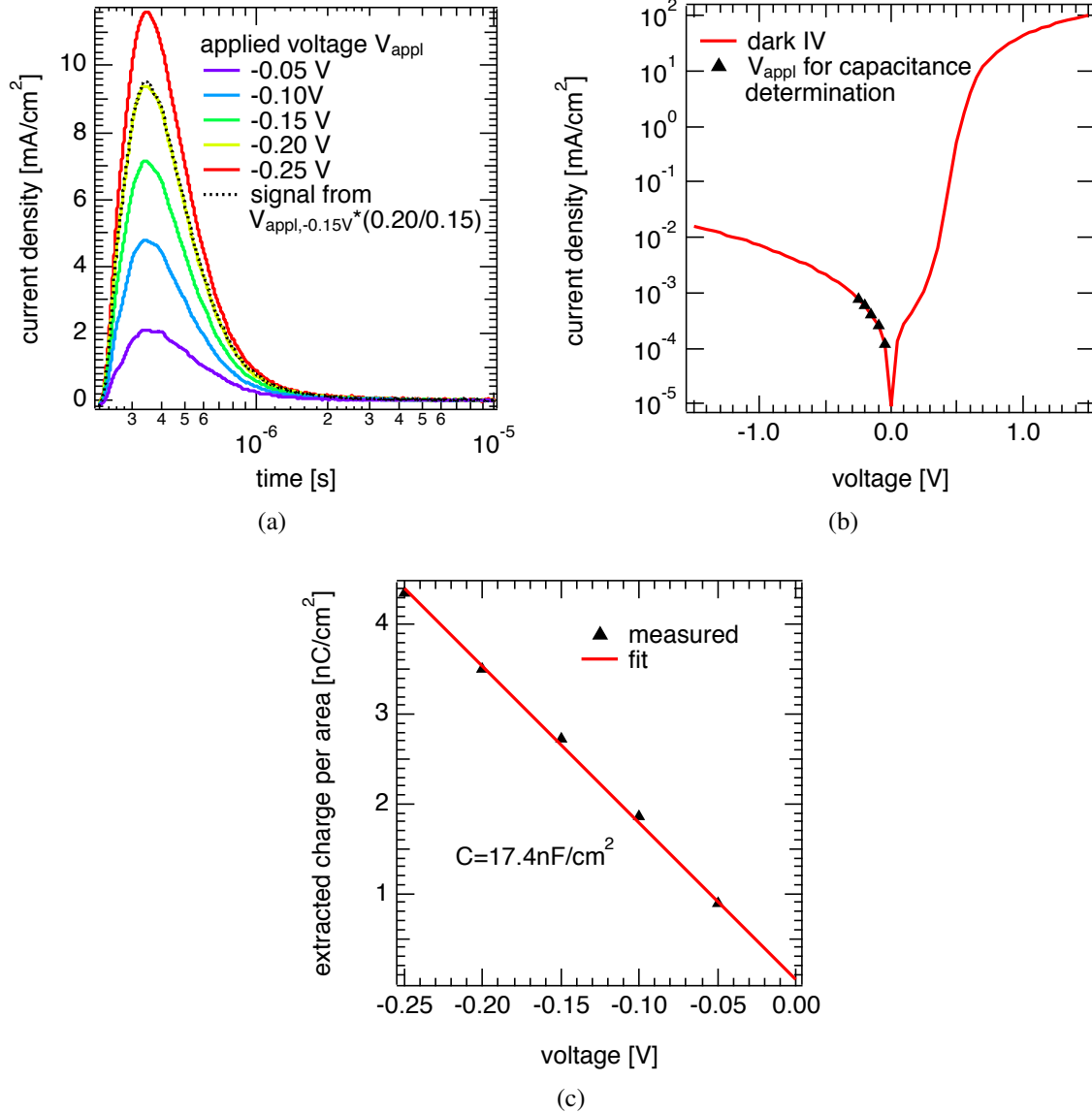


Figure 3.3.: Charge extraction signals, when applying only small voltages V_{appl} to the test cell in reverse bias in the dark without using the LED (a). Here the solar cell acts as a capacitor. At this voltages only a negligible amount of charge carriers is injected into the solar cell which can be seen in the dark IV-curve, the triangles indicate the used voltages (b). The amount of charges stored on the plates as result of the integration of the CE signals shown in (a) as function of V_{appl} shows a linear dependency of Q_{plates} on V_{appl} , where the slope yields directly the capacitance (c).

3. Experimental

In this voltage range the diode is reversed-biased and only a negligible current is flowing as can be seen from the dark IV curve (Fig. 3.3(b)). This implies that only an insignificant amount of charge carriers is injected into the active material and the number of charges stored on the electrodes Q_{plates} can be obtained by integrating the signal over time. Plotting Q_{plates} over the applied absolute voltage (Fig. 3.3(c)) results in a linear dependence as predicted by Eq. (3.3). From the fit one can determine C of the solar cell.

Another issue, which will be important when calculating the recombination of charge carriers during the extraction, is that the transients of the different signals for the capacitance determination only vary in height. In Fig. 3.3(a) the signal of $V_{appl}=-0.15$ V was multiplied by a factor of 4/3 and matches perfectly the signal of $V_{appl}=-0.2$ V. This implies the possibility to scale the capacitance signal to every applied voltage.

Recombination during Extraction

The first step to calculate the recombination losses during the charge extraction is to subtract the part of the signal originating from the capacitance from the charge extraction signal. This is for example done in Fig. 3.4(a) for a P3HT:PC₆₁BM cell under $P_L = 1, 0.1$ and 0.017 suns illumination at 300 K. It becomes obvious from the graph that the influence of the capacitance is higher for lower light intensities. Integration of the obtained signal leads to the charge carrier density $n_{extr,0}(t)$, where the index 0 denotes that $n_{extr}(t)$ is not recombination adjusted. To determine the recombination losses it is important to know the charge carrier density stored in the device at any time $n_{dev,0}(t)$, which is given by:

$$n_{dev,0}(t) = n_{extr,0} - n_{extr,0}(t) \quad . \quad (3.4)$$

$n_{extr,0}$ is equal to $(Q_{extr} - Q_{plates})/V$ as described above. $n_{extr,0}(t)$ and $n_{dev,0}(t)$ are shown in Fig.3.4(b) for $P_L=1$ sun.

The next step is to discretize the time t to t_i , here a step size of $\Delta t = t_{i+1} - t_i = 1$ ns was used. The recombination losses $n_{loss}(t_i)$ in the time interval from t_i to t_{i+1} is then given by:

$$n_{loss}(t_i) = R(n_{dev,0}(t_i)) \cdot n_{dev,0}(t_i) \cdot \Delta t \quad , \quad (3.5)$$

where R is the recombination rate, which was determined by transient photovoltage / transient photocurrent [100] measurements performed on the same device. It has to be noted that Eq. (3.5) is only valid when the difference between $n_{div}(t_i)$ and $n_{div}(t_{i+1})$ is small, which was ensured by using a narrow discretization. To calculate the whole recombination losses one has to sum up all $n_{loss}(t_i)$,

$$n_{loss,j+1}(t) = \sum_{t_i=0}^t R(n_{dev,j}(t_i)) \cdot n_{dev,j}(t_i) \cdot \Delta t \quad . \quad (3.6)$$

Together with

$$n_{dev,j+1}(t) = (n_{dev,0}(t) + n_{loss,j+1}(t)) \quad (3.7)$$

one can calculate the real $n_{dev}(t)$ by applying Eq. (3.6) and (3.7) iteratively, where j is the iteration step. The routine has to be continued until $n_{dev,j+1} - n_{dev,j} \rightarrow 0$. This is achieved in most cases after 4-5 iteration steps, nevertheless 10 steps were routinely performed.

The results for $n_{loss,10}$ as well as $n_{dev,10}$ are shown in Fig. 3.4(b). The recombination losses in this case ($P_L=1$ sun, $T=300$ K) were 6.1 %. For lower light intensities the losses decrease to

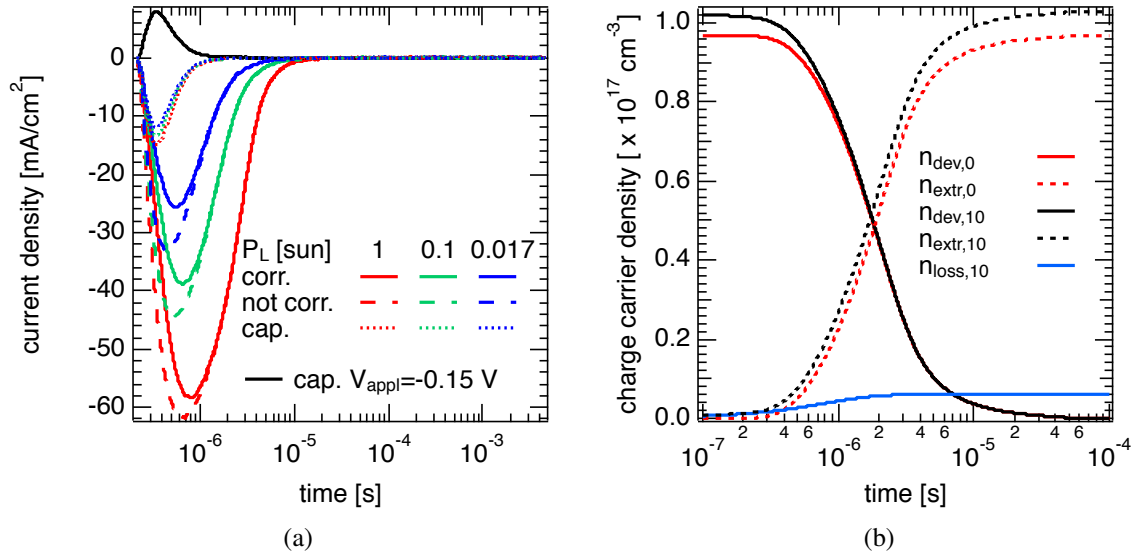


Figure 3.4.: Charge extraction measurements for different illumination levels. The raw signals (dashed lines) were corrected (solid lines) by their capacitive contribution (dotted lines). The black line is a capacitance signal measured at $V = -0.15$ V (a). The influence of recombination during a charge extraction measurement is shown exemplary for 1 sun illumination. The red dashed line shows the integral charge density extracted from the device where no recombination was taken into account, the red solid line is the corresponding stored charge carrier density. The black lines are corresponding data, where recombination during extraction was taken into account using the iteration described in the text. The blue line shows the recombination losses (b).

1.1 % for $P_L = 0.1$ suns and 0.3 % for $P_L = 0.017$ suns. At lower temperatures the recombination rate drops which implies that the recombination losses at lower temperature will decrease even if the extraction time increases.

Since most measurements were performed in the range of illumination intensities of 1 sun or only a bit higher, recombination losses can be neglected. Therefore, all data shown in the results are not corrected for recombination losses: their calculation is very time consuming and do not change the main statements of this work. Thus, all presented charge carrier densities were calculated by $(Q_{\text{extr}} - Q_{\text{plates}})/(V_s q)$.

3.2. Sample Preparation

The working principles of organic BHJ solar cells were discussed in chapter 2 from a physical point of view. In this part, the preparation of solar cells like those used in this work is described from a technical aspect. Deviations from the here presented standard routine will be given in the respective sections.

The standard organic BHJ SC device configuration is shown schematically in Fig. 3.5. As a transparent electrode indium tin oxide (ITO) coated on glass is used, which is the most important transparent conductive oxide (TCO) in the field of organic SCs or LEDs. ITO was purchased from PGO (*Präzisions Glas & Optik GmbH, CEC010S*) with a sheet resistance lower than $10 \Omega/\square$. The ITO layer is around 180 nm thick, the substrate consists of 1.1 mm thick HQ-float glass and a 25 nm thick SiO_2 passivation layer to prevent Na to diffuse into the ITO. In

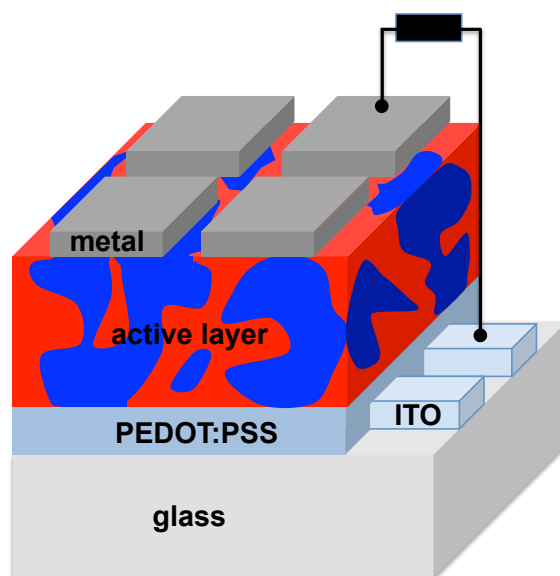


Figure 3.5.: Scheme of an organic solar cell as used in this work.

order to process more than one solar cell per substrate and to be able to define the area of a solar cell, a lithography based on wet chemical etching was performed to achieve two separate 3 mm thick ITO stripes.

Before starting with the lithography, the ITO coated glass substrates were cleaned by

- mechanical cleaning with soap water
- at least 10 min in soap water in an ultrasonic bath (USB)
- thoroughly rinsing under deionized water and drying
- at least 10 min in acetone in an USB
- at least 10 min in isopropyl alcohol in an USB
- drying by a nitrogen gas flow

The lithography itself was done by the following steps:

- 10 min heating of the substrates at 120 °C on a hot plate
- spin coating of the photoresist (*AZ 1518, MicroChemicals*) with 3000 rpm, 1 s acceleration for 60 s
- annealing for 50 s at 100 °C
- UV illumination through a shadow mask for 59 s
- developing of the photoresist (*AZ 351B, MicroChemicals*): 2× AZ 351B:H₂O=1:3 for 30 s
- removing of developer with deionized water
- annealing for 2 min at 120 °C
- etching of the ITO with H₂O:HCl:HNO₃=12:12:1 for 13 min in an USB
- removing of acid residues with deionized water
- removing of photoresist with acetone

After the lithography was finished, the substrates were treated by another cleaning run as described above.

On top, a thin layer (~40 nm) of PEDOT:PSS¹ (*Heraeus CLEVIOS™ P VP AI 4083*) was spin coated (3000 rpm, 1 s acceleration, 60 s) as a hole transport layer (HTL). Afterwards the substrates were transferred into a nitrogen filled glovebox to avoid contact of the solar cells with oxygen. Here the PEDOT:PSS coated substrates were at first heated at 130 °C for 10 min to remove residual water.

The active layer was spin coated from a solution of the donor–acceptor blend. To obtain a blend solution the respective materials were dissolved in an organic solvent such as chlorobenzene in a specific concentration. In most cases the single materials were dissolved in separate solutions for several hours and blended before application, in some cases the donor–acceptor blend was dissolved in one solution. The material concentration as well as the spin speed were used as parameters to obtain the favored film thickness. After spin coating of the active layer an optional annealing step was applied. This temperature treatment can beneficially influence the morphology and enhance the performance of the solar cells, especially of those consisting of P3HT as donor material. In contrast, in other material systems the heating can influence the solar cell performance negatively. Whether or not a heating step was applied will be stated in the specific sections.

Without breaking the nitrogen atmosphere the substrates were transferred into an evaporation chamber where the metal contacts were thermally evaporated on top of the active layer through a shadow mask. The base pressure was lower than 1×10^{-6} mbar. The contacts consisted of a 3 nm thin calcium (Ca) interlayer and a 100-120 nm thick aluminum (Al) layer.

The finished solar cells were directly measured under a solar simulator to determine their efficiencies before they were transferred into the cryostat to perform the charge extraction measurements.

¹poly(3,4-ethylenedioxythiophene):(polystyrenesulfonate)

3.3. Materials

In the field of OPV a vast range of different donor and acceptor materials with different physical and chemical properties exists. In the following the relevant properties of the materials used in this work are described, starting with the donor materials before going on to the acceptors.

Donor Materials

In the framework of this thesis many materials were utilized as donors, but only two polymers are mentioned in the experimental part: P3HT and PTB7. Their structural formulas are illustrated in Fig. 3.6. These two materials are polymers, as most donors in OPV are, but also different solution processable molecules such as cyanine salts can be used. The structural formulas of two cyanine salts which act as donors in combination with PC₆₁BM are shown in Fig. 3.7 [13].

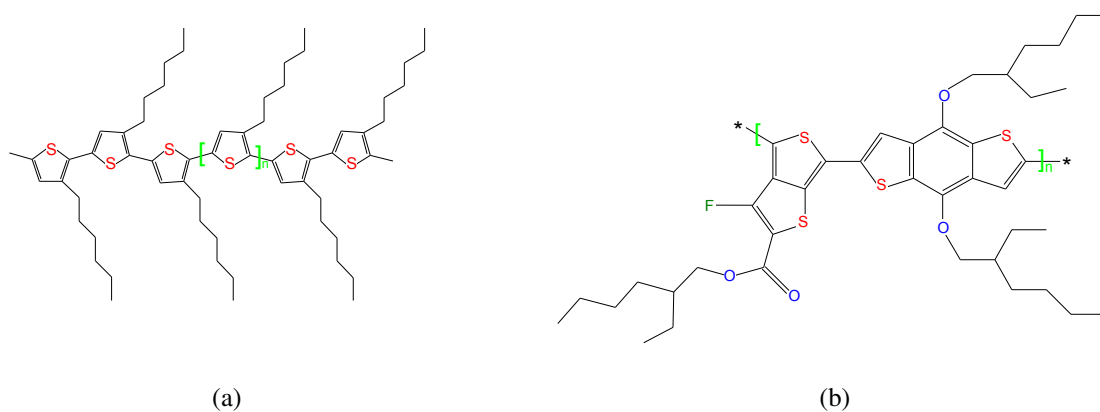


Figure 3.6.: Structural formulas of the the donors used in this work, P3HT (a) and PTB7 (b).

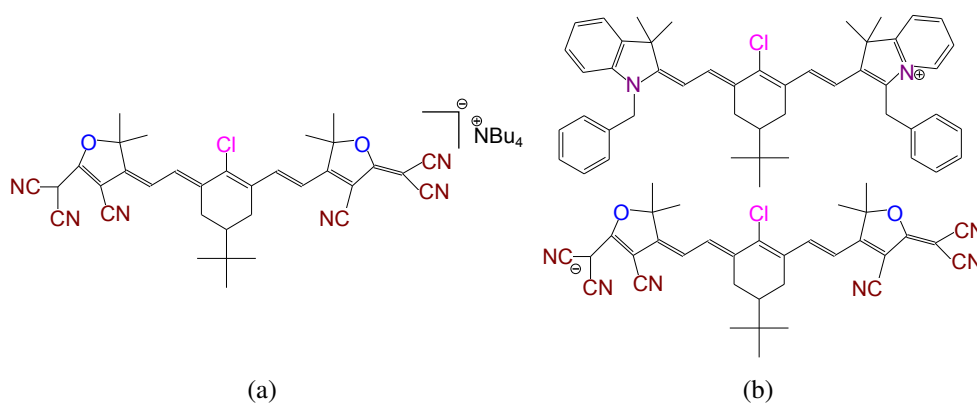


Figure 3.7.: Cyanine salts used as donors, which were characterized in BHJ SC in combination with PC₆₁BM as acceptor. Not discussed in this thesis, but published in cooperation with N. Martin *et al.* [13].

P3HT is the best investigated donor material since it was holding the efficiency record in OPV for a long time in combination with PC₆₁BM as acceptor (see below). Performing an internet search on *webofknowledge.com* with the keyword "P3HT" results in approximately 4.364 publications (as of 14. October 2011). Together with PC₆₁BM 1033 articles were published in the time range from 2002 to 2010 [24]. As a result many fundamental properties of this polymer are known, e.g. the energetics [27] and transport properties. The mobility is in the range of 10^{-4} cm²/(Vs) in diode configuration measured by time of flight measurements [21] and can reach values of up to 0.1 cm²/(Vs) in a field effect transistor [102]. The reason for these relatively high mobilities is that P3HT can form crystalline phases, as found by X-ray diffraction (XRD) (see Fig.3.8(a)). Also the density and energetic depth of trap states, which have a high impact on the transport of charge carriers, is known [91]. The major drawback of P3HT with respect to solar cells is the limited absorption in the visible range with an absorption edge at \sim 650 nm which allows to harvest only around 20 % of the solar photons. P3HT used in this work was purchased from *Rieke Metals, Inc. (BASF Sepiolid P200)* and was used without further purification. The average molecular weight was 20-40 kDa, the regioregularity, which describes the head to tail configuration, was higher than 95 % [47].

PTB7, in contrast to P3HT, is a very new material which was presented 2010 and was the first material reaching power conversion efficiencies higher than 7 % in combination with PC₇₁BM as acceptor [63]. Optimization of the device preparation yielded even 8.37 % [43], which makes it the best commercially available donor material. Up to date, only few publications about the properties of this material exist. The advantage in the view of solar cell performance in contrast to P3HT is the higher absorption range of up to 750 nm. Remarkable is the fact that the material is completely amorphous and does not show any crystallinity in the XRD spectrum (Fig. 3.8). PTB7 was purchased from *1-material*.

Acceptor Materials

Fullerene derivatives are commonly used in OPV as acceptor molecules due to various advantageous properties. The most important is the relative high electron affinity in comparison to the donors, which is responsible for the effective dissociation of excitons and the separation of the polaron pairs. Another beneficial property is the transport of the charge carriers, since the fullerene derivatives show mobility values in the same range as the donor materials which prevent that space charges build up in the active layer. A more practical property is the solubility in common organic solvents such as chlorobenzene to fabricate the solar cells from solution which is achieved by the side chain of the fullerene. All these three main requirements are fulfilled by the most famous acceptor material PC₆₁BM (Fig. 3.9(a)), which was used in most solar cells discussed in this thesis. It has a LUMO level of -3.72 eV [36], a solubility level in chlorobenzene of 25 mg/ml at room temperature [14] and relative high mobility values of 2×10^{-3} cm²/Vs measured in diode configuration [75].

To improve the solar cell efficiency a lot of research is focused on the synthesis of new acceptors. PC₆₁BM for example exhibits only a low absorption of photons in the solar spectrum and therefore contributes only very little to the photocurrent of the solar cells. So one important research topic is the creation of new acceptors which absorb in a supplementary spectral range to the donor material to increase j_{sc} . PC₇₁BM (Fig. 3.9(b)) for example shows similar properties (LUMO, mobility) to PC₆₁BM, but additionally absorbs photons in the visible spectra [14], which supports the generation of excitons and therefore increases the photocurrent.

3. Experimental

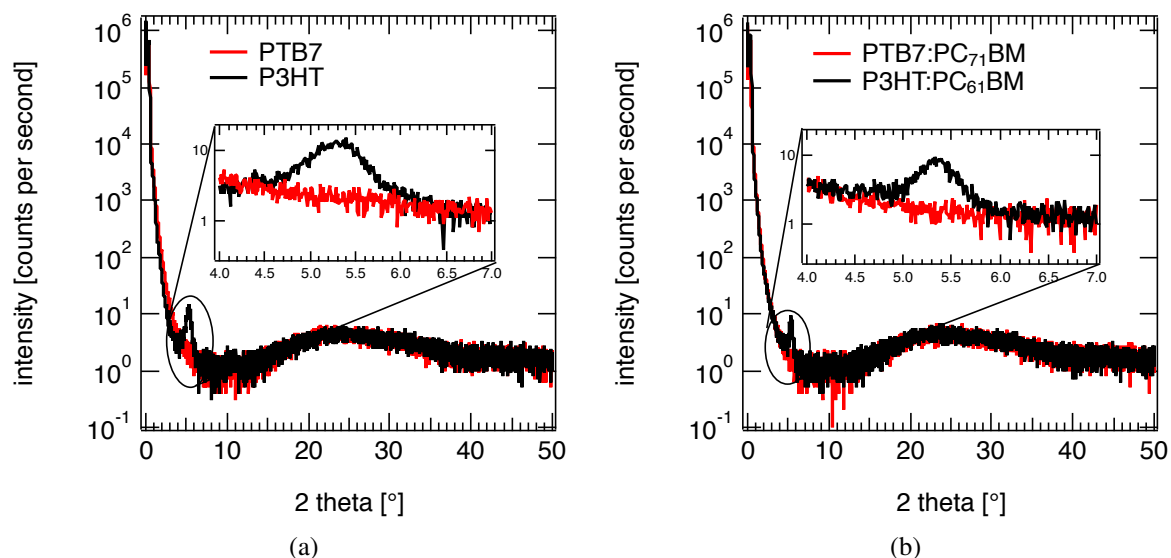


Figure 3.8.: XRD spectra of pure P3HT and PTB7 films (a) as well as P3HT:PC₆₁BM and PTB7:PC₇₁BM blends (b). The signature at $\sim 5.4^\circ$ in the P3HT and P3HT:PC₆₁BM spectra indicates the crystallinity of the P3HT phase, whereas no signature in the PTB7 and PTB7:PC₇₁BM spectra shows that these films are completely amorphous. The broad peak in the range $15\text{--}40^\circ$ results from the glass substrate.

It is often used in low bandgap materials such as PTB7. The second hot topic is shifting the LUMO level to higher values to increase the open circuit voltage of the system, which reduces the driving force ΔG for the charge carrier generation and can again have a negative impact (see section 2.2.1(III)). Here a trade-off between V_{oc} and j_{sc} has to be found. In this work bisPC₆₁BM (Fig. 3.9(c)), a fullerene derivative which consists of two side chains instead of one as in PC₆₁BM, having a considerably higher LUMO level of -3.56 eV [36] was used. A new class of fullerene derivatives are the Indene-C₆₀ adducts [42]. Thereby, the bisadduct ICBA¹ (Fig. 3.9(d)) fulfills the endeavor for high open circuit voltages and provided an efficiency record for P3HT based solar cells [119] and was also used in this work.

Not only the side chains of the fullerenes can be varied to change the acceptor properties, but also two fullerenes can be linked together. To investigate such acceptors, C₆₀–C₆₀, C₆₀–C₇₀ and C₇₀–C₇₀ homo- and heterodimers (Fig. 3.10) were characterized in solar cells in combination with P3HT as donor in collaboration with the work group of N. Martin [32]. The results are not discussed in this thesis, but mentioned here for the sake of completeness. For details, see Ref. [32].

¹Indene-C₆₀ Bisadduct

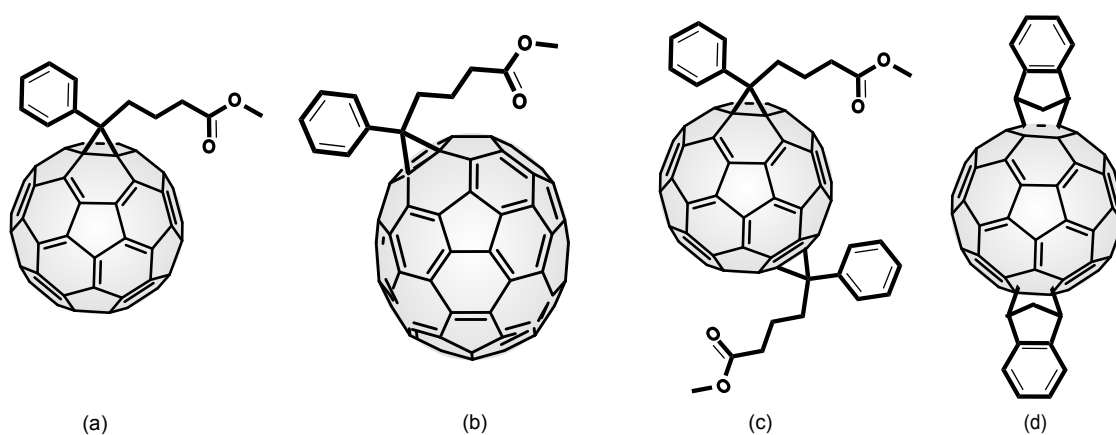


Figure 3.9.: Structural formulas of the the acceptors used in this work: PC₆₁BM (a), PC₇₁BM (b), bisPC₆₁BM(c) and ICBA (d).

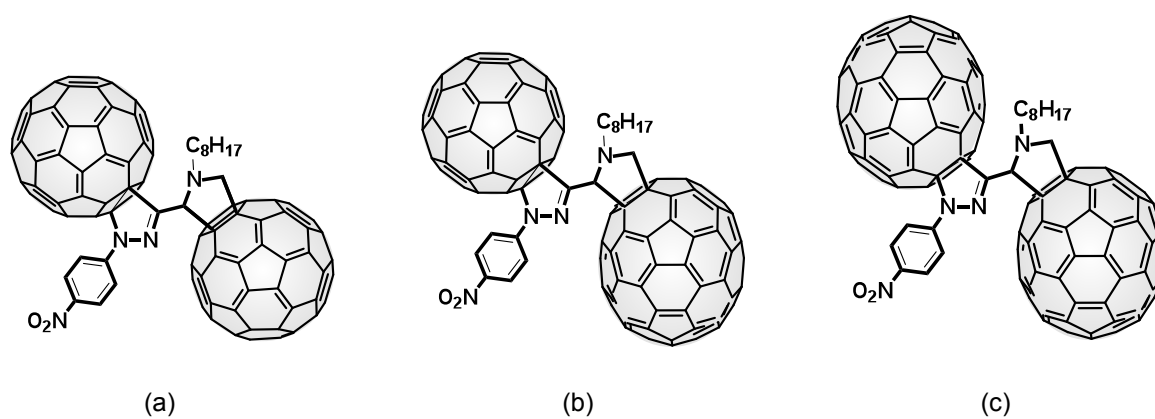


Figure 3.10.: Fullerene homo- and heterodimers (C₆₀-C₆₀ (a), C₆₀-C₇₀ (b) and C₇₀-C₇₀ (c)) used as acceptors, which were characterized in BHJ SC in combination with P3HT as donor. Not discussed in this thesis, but published in cooperation with N. Martin *et al.* [32].

4. Relation of Open Circuit Voltage to Charge Carrier Density in Organic Bulk Heterojunction Solar Cells ¹

4.1. Introduction

The open circuit voltage is one of the key parameters to optimize organic bulk heterojunction solar cells as already mentioned in section 2.3. A linear dependence of V_{oc} on the energy difference E_g between the acceptor LUMO_{acceptor} and polymer HOMO_{donor} was already shown in various publications [15]. This effective band gap E_g was later attributed to the energy of the charge transfer state [29, 114] and is determining the maximum value of the magnitude qV_{oc} that can be achieved in a particular system. This upper limit is reduced by surface [87] and bulk recombination [114] by 0.3 to 0.5 eV [94, 113]. Choosing the right electrode materials can minimize the influence of the surface losses.

As already described in section 2.2.3 Koster *et al.* derived an analytical equation for V_{oc} based on Shockley, drift and continuity equation under assumption of Langevin recombination resulting in Eq. (2.16). Transforming this equation to Eq. (2.18) yields a direct connection of the open circuit voltage to the inherent charge carrier density in the device at open circuit conditions. Under assumption of a constant effective density of states N_c for a specific donor–acceptor blend, a higher steady-state charge carrier concentration leads to an increase of V_{oc} . In principle, there are two ways to get a higher equilibrium charge carrier density in the device at open circuit conditions: a higher generation rate of polarons and/or a lower recombination rate. Internal quantum efficiency values close to 100 % were reported for P3HT:PC₆₁BM [95] at short circuit conditions. In addition, photocurrent measurements on the same material system showed, that the polaron pair dissociation yield P at room temperature has only a weak voltage dependence in the range between short circuit and open circuit [28, 66]. Therefore, the gain in carrier concentration at a constant light illumination by increasing the generation rate and thus V_{oc} is very limited. This leads to the second and more promising point: the influence of nongeminate recombination. Reducing the recombination rate will increase the steady state polaron concentration and thus the open circuit voltage.

In this section the open circuit voltage is investigated temperature and illumination dependent together with the corresponding charge carrier density n in the device. It is shown that, depending on temperature, the V_{oc} is mainly determined either by the effective bandgap of the donor–acceptor blend or by the metal–insulator–metal model.

¹Parts of this chapter have been published in Rauh *et al.* *Appl. Phys. Lett.*, 98, 133301 (2011) [90]

4.2. Experimental

In this investigation three different types of solar cells were processed as described in section 3.2. Two devices had an active layer consisting of P3HT as donor blended with PC₆₁BM as acceptor in the ratio of 1:0.8. For one solar cell a Ca (3 nm) / Al (100 nm) cathode was used, for the other a Cr (3 nm) / Al (100 nm) cathode, known to form an injection barrier. For the third solar cell bisPC₆₁BM was used as acceptor in a ratio of 1:1 with P3HT and a Ca (3 nm) / Al (100 nm) contact. The active layers were spin coated from chlorobenzene solutions to gain an active layer thickness for all three cells of about 200 nm. All samples were annealed for 10 min at 130 °C before the metal contacts were thermally evaporated.

All temperature dependent current–voltage characteristics and charge extraction measurements were performed in a cryostat as described in section 3.1.

4.3. Results and Discussion

The IV–characteristics in dark as well as under 1 sun illumination using the solar simulator for all three devices measured in a nitrogen filled glovebox are shown in Fig. 4.1. The extracted parameters j_{sc} , V_{oc} , FF together with the overall efficiency are summarized in table 4.1.

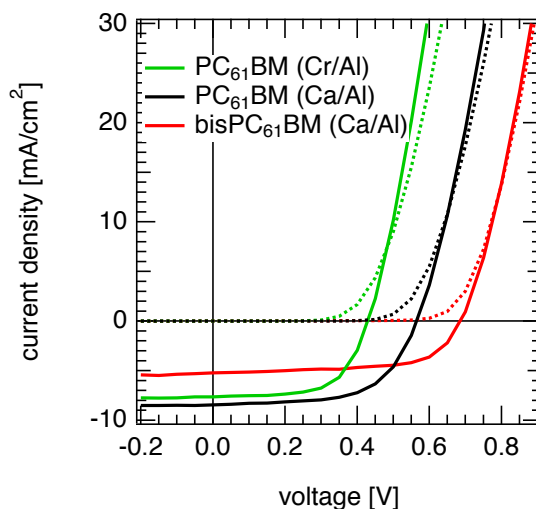


Figure 4.1.: IV–characteristics of all three devices in dark (dotted lines) and under 1 sun illumination (solid lines). The respective parameters are given in table 4.1.

	j_{sc} [mA/cm ²]	V_{oc} [V]	FF [%]	η [%]
PC ₆₁ BM (Ca/Al)	8.4	565	61	2.9
PC ₆₁ BM (Cr/Al)	7.6	430	63	2.1
bisPC ₆₁ BM (Ca/Al)	5.2	690	64	2.3

Table 4.1.: Parameters extracted from the IV–characteristic (Fig. 4.1)

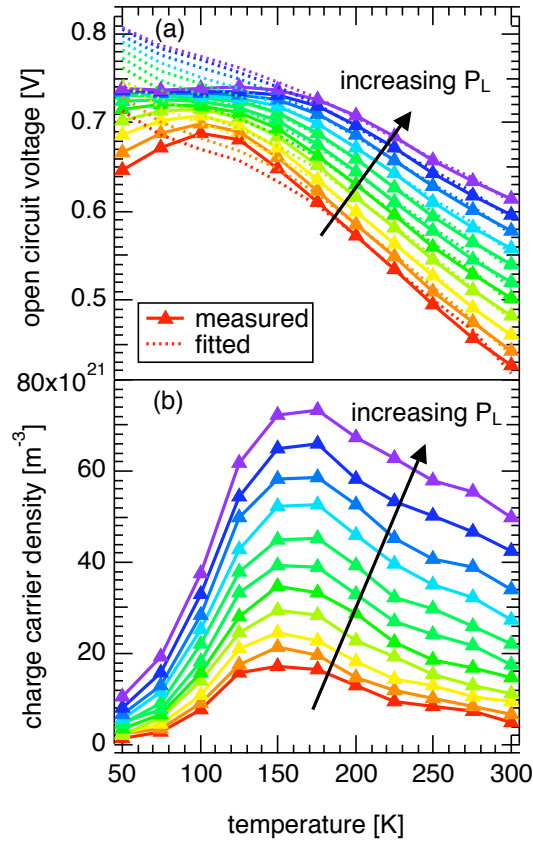


Figure 4.2.: Temperature dependent V_{oc} (a) and corresponding charge carrier density (b) for different illumination levels ranging from 0.01 to 3.16 suns of an annealed P3HT:PC₆₁BM solar cell. The dotted lines in (a) indicate the fit using Eq. (2.18) as fit function.

In Fig. 4.2 temperature and illumination dependent V_{oc} and the corresponding charge carrier densities n are shown for the P3HT:PC₆₁BM solar cell with Ca/Al contacts. Similar dependencies of V_{oc} have been previously reported for MDMO-PPV¹:PC₆₁BM [33]. Two different temperature ranges can be observed. In the high temperature regime (HTR) between around 150 to 300 K, the open circuit voltage is decreasing with increasing temperature as well as the extracted charge carrier density. The low temperature regime (LTR), ranging from 50 to 150 K, shows an increase of n stored in the device with raising temperature and a saturation effect for the V_{oc} at high light intensities. For lower light intensities an increase of open circuit voltage with increasing temperature is observed. The illumination level was varied more than two orders of magnitude from 0.01 to 3.2 suns leading to an increase of both n and V_{oc} . At 300 K the extracted charge carrier density increases only by a factor of ~ 10 despite the more than 300-fold increase in illumination. This nonlinear behavior can be explained by the dependence of the recombination rate on the charge carrier density $R = k_{\lambda} n^{\lambda+1}$, where λ was shown to be in the range of 1.3 to 1.75 for P3HT:PC₆₁BM solar cells at room temperature (see chapters 5, 6 or Ref. [35]).

The temperature dependent open circuit voltages for all investigated solar cells at 1 sun are

¹Poly(2-methoxy-5-(3',7'-dimethyloctyloxy)-1,4-phenylenevinylene)

4. Relation of Open Circuit Voltage to Charge Carrier Density in Organic Bulk Heterojunction Solar Cells

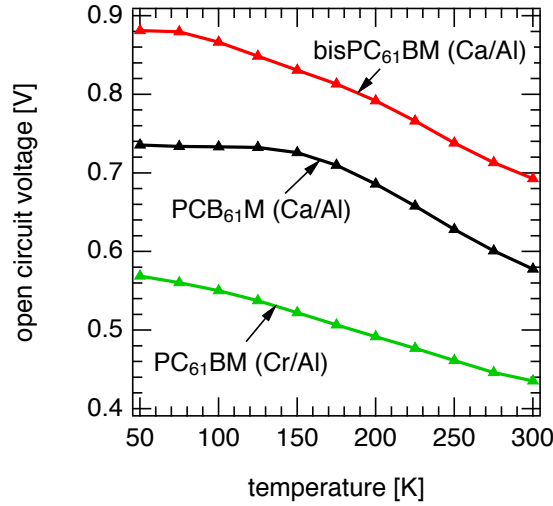


Figure 4.3.: Temperature dependent V_{oc} behavior for three different solar cells. $PC_{61}BM$ and $bisPC_{61}BM$ were used as acceptor in blends with P3HT, the cathodes used are indicated in brackets.

shown in Fig. 4.3. The P3HT: $bisPC_{61}BM$ SC has an overall higher V_{oc} than the P3HT: $PC_{61}BM$ solar cell with the same Ca/Al contact, which is due to the higher LUMO level of $bisPC_{61}BM$ compared to $PC_{61}BM$ [60]. The saturation effect in the LTR is also visible, although it is not as pronounced. The P3HT: $PC_{61}BM$ solar cell with Cr/Al contact has a lower open circuit voltage than the cell with the Ca/Al contact, indicating that in this case the contact is limiting, since the bulk properties have not changed. The temperature dependence of n for the P3HT: $bisPC_{61}BM$ and the Cr/Al P3HT: $PC_{61}BM$ cell show the same behavior as the Ca/Al P3HT: $PC_{61}BM$ cell, but with slightly lower values (not shown).

Investigating the influence of the charge carrier density generated in the solar cell on the open circuit voltage, the $V_{oc}(T)$ was fitted using Eq. (4.1) under the assumption of $n = p$. $n(T)$ obtained from CE measurements provides E_g and N_c as fitting parameters. For the fits shown in Fig. 4.2(a) (dotted lines) only the HTR was used, where Eq. (4.1) describes the V_{oc} behavior very well. Expanding the fit using E_g and N_c from the HTR to the LTR shows a clear discrepancy between the fit and the measured voltage. This implies that the polaron concentration is not responsible for the saturation of V_{oc} at low temperatures, although it can explain the HTR range well. Hence, it can be proposed that the saturation effect at low temperatures is not caused by bulk properties but by the contacts, limiting the maximum achievable voltage.

To support this proposition macroscopic simulations of temperature dependent IV-characteristics were performed. There, Poisson, continuity and drift-diffusion equations were solved simultaneously by an iterative approach explained in Ref. [30, 116] in more details. The mobilities of electrons and holes were assumed to be balanced, their temperature dependencies were calculated by the Gaussian disorder model [8] by $\mu(T) = \mu_0 \exp(-(\frac{2\sigma}{3k_B T})^2)$, with $\mu_0 = 1.1 \times 10^{-7} \text{m}^2 \text{V}^{-1} \text{s}^{-1}$ and $\sigma = 0.06 \text{eV}$ as width of the Gaussian density of states. Recombination was considered by the reduced Langevin model, whereas field and temperature dependent polaron pair dissociation was not taken into account. The other parameters used are summarized in table 4.2.

In addition, different energy barrier heights for charge injection into the blend for electrons

parameter	symbol	value	unit
effective band gap	E_g	1.10	eV
relative dielectric constant	ϵ_r	3.3	
active layer thickness	L	100	nm
effective density of states	N_c, N_v	1.0×10^{26}	m^{-3}
generation rate	G	6.0×10^{27}	m^3s^{-1}
exciton binding distance	a	1.3	nm
decay rate	k_f	1.0×10^5	$\text{m}^{-3}\text{s}^{-1}$

Table 4.2.: Parameters used for simulation.

Φ_n and holes Φ_p were considered in order to investigate their influence on the temperature dependence of the simulated open circuit voltage.

The results are depicted in Fig. 4.4 (a). Without an injection barrier, implying *perfect* ohmic contacts at both electrodes, a linear temperature dependence of V_{oc} over the whole temperature range from 100 to 400 K is determined. A linear fit of this data leads to an intersection at $T=0$ K about 1.2 eV which is above the given E_g of 1.1 eV. Based on the square root shaped density of states as necessary approximation for the numerical calculations, this effect originates from the fixed boundary conditions of thermionic emission at the contacts and charge carrier densities above the effective density of states in the bulk (see Fig. 4.4 (b)). Including a barrier for electrons of 0.1 eV and holes of 0.2 eV already shows a saturation effect of V_{oc} at lower temperatures at 0.8 V. For higher temperatures these relatively low barrier heights can still be considered as ohmic contacts, reducing the open circuit voltage only slightly. Raising the sum of the electron and hole injection barrier to 0.8 eV shows a high impact on V_{oc} even at high temperatures. The difference in V_{oc} compared to the cell with ohmic contacts of 0.53 V at 300 K implies that non-ohmic contacts limit the open circuit voltage at room temperature. Furthermore, it can be seen that it is not appropriate to extrapolate the linear V_{oc} range to $T=0$ K and use this intersection point as E_g/q , as long as the contacts barriers are not zero. The simulation explains the saturation behavior of V_{oc} at low temperatures and can also predict the value at which it occurs, namely $qV_{oc} = E_g - (\Phi_n + \Phi_p)$. For example in the simulation with an injection barrier for the electrons of 0.1 eV and for the holes of 0.7 eV, together with $E_g=1.1$ eV, the saturated V_{oc} is 0.3 V. This makes it possible to determine the sum of the barriers by temperature dependent IV measurements and determine the built in voltage V_{bi} , which is the value at which V_{oc} saturates.

The simulated charge carrier density n under open circuit conditions is given in Fig. 4.4 (b) in dependence of the temperature and for all three injection barrier variations. Here $n = \sqrt{\int_0^L p(x)n(x)dx}$, with $p(x)$ and $n(x)$ the spatial profile of the hole and electron density and L the thickness of the cell. This charge carrier density is different from that one measured experimentally, nevertheless, n taken from the simulation decreases with increasing temperature in the HTR similar to the experimental results shown in Fig. 4.2 (b). In the LTR of the simulated solar cells, this trend is continued, whereas in the experiment n is decreasing with decreasing temperature, which can be an indication for a hindered extraction of the generated charge carriers at lower temperatures resulting in an underestimation of the experimental n . Anyhow, even the low experimental charge carrier densities in the LTR would result in a higher V_{oc} in terms of Eq. (2.18) than the measured values which can be seen by the fits in Fig. 4.2 (a). Inserting the

4. Relation of Open Circuit Voltage to Charge Carrier Density in Organic Bulk Heterojunction Solar Cells

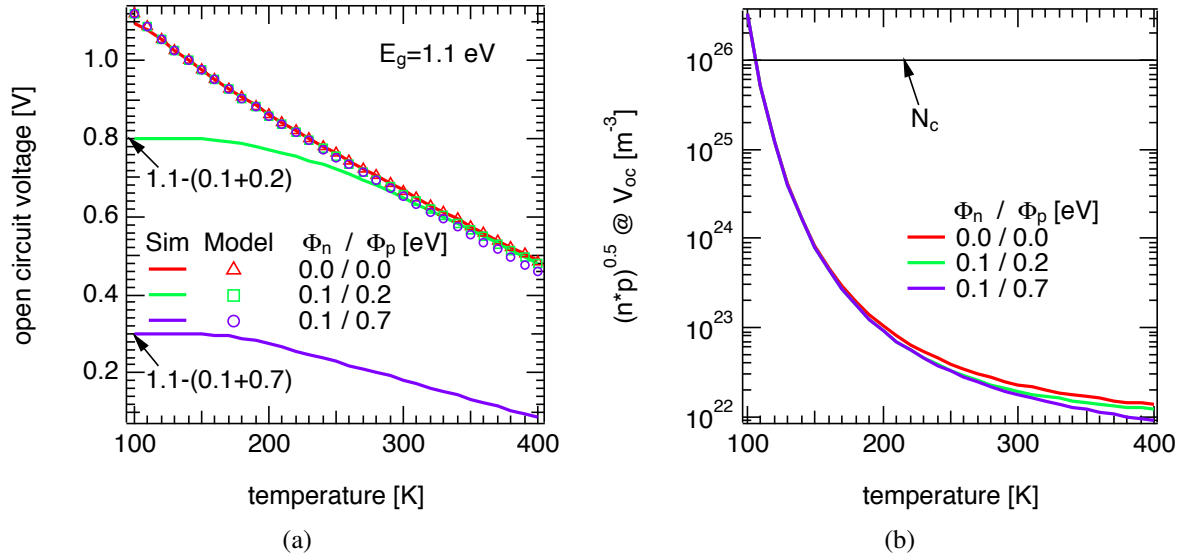


Figure 4.4.: Temperature dependent open circuit voltage (a, solid line) and respective charge carrier densities $\sqrt{n^*p}$ under open circuit conditions (b) obtained from macroscopic simulations with varying electron Φ_n and hole Φ_p injection barriers at the contacts. Applying the simulated charge carrier densities to Eq. (2.18) results in calculated V_{oc} values (a, symbols) higher than the simulated ones.

simulated charge carrier densities into Eq. (2.18) results in V_{oc} values (marked with symbols in Fig. 4.4 (b)) that equals those simulated using *perfect* ohmic contacts.

Comparing the experimental results in terms of V_{oc} with the simulated ones shows qualitatively good agreement. In both solar cells with Ca/Al contact the saturation of the open circuit voltage can be observed at low temperatures. If the work function of the Ca/Al cathode was the same for these two cells, implying the same V_{bi} , both cells should saturate at the same voltage. It is proposed that the difference of ~ 0.1 V in the saturation voltage can be explained by different interface dipoles between the PC₆₁BM/Ca and bisPC₆₁BM/Ca interface, thus changing the corresponding work functions. Indeed, interface dipoles have often been observed for interfaces of evaporated small molecules to metals [44] and polymer:fullerene blends to metals [41], and it is a credible assumption that different material combinations will influence the magnitude of the dipole. Thus, within this scenario, V_{oc} in the LTR is limited by the contacts and only slightly influenced by bulk effects such as the charge generation (see light intensity dependence in Fig. 4.2 (a)).

The difference of V_{oc} in the HTR is mainly caused by the difference of the LUMO levels of PC₆₁BM (-3.7 eV [71]) and bisPC₆₁BM (-3.56 eV) [34, 36], as the charge density is in the same range. This indicates that in this temperature range the open circuit voltage is mainly affected by bulk properties such as the photogeneration and recombination of polarons. Thus, the equation given by Brabec et al. [15], $V_{oc} \approx |E_{HOMO_{donor}} - E_{LUMO_{acceptor}}|/q - 0.3$ V, can be used as a rule of thumb.

Simulation and experiment are also consistent for the solar cells with a limiting contact, as experimentally demonstrated by using a Cr/Al cathode, because of the low workfunction of Cr creating a non-ohmic contact. In this case, the open circuit voltage is limited even in the HTR,

in contrast to the P3HT:PC₆₁BM solar cell with the Ca/Al cathode, although the bulk properties are the same. Such a device is completely contact limited, despite the V_{oc} slightly increases with lower temperature. Thus, it can be concluded, that in the case of limiting contacts, V_{oc} is determined by the MIM model [74].

In the description of Fig. 4.3 it was already mentioned that for lower light intensities in the LTR the open circuit voltage is lower than $(E_g - (\Phi_n + \Phi_p))/q$. To find the origin of this effect, temperature dependent simulations using fixed injection barriers of $\Phi_n=0.1$ eV and $\Phi_p=0.2$ eV, but varying generation rates to account for different light intensities were performed. Fig. 4.5 (a) shows the results, where no decrease of V_{oc} below $E_g - \Phi_n - \Phi_p$ for low generation rates in the LTR can be observed. This is a first evidence that the nature of this effect is not lying

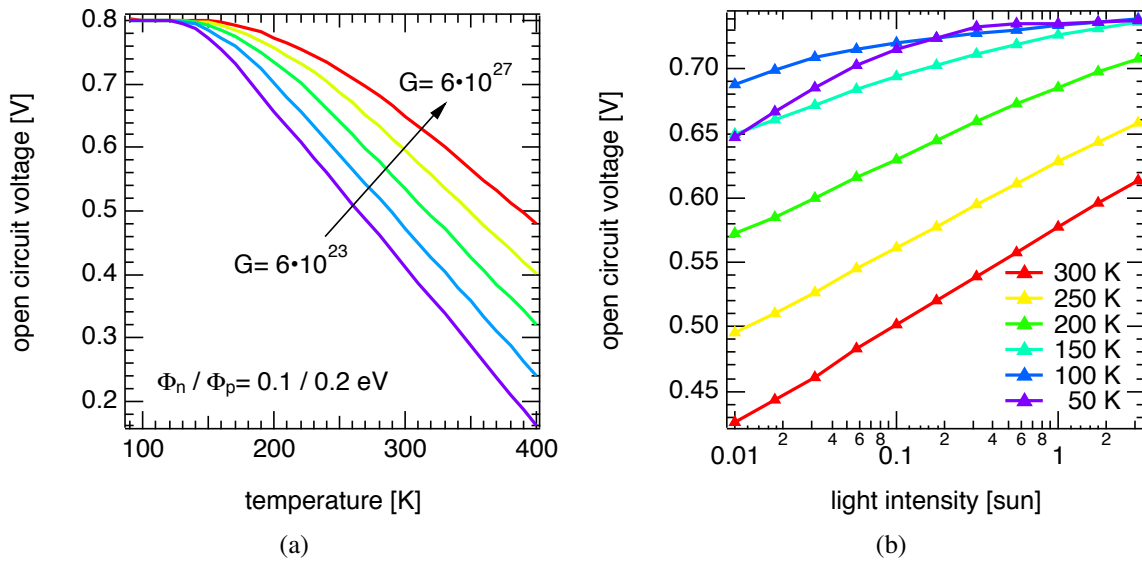


Figure 4.5.: Simulated V_{oc} in dependence of the temperature using fixed injection barriers for electrons and holes ($\Phi_n=0.1$ eV, $\Phi_p=0.2$ eV) with varying generation rates, representing varying illumination levels (a). No decrease of V_{oc} below $E_g - \Phi_n - \Phi_p$ for low generation rates in the LTR can be observed. Plotting the V_{oc} data of the P3HT:PC₆₁BM (Ca/Al) solar cell (Fig. 4.2 (a)) versus the light intensity results in a similar curve as given in section 2.2.3 Fig. 2.7 (b), where it was shown that the parallel resistance of the solar cell can limit the open circuit voltage with a higher influence at lower photocurrents.

in the elementary bulk properties or the contacts. A reasonable explanation for the measured behavior could be, that V_{oc} is suppressed by a too low parallel resistance, an effect which is more pronounced for lower photocurrents (see section 2.2.3, Fig. 2.7 (b)) which are generated at low illumination levels and temperatures. Since the experimentally obtained light intensity dependence of V_{oc} for the P3HT:PC₆₁BM (Ca/Al) solar cell (see Fig 4.5 (b)) shows a similar curve like $V_{oc}(j_{ph})$ in the case of low R_p as calculated by the Shockley equation (Fig. 2.7 (b)), this proposition can be seen as very probable.

4.4. Conclusion

In conclusion, IV and CE measurements of organic BHJ solar cells were performed at various temperatures and illumination intensities to investigate the relation between the open circuit voltage and corresponding charge carrier density. At HTR a linear increase of V_{oc} with decreasing temperature was observed. The saturation at LTR was identified to be caused by injection barriers for charge carriers at the contact, as verified by macroscopic simulations. If these barriers are high and lead to non ohmic contacts, they can reduce V_{oc} and therefore the solar cell efficiency at device operation conditions.

5. Charge Density Dependent Nongeminate Recombination in Organic Bulk Heterojunction Solar Cells ¹

5.1. Introduction

One of the unresolved issues in OSC concerns the exact loss mechanism limiting the device performance. Therefore, the recombination of charge carriers will be discussed in this section in more details. The different recombination processes that can occur in OSC were already introduced in section 2.2.2, nevertheless they will be summarized once again here. The recombination rate R can be expressed empirically as $R = k_\lambda n^{\lambda+1}$ (see Eq. (2.7)), where $\lambda + 1$ means the order of decay and k_λ the recombination prefactor, here defined to be independent of the charge carrier density n . In this simple equation, the concentration of electrons n and holes p is not distinguished, as this is usually not possible by experiment. Many authors explain their experimental results by Langevin recombination [25, 59], in which the annihilation rate of electrons with holes is determined by the mobility. For pure Langevin recombination (Eq. (2.9)), k_λ can be described by the Langevin recombination prefactor $\gamma = (q/\epsilon)(\mu_n + \mu_p) \approx (q/\epsilon)\mu$ (see Eq. (2.10)). Nongeminate recombination was also reported to occur via interface states [23] or trap states [10, 52], described by Shockley–Read–Hall recombination [110]. These processes change the recombination dynamics towards first order, as electron and hole concentrations become imbalanced. For first order recombination, $1/k_\lambda$ is the lifetime. However, several studies reported recombination orders exceeding two [22, 35, 78, 100].

For apparent recombination orders between one and two, or exceeding two, the prefactor k_λ is empirical. The former case can usually be explained by a combination of Langevin and SRH recombination rates. The origin of the higher recombination orders, however, is still under discussion [22, 35, 98].

All approaches to explain the high orders of decay have in common that the recombination process is basically of Langevin type, with the disordered nature of the organic semiconductor blend being responsible for trapping of charge carriers. The influence of energetic disorder on the charge carrier mobility is already known for decades: the thermally activated hopping process of charge carriers, which can also be described by the multiple trapping and release approach, leads to a charge carrier concentration dependent mobility [7, 77, 80]. Charge carriers located in the density of states below the transport energy are trapped and immobile (with density n_t) whereas charge carriers above (with density n_c) are free and have the mobility μ_0 . The overall mobility of all charge carriers (with density $n = n_c + n_t$) corresponds to the measured mobility μ defined by $\mu_0 \cdot n_c = \mu \cdot n$. Nelson [79] used one-dimensional Monte Carlo simula-

¹Parts of this chapter have been published in Rauh et. al. *Adv. Funct. Mater.* 22, 3371 (2012) [89]

5. Charge Density Dependent Nongeminate Recombination in Organic Bulk Heterojunction Solar Cells

tions to understand the stretched exponential decays of the charge carrier concentration found in transient absorption experiments. Trapping of charge carriers in the tails of the density of states distribution was found to be responsible for this finding, as it slowed down nongeminate recombination. Recently, Shuttle *et al.* [98] investigated P3HT:PC₆₁BM solar cells experimentally at 300 K. They showed that $k(n) \propto \mu(n)$ completely accounted for the charge carrier concentration of the recombination rate in excess of the expected value of two, i.e., $R = k(n)n^2$ where $k(n) \propto n^{\lambda-1}$.

In this section, experimental evidence that the observed order of decay can only partly be explained by the charge carrier concentration dependent mobility will be presented. This discrepancy will be quantified for P3HT:PC₆₁BM solar cells at temperatures below 300 K and for PTB7:PC₇₁BM cells at room temperature. Although the MTR model already includes the existence and influence of trap states it will be demonstrated that in addition to the influence on the charge carrier mobility, the donor–acceptor phase separation can protect trapped charge carriers from recombination. The spatial separation of electrons and holes implies that charge carriers trapped within the tail of the density of states distribution cannot be reached by an oppositely charged mobile charge carrier until the trapped charge carrier is emitted from the deep state and becomes mobile. Only then this charge carrier can participate in the recombination process. Thus, the emission rates from the trap states slow down the recombination rate even more than the charge carrier mobility, i.e., the impact of trapping on the recombination prefactor alone, can account for. This model is able to explain the experimentally observed high recombination orders, in contrast to earlier approaches.

5.2. Experimental

In this investigation two different active layer material systems were used: P3HT:PC₆₁BM as reference system and the new and high efficient blend PTB7:PC₇₁BM. Molecular structures and more details concerning the single materials are given in section 3.3. The general fabrication steps were similar to those described in section 3.2. In the case of the P3HT:PC₆₁BM SC, the active layer was spin coated from a 30 mg/ml chlorobenzene solution with a DA weight ratio of 1:0.8, resulting in a 200 nm thick film. The PTB7:PC₇₁BM film was spin coated from a 20 mg/ml chlorobenzene solution where 3 volume % 1,8-diiodooctane was added to influence the morphology of the film. The DA blend ratio was 1:1.5 and the resulting layer thickness was 105 nm. Before the thermal evaporation of the Ca/Al metal contacts the P3HT:PC₆₁BM film was annealed at 130 °C for 10 min, the PTB7:PC₇₁BM film was left as cast.

Since the spectral mismatch M for the solar simulator calibration using the direct method (see section 2.3) was close to 1 ($M=0.96$ for P3HT:PC₆₁BM, $M=1.04$ for PTB7:PC₇₁) the light intensity was not readjusted for exact efficiency determination because the error of spatial inhomogeneity of the light beam was in the same range.

All temperature dependent current–voltage characteristics and charge extraction measurements were performed as described in section 3.1. In this investigation it is distinguished between two different CE measurements: charge carrier generation (illumination) under open circuit and short circuit conditions to measure the respective equilibrium charge carrier density. An example for the charge extraction signal for the determination of n under short circuit conditions is given in section 7 (Fig. 7.6(a)). Since the solar cell is held at $V=0$ V during the complete measurement, the current in the time range $t_0 \leq 0$ s is equal to the short circuit current.

Switching the LED off at t_0 leads to a decrease of the current, integration of the current signal from t_0 to t , where the current is dropped to zero, leads to the equilibrium charge present under short circuit conditions.

5.3. Theory

As already explained in section 2.2.2 it is preferable to study recombination processes by analyzing the charge carrier density at open circuit conditions for different illumination levels and temperatures, as at V_{oc} all charge carriers generated with generation rate G have to recombine ($G = R$). From CE measurements it is not possible to determine the recombination rate directly which is compensated by the calculation of G , which can be extracted from the current–voltage characteristics under illumination. Therefore, the assumption is needed that at sufficiently high voltages in reverse direction, all generated charge carriers will contribute to the saturated photocurrent density $j_{sat,ph}$ and will not recombine. G can then be derived by $G = j_{sat,ph}/(qL)$ (see Eq. (2.6)), where the photocurrent density is derived by subtracting the dark IV-curve from the illuminated one. Using $G = R$ and the charge carrier density n measured under open circuit conditions, $R(n)$ can be obtained and from the slope dR/dn the recombination order (Eq. (2.7)). Here, it is assumed that the polaron pair dissociation is independent of the electric field in the device, i.e., that the generated number of polarons at V_{oc} and at reverse bias, where $j_{sat,ph}$ is calculated, is equal. This assumption is so far justified for P3HT:PC₆₁BM between short circuit and open circuit [53, 66, 104].

As the aim of the investigations in this section is to find out whether the charge carrier concentration dependent mobility alone can explain the recombination orders exceeding two, the different charge carrier concentration dependent contributions to the Langevin recombination rate were analyzed: Therefore, the prefactor

$$k(n) = \frac{R}{n^2} \propto n^\beta, \quad (5.1)$$

determined as described in the previous paragraph was compared to the independently measured mobility $\mu(n) \propto n^\alpha$ as outlined below. If the recombination order could be completely described by the charge carrier concentration dependent mobility (together with the order of 2 for bimolecular recombination), then $k(n) \propto \mu(n)$, i.e., $\alpha = \beta$ should be found.

In order to determine the charge carrier density dependence of the mobility, the short circuit current density j_{sc} was assumed to be drift-dominated [98],

$$j_{sc} \approx j_{drift} = \mu_{drift} n F. \quad (5.2)$$

Here n is the charge carrier density measured under short circuit conditions, F the electric field given by the built-in potential and μ_{drift} the mean drift mobility. In well optimized solar cells, unbalanced electron and hole mobilities would inevitably lead to a drop of the FF and the open circuit voltage [68], which is not the case in the devices investigated here, at least at room temperature. Therefore, it is assumed that μ_{drift} approximately equals the mobility of electrons and holes. As only the charge carrier concentration dependence, i.e. the exponent α ($\mu(n) \propto n^\alpha$) is important in the following argumentation, it is sufficient to calculate a parameter proportional to μ ,

$$\mu \propto \frac{j_{sc}}{n} \equiv \tilde{\mu} \quad (5.3)$$

5. Charge Density Dependent Nongeminate Recombination in Organic Bulk Heterojunction Solar Cells

for constant F . Thus one obtains

$$\mu(n) \propto \tilde{\mu}(n) \propto n^\alpha. \quad (5.4)$$

The same proportionality (j_{sc}/n) results assuming the current to be dominated by diffusion, only the proportionality factor is different.

In the framework of the MTR model it is possible to calculate a theoretical $\mu(n)$ dependence for different density of states distributions when the system is in equilibrium. Although, in most cases the DOS is assumed to be of Gaussian type for organic semiconductors, the here presented calculations consider the case of an exponential DOS $g(E)$ (2.24), as the tail of a Gaussian distribution is similar to an exponential shape and the calculations using an exponential DOS is much simpler. Starting from the charge carrier trapping and release equations [3] together with the density of occupied states $\rho(E)$ being

$$\rho(E) = \frac{g(E)}{1 + \exp\left(-\frac{E-E_F}{k_B T}\right)}, \quad (5.5)$$

where E_F is the Fermi energy, the dependence of the free charge carrier density on the total charge carrier density can be calculated, resulting in

$$n_c(n) = v_0 \tau_0 N_t \left(\frac{n}{N_t}\right)^{\frac{E_0}{k_B T}}. \quad (5.6)$$

τ_0 is the lifetime of free charge carriers until they are trapped. Using $\mu_0 \cdot n_c = \mu \cdot n$, this leads directly to the following theoretical mobility dependence on the charge carrier density

$$\mu(n) = \mu_0 v_0 \tau_0 \left(\frac{n}{N_t}\right)^{\frac{E_0}{k_B T} - 1}. \quad (5.7)$$

As mentioned above, Eq. (5.6) and (5.7) were derived for a system in equilibrium without recombination effects being considered. Despite the charge carriers are extracted from a solar cell which is held in equilibrium, the continuous generation of charge carriers in the complete DOS will lead to a proportionally higher ratio of free to trapped charge carriers, as some charge carriers are still in the thermalization process (see section 2.2.1). Nevertheless, Eq. (5.6) and (5.7) can be used for first estimations.

It was already pointed out that the aim of this investigation was to show that α is not always equal β , i.e. that the high recombination orders can generally not be solely explained by the charge carrier concentration dependent mobility. Instead, a more general recombination rate based on the Langevin rate and prefactor is considered,

$$\begin{aligned} R &= \frac{q}{\varepsilon} (\mu_n + \mu_p) (n_c + n_t) (p_c + p_t) \\ &= \frac{q}{\varepsilon} ((\mu_n + \mu_p) n_c p_c + \mu_n n_c p_t + \mu_p p_c n_t + 0 \cdot n_t p_t) \end{aligned} \quad (5.8)$$

With the assumptions made before, this equation can be simplified to

$$R \propto \underbrace{\mu(n)}_{\propto n^\alpha} \underbrace{(n_c p_c + n_c p_t + p_c n_t)}_{\propto n^{\beta - \alpha n^2}} \propto n^{\beta + 2}. \quad (5.9)$$

Here, the charge carrier mobility depends on the charge carrier concentration due to trapping and release. The first term on the right hand side of Eq. (5.9) corresponds to Langevin recombination, but only of mobile charge carriers. The second and third term are equivalent to SRH recombination, i.e., recombination of a (previously) trapped with a free charge carrier, and is proportional to the mobility of the respective mobile charge carriers. Therefore, the Langevin prefactor can be adapted for this case as well. As trapped charge carriers are immobile, the term $n_t p_t$ does not contribute to the recombination rate. The advantage of Eq. (5.9) is its higher degree of transparency as compared to the superposition of Langevin and SRH recombination. Bear in mind that free and trapped charge carriers are not completely separate reservoirs of charge carriers, but that free charge carriers can be trapped and trapped ones can be reemitted as described by the MTR framework. Due to Fermi–Dirac statistics, $n_t > n_c$ in steady state. It has to be mentioned that in the case of a significant donor–acceptor phase separation, recombination can only take place at the heterointerface. Thus, only mobile charge carriers could recombine directly, as trapped charge carriers would be protected from recombination within their respective material phase. Thus, Eq. (5.9) would simplify to $R \propto \mu(n)n_c p_c$, where the free carrier reservoirs are refilled by reemission from trapped charge carriers, this thermal activation process becomes the limiting factor for the recombination rate instead of the mobility. This case leads to a slower decay of the overall charge carrier concentration, corresponding to a higher recombination order going beyond the impact of the mobility. Fig. 5.1 summarizes schematically all possible recombination mechanisms that can occur in OSC.

5.4. Results and Discussion

5.4.1. Results

The measurements were performed on P3HT:PC₆₁BM and PTB7:PC₇₁BM solar cells showing photovoltaic behavior comparable with literature [16, 63]. The P3HT:PC₆₁BM solar cell had an efficiency of $\eta=3.4\%$ ($V_{oc}=570$ mV, $j_{sc}=8.6$ mA/cm², $FF=69\%$) under 1 sun illumination, the PTB7:PC₇₁BM $\eta=7.0\%$ ($V_{oc}=700$ mV, $j_{sc}=15.0$ mA/cm², $FF=67\%$). The IV curves in dark and for 1 sun illumination are shown in Fig. 5.2.

Fig. 5.3 shows $\tilde{\mu}(n)$ and $k(n)$ obtained from CE and IV measurements for light intensities ranging from 0.01 to 0.5 suns. For both material systems and at all temperatures the power law dependence of $k(n)$ and $\tilde{\mu}(n)$ as described by Eq. (5.1) and Eq. (5.4) can be observed. The slopes of $\tilde{\mu}(n)$ and $k(n)$ are different, implying that the charge carrier density dependence of the mobility alone cannot explain the $k(n)$ dependence.

The recombination prefactor $k(n)$ was calculated using Eq. (2.9) and Eq. (2.6), where for $j_{sat,ph}$ the value at -3.5 V was used. At this negative bias the photocurrent was saturated for all temperatures which was proven by the linear dependence of the calculated generation rate vs. the light intensity P_L . The exponent δ from $G \propto P_L^\delta$ ranged from 0.95 at 300 K to 0.92 at 150 K for P3HT:PC₆₁BM and from 0.95 to 0.94 for PTB7:PC₇₁BM. Recombination losses during the extraction in the CE measurements were in the range of only a few percent and therefore not taken into account. The steady state charge carrier density under short circuit conditions was always lower than under open circuit conditions at the same illumination level because of the continuous sweep out of charge carriers before extraction.

The $V_{oc}(T)$ dependence for both material systems is shown in Fig. 5.4, where the linear

5. Charge Density Dependent Nongeminate Recombination in Organic Bulk Heterojunction Solar Cells

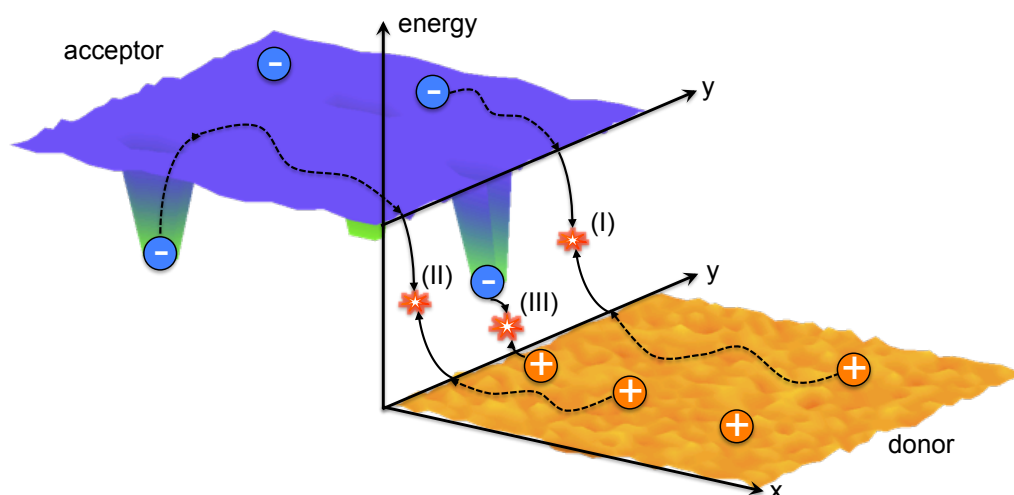


Figure 5.1.: The three possible recombination mechanisms that can occur in a BHJ solar cell. (I): Recombination of two oppositely charged free charge carriers. This process is called Langevin recombination. (II): Recombination of two oppositely charged free charge carriers, whereas at least one of the two charge carriers was captured for a certain time in a trap before it was emitted to participate in the recombination process. In the framework of this thesis this process is called trap limited recombination. (III): A trapped charge carrier recombines directly with an oppositely charged free carrier. Due to the DA phase separation this process can only take place when the trapped charge carrier is very close to the interface in such a way that it can overcome the spacial distance to the interface by tunneling with a reasonable probability. This type of recombination is called trap assisted recombination or SRH recombination.

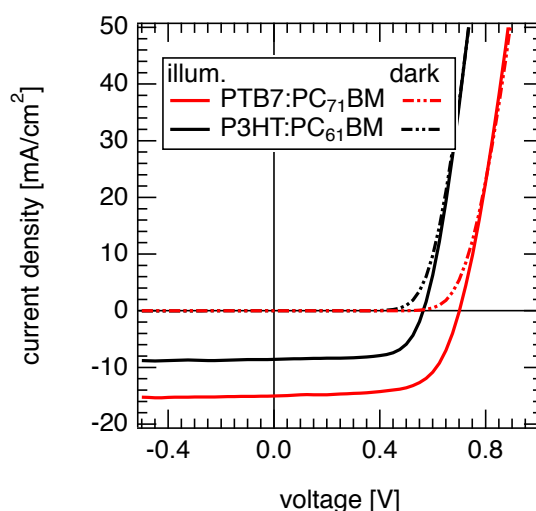


Figure 5.2.: Current–voltage characteristics of P3HT:PC₆₁BM and PTB7:PC₇₁BM solar cells under 1 sun illumination conditions and in the dark.

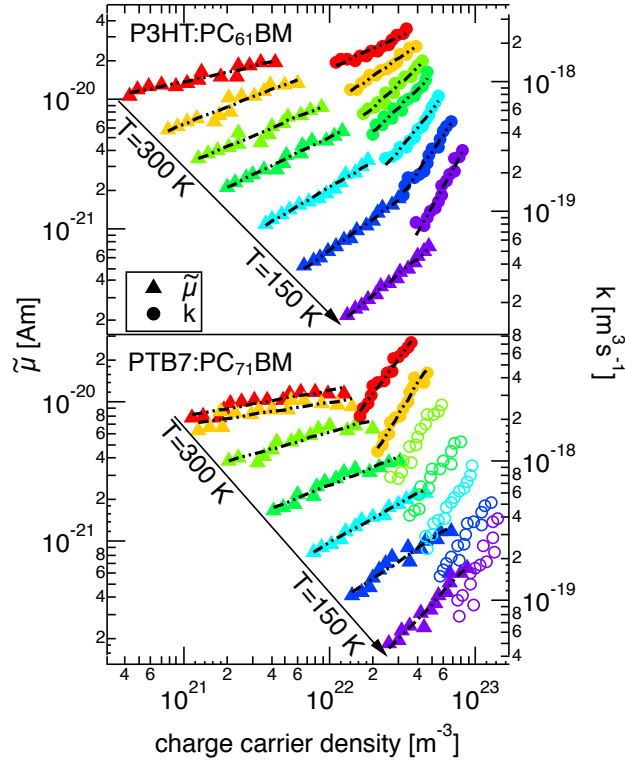


Figure 5.3.: Charge carrier dependence of $\tilde{\mu}$ (Eq. (5.3)) (triangles, left axis) and the Langevin recombination prefactor k (circles, right axis) for P3HT:PC₆₁BM (top) and PTB7:PC₇₁BM (bottom). Solid circles were used for temperatures where the contacts are ohmic, open circles where the solar cell was limited by injection barriers. Details are given in the text. The dashed–dotted lines indicate the fits to Eq. (5.4) and Eq. (5.1), respectively.

5. Charge Density Dependent Nongeminate Recombination in Organic Bulk Heterojunction Solar Cells

increase of the open circuit voltage with decreasing temperature in the case of P3HT:PC₆₁BM indicates that the contacts have an ohmic behavior with negligible injection barriers (chapter 4). Therefore, V_{oc} is directly related to the charge carrier density at open circuit conditions by

$$V_{oc} = \frac{E_g}{q} + \frac{n_{id}k_B T}{q} \ln\left(\frac{np}{N_c^2}\right) \quad , \quad (5.10)$$

with E_g the effective band gap, n_{id} the ideality factor, k_B Boltzmann's constant and N_c the effective density of states [20, 54]. The situation changes regarding the PTB7:PC₇₁BM solar cell, where a linear increase of V_{oc} with decreasing temperature can only be observed in the range of around 250 to 300 K, whereas at lower temperatures the open circuit voltage is limited by injection barriers that are dominant then (chapter 4). In this regime Eq. (5.10) is not valid and the measured charge carrier density can also be affected by the barriers. Hence, no further evaluation of the $k(n)$ data in the temperature range of 150 to 250 K for PTB7:PC₇₁BM was performed, as indicated in Fig. 5.3 by open instead of solid circles.

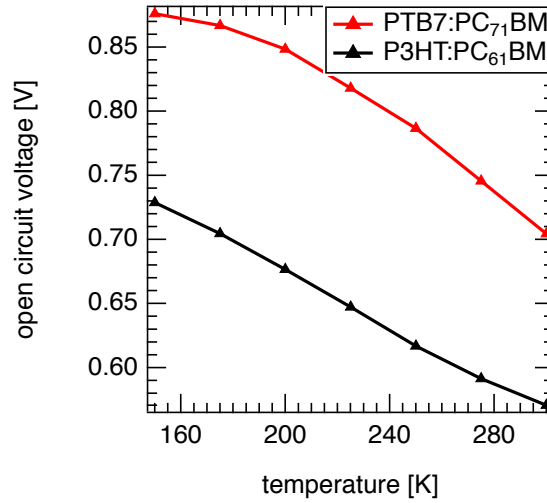


Figure 5.4.: The open circuit voltage versus temperature at 1 sun. For the P3HT:PC₆₁BM solar cell the contacts are not limiting the V_{oc} justified by the linear behavior, for the PTB7:PC₇₁BM solar cell, the contacts influence the V_{oc} , especially at lower temperatures which becomes visible by a saturation of V_{oc} .

β was obtained from the data presented in Fig. 5.3 by using the slope of the linear fit of $\ln(k)$ vs. $\ln(n)$ over the whole data set (Eq. (5.1)), α from the $\ln(\tilde{\mu})$ vs. $\ln(n)$ fit (Eq. (5.4)). The fits are presented in Fig. 5.3 as dash-dotted lines. The determined values of β and α are summarized in Fig. 5.5. The case of $\beta = \alpha$ would imply that the recombination orders higher than two can be explained completely by pure Langevin recombination with an additional charge carrier density dependent mobility.

5.4.2. Discussion

For the P3HT:PC₆₁BM solar cell at 300 K (Fig. 5.3), the mobility (α) shows nearly the same carrier concentration dependence as the recombination prefactor k (β), i.e. the apparent recom-

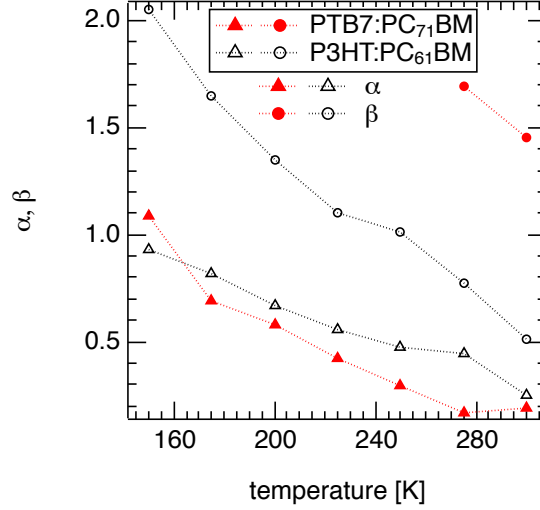


Figure 5.5.: The values of α and β obtained from Fig. 5.3 using Eq. (5.4) (triangles) and Eq. (5.1) (circles) for P3HT:PC₆₁BM (black) and PTB7:PC₇₁BM (red) versus temperature. β for PTB7:PC₇₁BM at lower temperatures was not evaluated because of the contact limitation of V_{oc} in this temperature range.

bination order above two is due to the charge carrier concentration dependent mobility in accordance with literature [98]. At lower temperatures, however, it becomes clear that α and β are not increasing by the same amount with decreasing temperature, resulting in $\alpha < \beta$. The temperature behavior of β for P3HT:PC₆₁BM (Fig 5.5), determined independently, is in accordance with literature [35].

The 275 K and 300 K data of PTB7:PC₇₁BM hold a clear statement. Whereas the values of α are similar to those of the P3HT:PC₆₁BM device, β is higher. This results in a high discrepancy between β and α even at room temperature for PTB7:PC₇₁BM in contrast to P3HT:PC₆₁BM.

In both material systems the charge carrier density dependence of the mobility alone cannot explain the recombination order being higher than two and a trap limited recombination mechanism has to be taken into account.

Generally, the temperature dependence of the charge carrier concentration dependent mobility (i.e., α) is experimentally not well investigated. Tanase *et al.* [107] showed charge carrier dependent mobility data of P3HT diodes and field effect transistors (FET). In the regime of low charge carrier densities ($1 \times 10^{21} - 4 \times 10^{22} \text{ m}^{-3}$) occurring in solar cells under standard light intensities, they observed almost no $\mu(n)$ dependence by determining the mobility in the space charge limited regime. The data from the FET measurements at higher charge carrier densities ranging from $2 \times 10^{24} - 3.5 \times 10^{25} \text{ m}^{-3}$ showed a clear $\mu(n)$ dependence. Overall they proposed $\mu \propto n^{(E_0/(k_B T)) - 1}$. This implies an increasing α with decreasing temperature, which is in good agreement with our measurements. The same trend for $\alpha(T)$ was predicted by Pasveer *et al.* from numerical simulations of the hopping transport in a master equation approach [83].

The temperature dependence of the difference between $\mu(n)$ (i.e., α) and $k(n)$ (i.e., β) reinforces the assumption, that at lower temperatures the influence of trapping on recombination becomes more pronounced. Under these conditions the release of a trapped charge carrier into a transport state is less probable than at room temperature, as the emission is thermally activated

5. Charge Density Dependent Nongeminate Recombination in Organic Bulk Heterojunction Solar Cells

by a Boltzmann factor. The existence of a broad distribution of traps in P3HT:PC₆₁BM ranging from 20 to 400 meV was confirmed by thermally stimulated current (TSC) technique with the distribution maximum at 105 meV [92].

Considering the contributions to the recombination rate discussed in section 5.3 in the context of Eq. (5.9), three contributions can be separated, two of them are directly apparent:

1. The recombination of mobile charge carriers, $n_c p_c$, corresponds to the classical Langevin picture, with the difference that not all charge carriers participate. Depending on the dynamics of trapping and emission, the order of recombination in view of the *overall* charge carrier concentration n can exceed the value of two. An additional contribution to the charge carrier concentration dependence is due to the recombination prefactor, i.e., the mobility $\mu(n)$, as described e.g. by Nelson [79].
2. The recombination of mobile charge carriers with trapped ones, $n_c p_t$ and $p_c n_t$. The prefactor is proportional to the mobility of the free charge carriers [52], leading again to a recombination rate in accordance with Langevin theory. Alternatively, this contribution can be described by SRH, although the charge carrier concentration dependence of the mobility does not automatically follow from the trap population—in contrast to MTR. Accordingly, more fit parameters are required for SRH.
3. Contributions to recombination of free with free and free with trapped charge carriers, as described in the previous two scenarios, considering (partial) phase separation. Experimentally, phase separation has been reported at least for P3HT:PC₆₁BM, see e.g. Ref. [2]. Charge carriers trapped within their respective material phase cannot be reached by their oppositely charged recombination partners residing in the other material. Only upon thermal activation of the trapped charge carriers from the deep states they are able to recombine at the heterointerface. This third contribution therefore increases the first one, $n_c p_c$, combined with a reduced second contribution due to the phase separation. Consequently, the recombination rate is decreased due to the slow emission process, leading to high orders of decay.

It has to be pointed out that for P3HT:PC₆₁BM the impact of trapping is more pronounced for lower temperatures due to a higher effective disorder, i.e. a much slower emission rate from traps, directly influencing the third contribution. Similarly, in P3HT:bisPC₆₁BM films a significantly slower decay of the polaron signal than for P3HT:PC₆₁BM was found by transient absorption measurements [34]. This corresponds to a higher apparent recombination order and is consistent with bisPC₆₁BM exhibiting more and deeper traps than PC₆₁BM, as observed by TSC [93].

The importance of the phase separation gets also apparent, when using Eq. (5.6) and (5.7) to calculate the recombination order after Eq. (5.9) in the case of $\mu_n = \mu_p$ and $n = p$, which is a valid assumption for describing both material systems because of the high solar cell FF . In this approach no phase separation is integrated, which indeed results in recombination orders higher than two, but in this case the apparent recombination orders can be completely explained by the n dependence of the mobility. These calculation supports the assumption that the discrepancy between α and β is a result of DA phase separation. Nevertheless, the calculation can be used to get an impression of the dependencies of the recombination order on the depth of the traps, which is implicitly included in the parameter E_0 or the number of trap states N_t . Fig. 5.6(a)

displays clearly that with deeper traps (higher E_0), the recombination order strongly increases to values much higher than two. Increasing the number of trap states without changing the overall shape of the exponential DOS does not lead to an increase of the apparent recombination order but only to a reduction of the overall recombination rate which is shown in Fig. 5.6(b).

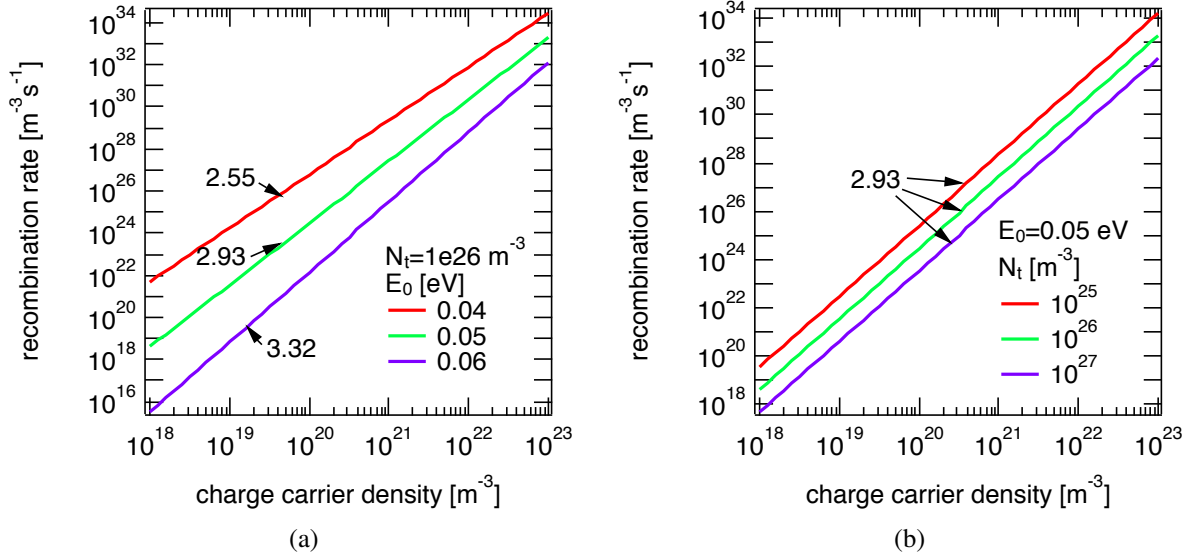


Figure 5.6.: The calculated Langevin recombination rate in dependence of the charge carrier density using the $\mu(n)$ dependence after Eq. (5.7) with varying E_0 (a) and N_t (b). Both show recombination orders higher than two (numbers according to the lines). The deviation from the recombination order of two increases with increasing E_0

From the given experimental results as well as the theoretical calculations, it is clear that trap states have a strong impact on the apparent recombination order, in terms of the charge carrier mobility and the populations of charge carriers which are available for recombination. The impact on the device performance needs to be considered accordingly.

5.5. Conclusion

In this section the charge carrier dependence of the mobility μ and the recombination prefactor k were determined for various temperatures by independent experimental techniques. For P3HT:PC₆₁BM solar cells at 300 K, the mobility showed nearly the same dependence as k on the charge carrier density in accordance with literature [98]. At lower temperatures the discrepancy between the $\mu(n)$ and $k(n)$ increased. Investigations of a highly performing PTB7:PC₇₁BM solar cell showed the discrepancy between $\mu(n)$ and $k(n)$ dependency already at room temperature. These findings substantiate the proposition that not only the impact of trapping on the recombination prefactor proportional to the charge carrier mobility is responsible for increasing the order of charge carrier decay beyond the value of two expected for bimolecular recombination. Instead, for systems with (partial) phase separation, trapped charge carriers can be protected from recombination. Only after their thermally activated release from the deep states they are able to contribute to the recombination rate, leading to an additional increase of the

5. Charge Density Dependent Nongeminate Recombination in Organic Bulk Heterojunction Solar Cells

recombination order. This scenario implies that in PTB7:PC₇₁BM the influence of trapping in combination with phase separation is more significant than in P3HT:PC₆₁BM, lowering the charge carrier recombination rate. Therefore, the apparent recombination orders higher than two should be an inherent property of disordered organic semiconductor blends.

6. Influence of Trap States on the Open Circuit Voltage and the Recombination Dynamics in Organic Solar Cells

In this section the influence of trap states within the band gap of the active material will be discussed, where the main focus is on their influence on the solar cell parameters — especially V_{oc} — and the recombination dynamics of photogenerated charge carriers. The first and easiest possibility to introduce trap states into organic solar cells is to expose them to oxygen. The results of this study are shown in section 6.1. Another possibility is to add a second acceptor material (guest molecule) to the DA blend (host molecules). When the LUMO level of the guest molecule is significantly lower than that of the host molecule, the LUMO levels of the guest molecule act as electron trap states. In the here presented study (section 6.2), TCNQ¹ as guest molecule was used in a P3HT:PC₆₁BM blend system.

6.1. Influence of Oxygen Exposure on the Open Circuit Voltage and Recombination Dynamics in P3HT:PC₆₁BM

6.1.1. Introduction

Beside the efficiency and the costs of organic solar cells, the lifetime of these devices is crucial before they can make their way in the mass market, away from just being a niche product. Therefore, degradation measurements are important to identify the mechanisms leading to the decrease of efficiency with time. Many publications concerning the lifetime of solar cells were presented, where the measurements were performed in a variety of different conditions that are crucial for their degradation behavior: encapsulated or not, in dark or under illumination, under nitrogen, ambient or synthetic air. In this subsection the influence of synthetic air (80 % N₂, 20 % O₂, < 1 ppm H₂O) in dark and under illumination is investigated. Thereby, the main focus is set on the open circuit voltage, also the light intensity dependence of V_{oc} , as well as the recombination dynamics of charge carriers.

6.1.2. Experimental

The investigated solar cell was prepared as described in section 3.2. The 190 nm thick active layer consisted of P3HT:PC₆₁BM blend using a weight ratio of 1:0.8. As cathode a Ca (3 nm)/Al (90 nm) electrode was used, the active area of the complete solar cell was 9.32 mm². After IV-characterization under AM1.5g simulated illumination the solar cell was

¹7,7,8,8-Tetracyanoquinodimethane

6. Influence of Trap States on the Open Circuit Voltage and the Recombination Dynamics in Organic Solar Cells

directly transferred to the cryostat, where the degradation measurements were performed. During the transfer, the solar cell was exposed to ambient air for a few minutes. During the measurements the solar cell was stored in He atmosphere, during the degradation steps the cryostat was filled with synthetic air. The calibration of the illumination level was performed as described in section 3.1. At every degradation step the light intensity was varied from 0.001 to 3.98 suns and at every single illumination level an IV-curve as well as a charge extraction measurement to deduce the charge carrier density under open circuit conditions was performed. Additionally, a V_{oc} transient was recorded for an initial illumination level of 1.58 suns. The measurement cycle was performed before starting the degradation, and after 1, 3, 10 and 30 h in dark. Afterwards, the degradation under 1 sun illumination on the same solar cell was started and was characterized again after 1, 3, 10 and 30 h.

6.1.3. Results and Discussion

The solar cell used for the degradation study exhibited photovoltaic performance like P3HT:PC₆₁BM solar cells described in literature or chapter 5, e.g. $V_{oc} = 0.57$ V, $j_{sc} = 8.2$ mA/cm², $FF = 69$ % leading to $\eta = 3.2$ % under AM1.5g illumination using a solar simulator. The IV-curves measured under 1 sun LED illumination for every degradation step are depicted in Fig. 6.1(a).

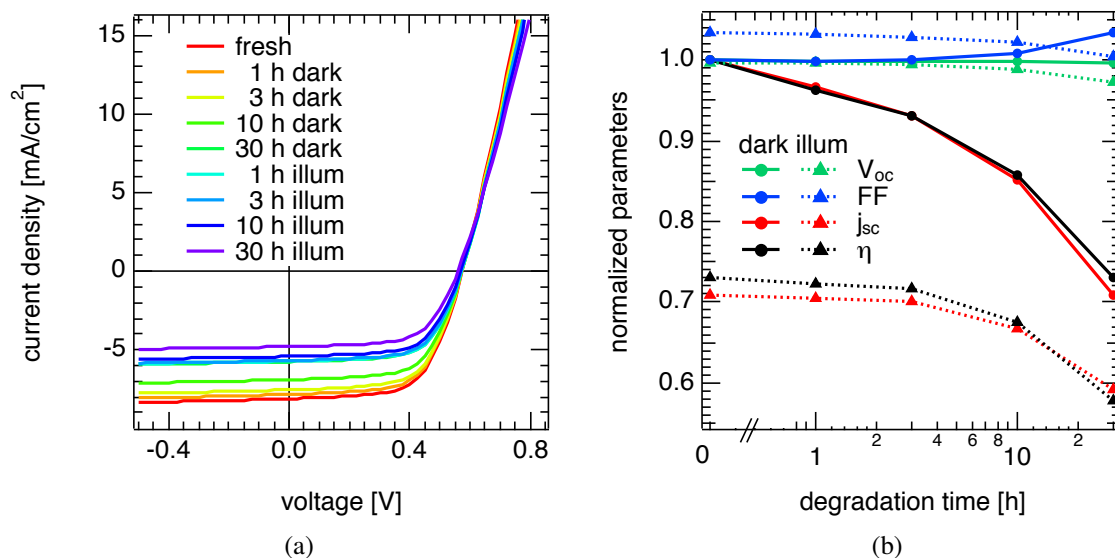


Figure 6.1.: IV-curves of P3HT:PC₆₁BM under 1 sun illumination (a) and the respective parameters V_{oc} , j_{sc} , FF and η normalized to the initial values (b) extracted from these curves for different degradation steps.

The normalized respective parameters extracted from the curves are shown in Fig. 6.1(b). They show similar behavior to the already published data by Schafferhans *et al.* [92]. In the dark only the short circuit current drops to 71 % of the initial value after 30 h, whereas the open circuit voltage remains unaffected and the fill factor even increases slightly (103 % of the initial value after 30 h). This was explained by doping of the active material and confirmed by macroscopic simulations. For the degradation under illumination the behavior differs a bit from

[92], where V_{oc} , j_{sc} and FF dropped all by 10 % after 3h of degradation under illumination whereas in this study all parameters dropped at a much slower rate: j_{sc} from 71 % to 59 %, FF from 103 % to 100 % and V_{oc} from 100 % to 97 % of the initial value after additional 30 h under illumination.

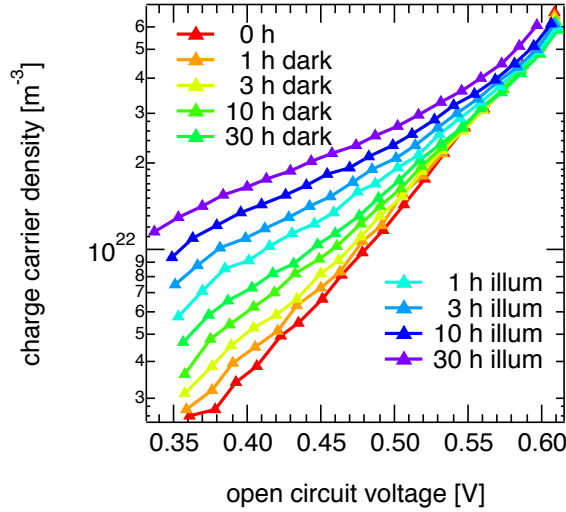


Figure 6.2.: The charge carrier density under open circuit conditions of P3HT:PC₆₁BM as obtained from charge extraction measurements for the different degradation steps.

The results of the charge extraction measurements to obtain the charge carrier density n under open circuit conditions is illustrated in Fig. 6.2. For the not degraded solar cell, n shows the typical exponential dependence on V_{oc} ($n = n_0 \exp(c_n V_{oc})$, where c_n is a proportionality factor). With increasing degradation time n_0 increases and c_n decreases, their values are summarized in table 6.1. Since for higher V_{oc} values at longer degradation times the slope $c_n = d \ln(n) / dV_{oc}$ is not constant but a bending appears in the $\ln(n)(V_{oc})$ curve, the fits for the calculation of n_0 and c_n were performed in the linear range of the logarithmic plot, namely for the values obtained for light intensities from 0.001 to 0.63 suns. For the calculation of n as described in section 3.1 the capacitance of the fresh solar cell was used for all degradation steps, since it is very unrealistic that the geometric capacitance changes from 2.20 nF to 6.62 nF (see also table 6.1).

Fig. 6.3 shows the decay of the open circuit voltage after switching of the light with an illumination level of 1.58 suns. It can clearly be seen that in the time range of $\sim 10^{-6}$ s to 5×10^{-4} s the decay is similar for all degradation steps, whereas for longer times the decay is slower for the more degraded solar cells. It has to be noted, that the open circuit voltage at 5×10^{-4} s of around 0.36 V is the same as V_{oc} achieved in steady-state IV-measurement using 0.001 suns background illumination.

To ensure that the measured voltage is correct one has to keep in mind that in this case, the solar cell at open circuit conditions (which acts here as voltage source) must have a low resistance in comparison to the input resistance of the oscilloscope, which is 1.5 G Ω in this case. To prove if this prerequisite is fulfilled over the whole time range the resistance at V_{oc} ($R_{V_{oc}}$) was first calculated for every IV-curve measured. Therefore, the IV-curve was fitted around V_{oc} using three measurement points below and above V_{oc} with a 4th order polynomial function and taking the inverse of the slope of this fit at V_{oc} as resistance. Fig. 6.4(a) depicts

6. Influence of Trap States on the Open Circuit Voltage and the Recombination Dynamics in Organic Solar Cells

degradation time	c_n	n_0 [m^{-3}]	C [nF]	R_p [$k\Omega$]
0 h	12.9	2.1×10^{19}	2.20	637
1 h dark	12.2	3.3×10^{19}	2.26	675
3 h dark	11.2	5.5×10^{19}	2.29	722
10 h dark	10.2	9.8×10^{19}	2.39	805
30 h dark	9.0	1.9×10^{20}	2.57	952
1 h illum	7.9	3.7×10^{20}	3.18	485
3 h illum	6.9	6.8×10^{20}	3.92	448
10 h illum	6.0	1.2×10^{21}	5.02	394
30 h illum	5.1	2.1×10^{21}	6.62	384

Table 6.1.: The slope c_n of the semilogarithmic plot $\ln(n)$ vs V_{oc} as well as n_0 as obtained from Fig 6.2 using the expression $n = n_0 \exp(c_n V_{oc})$ for all degradation steps. The fits were performed in the linear range of $\ln(n)$ vs V_{oc} where the light intensity was varied from 0.001–0.63 suns. C is the measured capacitance as described in section 3.1 by charge extraction measurements in the dark for small bias voltages in reverse direction. R_p is the parallel resistance obtained from the respective dark IV-curves.

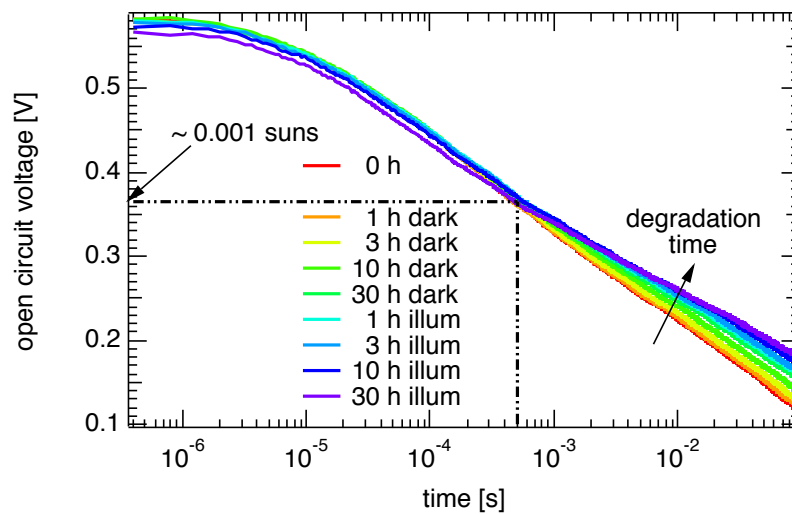


Figure 6.3.: Time evolution of the open circuit voltage for every degradation step after switching off the background light ($P_L=1.58$ suns). In the time range up to 5×10^{-4} s (dash-dotted line) the decay is similar for all degradation steps, whereas for longer times the decay is slower for the more degraded solar cells. At 5×10^{-4} s V_{oc} is around 0.36 V, which is the same as V_{oc} achieved in steady-state IV-measurement using 0.001 suns background illumination.

that this procedure works well for IV-curves under low light intensities (0.001 suns) as well as under higher illumination levels (1 sun). Since the open circuit voltage from the illuminated IV-curves only reached 0.35 V for the lowest measured light intensity of 0.001 sun, whereas in the V_{oc} transients values down to 0.12 V were measured in the detected time scale, one can not say for sure if $R_{V_{oc}}$ at these voltages is low enough for a correct measurement in basis of this data. To substantiate the assumption of a correct $V_{oc}(t)$ measurement $R_{V_{oc}}$ was plotted semilogarithmic against V_{oc} (Fig. 6.4(b)), where an exponential behavior $R_{V_{oc}} \propto \exp(V_{oc})$ can be observed in the range of lower V_{oc} . However, without the justification of any physical theory, since to best of my knowledge no theory concerning $R_{V_{oc}}$ in organic BHJ solar cells exists,¹ one can extrapolate the exponential behavior to even lower V_{oc} values, which is marked in Fig. 6.4(b) as "guide to the eye". With the assumptions that the extrapolation is valid and the oscilloscope measures V_{oc} with only negligible errors as long as $R_{V_{oc}}$ is lower than 1 % of the input resistance of the oscilloscope, which is marked as line in Fig. 6.4(b), the lower limit for the V_{oc} transient is ~ 0.18 V. Since in the V_{oc} transient, as already mentioned above, the lowest V_{oc} value is 0.12 V, at least the lowest V_{oc} have to be treated with special care².

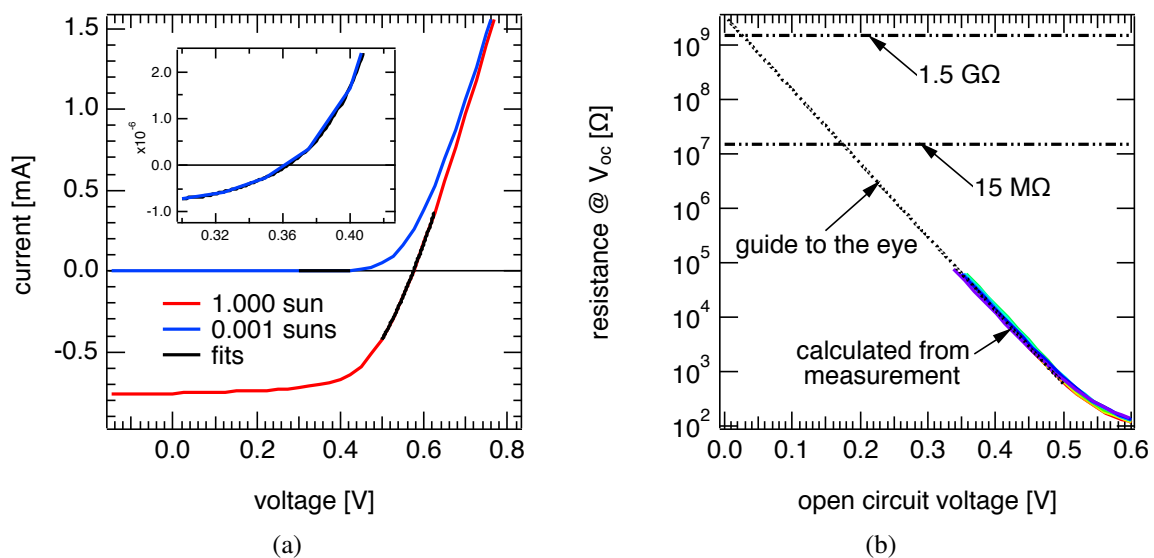


Figure 6.4.: Illuminated IV-curves ($P_L=0.001$ suns and $P_L=1$ sun) with the respective fits using a 4th order polynomial function to obtain the resistance at open circuit conditions $R_{V_{oc}}$ (a). Variation of $R_{V_{oc}}$ in dependence of the open circuit voltage for all degradation steps. By extrapolating the exponential part of the curve to lower V_{oc} values it is possible to estimate the limits of the $V_{oc}(t)$, that is when the resistance at V_{oc} is not negligibly small compared to the input resistance of the used oscilloscope (1.5 G Ω) (b).

¹In the case of organic bilayer cells Cheyins *et al.* [20] gave an analytical expression for $R_{V_{oc}}$. It can be assumed, that a similar approach can lead to a theoretical description for $R_{V_{oc}}$ in organic BHJ solar cells.

²For an identical fabricated P3HT:PC₆₁BM solar cell IV-measurements were performed with illumination intensities down to 10^{-6} suns in a different setup. Evaluation of $R_{V_{oc}}$ showed that in this device at 10^{-6} suns, which resulted in a V_{oc} of around 0.23 V, $R_{V_{oc}}$ was low enough that V_{oc} could be correctly measured with the 1.5 G Ω input resistance of the oscilloscope.

6. Influence of Trap States on the Open Circuit Voltage and the Recombination Dynamics in Organic Solar Cells

Together with the $n(V_{oc})$ data as shown in Fig.6.2 it is possible to calculate a $n(t)$ dependence to investigate the change of the recombination order with degradation time. Therefore, to reduce the amount of data points, corresponding V_{oc} and t data pairs were created in steps of 1 mV over the whole voltage range of the transients by interpolation of the raw data. The corresponding n values were obtained by $n = n_0 \exp(c_n V_{oc})$ using the fit parameters given in table 6.1. The results are shown in Fig. 6.5 for every degradation step.

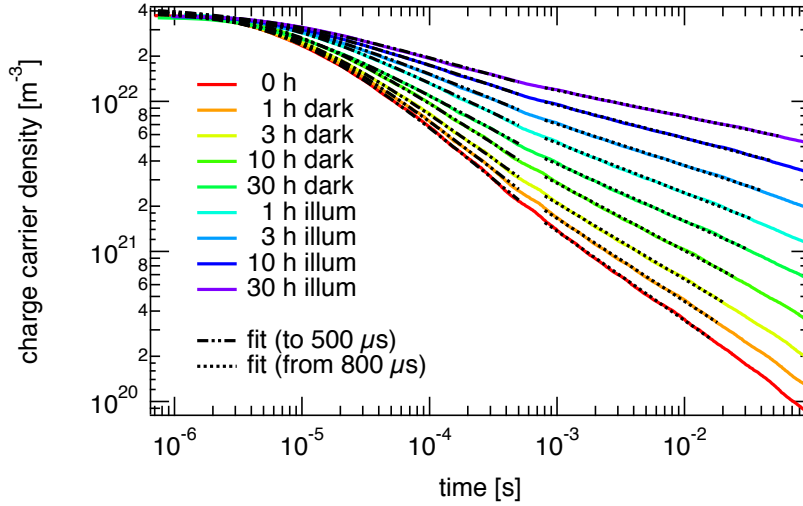


Figure 6.5.: Time evolution of the charge carrier density under open circuit conditions after switching the illumination off for all degradation levels. The data were obtained by a combination of $V_{oc}(t)$ (Fig. 6.3) and $n(V_{oc})$ (Fig. 6.2). The dash-dotted lines indicate the fits to Eq. (6.1) for times up to $500 \mu\text{s}$ to obtain the recombination order $\lambda + 1$. The dotted lines show linear fits in the double logarithmic plot starting from $800 \mu\text{s}$, used to calculate $\lambda_l + 1$.

With degradation time, the decay of the charge carrier density is slowed down, which indicates a change in the dominating recombination mechanisms. The recombination order $\lambda + 1$ can be obtained by fitting the $n(t)$ curve using

$$n(t) = \left(n_{t=0}^{-\lambda} + k_{\lambda} \lambda t \right)^{-1/\lambda}, \quad (6.1)$$

which directly follows from the integration of $dn/dt = k_{\lambda} n^{\lambda+1}$. Here $n_{t=0}$ is the charge carrier density at $t = 0$. However, because of the two different regimes in the $n(t)$ behavior, the fits using Eq. (6.1) were only performed in the time range up to $500 \mu\text{s}$, indicated in Fig. 6.5 as dash-dotted lines. The fit parameters $n_{t=0}$, k_{λ} and the recombination order $\lambda + 1$ are summarized in table 6.2. In the second regime at longer times, where the decay is slower, the recombination order, in this case called $\lambda_l + 1$, was determined using the negative inverse of the slope of the linear fit of $\ln(n)$ vs $\ln(t)$.

The observation of two different time regimes of recombination can be explained as follows: At first mainly two types of charge carriers recombine: free charge carriers of opposite sign with each other (Langevin) and/or a free charge carrier with a second one just emitted from a shallow trap (delayed Langevin). Deeper trapped charge carriers do not significantly contribute

6.1. Influence of Oxygen Exposure on the Open Circuit Voltage and Recombination Dynamics in P3HT:PC₆₁BM

degradation time	$\lambda + 1$	$n_{t=0}$ [m ⁻³]	k_λ	$\lambda_l + 1$	$\lambda_G + 1$
0h	2.40	4.18×10^{22}	1.94×10^{-27}	2.68	2.40
1h dark	2.50	4.13×10^{22}	1.25×10^{-29}	2.81	2.50
3h dark	2.63	4.11×10^{22}	1.38×10^{-32}	2.97	2.69
10h dark	2.80	4.23×10^{22}	1.16×10^{-36}	3.22	2.92
30h dark	3.12	3.98×10^{22}	7.08×10^{-44}	3.63	3.23
1h illum	3.41	4.18×10^{22}	1.97×10^{-50}	4.01	3.64
3h illum	3.81	4.03×10^{22}	1.09×10^{-60}	4.63	4.17
10h illum	4.51	3.96×10^{22}	2.59×10^{-75}	5.54	4.80
30h illum	5.19	4.00×10^{22}	1.13×10^{-90}	6.73	5.89

Table 6.2.: The recombination orders for all different degradation times as obtained from the fitted (Eq. (6.1)) $n(t)$ data (Fig. 6.5) up to 500 μ s together with the two other fit parameters n_0 and k_λ . $\lambda_l + 1$ is the recombination order extracted also from $n(t)$ but at longer times ($>800 \mu$ s), whereas $\lambda_G + 1$ was derived by calculating the generation rate under illumination as described in chapter 5.

to the recombination process in this time regime. The delayed recombination mechanism is the reason for the apparent recombination orders higher than two as already discussed in chapter 5. The ratio between trapped and free charge carriers increases and the apparent recombination order $\lambda + 1$ is further raised with increasing time. Additionally charges are emitted from deeper trap states causing a longer delay of the recombination, which leads to higher apparent recombination orders in the second time regime at longer times. The appearance of two different time regimes was recently shown in high sensitive charge extraction measurements under short circuit conditions [101]. In PBDTTPD¹:PC₆₁BM devices, a material system exhibiting deep trap states, both regimes were obtained, where the first was attributed to charge carriers in mobile states and/or shallow traps and the second to charge carriers in deep traps. In P3HT:PC₆₁BM devices the second regime was not visible, which is in accordance to the interpretation of the $n(t)$ transient of the not degraded solar cell, where the difference between $\lambda + 1 = 2.40$ and $\lambda_l + 1 = 2.68$ is very small and no second regime is visible.

With increasing degradation time in the dark, the recombination order increases only to $\lambda+1=3.12$ and $\lambda_l + 1 = 3.63$ after 30 h of degradation. This is only a small change indicating that the incorporation of additional traps is negligible which was experimentally proven by thermally stimulated currents (TSC), where the lower limit of the density of trapped charges increased only a bit [92]. Since the increase of $\lambda_l + 1$ ($\Delta(\lambda_l + 1)=0.95$ from 0 h to 30 h dark degradation) was stronger than for $\lambda + 1$ ($\Delta(\lambda + 1)=0.72$), one can conclude that proportionally more deeper trap states are introduced than shallow ones. This is again in accordance with TSC measurements where an increase of the density of deeper trap states was detected [92].

In the case of light induced degradation the recombination rate increases stronger on shorter time scale. After 3 h of illumination in synthetic air, $\lambda + 1$ increased further to 3.81, which is a similar increase (0.69) as the in the dark degradation case in the tenfold time. After 30 h $\lambda + 1$ even shows values of 5.19. Additionally, in the longer time range recombination orders up to

¹poly(di(2-ethylhexyloxy)benzo[1,2-b:4,5-b']dithiophene-co-octylthieno[3,4-c]pyrrole-4,6-dione)

6. Influence of Trap States on the Open Circuit Voltage and the Recombination Dynamics in Organic Solar Cells

6.73 are reached.

To substantiate the recombination order data obtained from the open circuit voltage transients, $\lambda + 1$ was additionally evaluated using the approach presented in chapter 5. Here again, the generation rate G was determined by the photocurrent at $V = -3.5$ V for every illumination level, which was assumed to be saturated at this negative bias. The slope of $\ln(G)$ vs. $\ln(n)$ is equal to the recombination order and was determined for the data obtained from illumination levels ranging from 0.001 to 0.63 suns. The values are summarized in table 6.2, where they are named $\lambda_G + 1$, to distinguish them from the two other recombination order values obtained from the transient V_{oc} approach. For the not degraded solar cell $\lambda_G + 1$ equals the values of $\lambda + 1$. With increasing degradation, when the influence of deep traps gets more pronounced resulting in an increasing difference between $\lambda + 1$ and $\lambda_l + 1$, $\lambda_G + 1$ is always between both recombination order values but slightly closer to $\lambda + 1$. The reason therefore is, that $\lambda_G + 1$ was calculated for illumination levels down to 0.001 suns, the same range which was evaluated in the $n(t)$ plot for the calculation of $\lambda + 1$.

A more qualitative approach to investigate the dominating recombination process is the evaluation of light intensity dependent V_{oc} data. The origin of this method is again the Shockley equation for pn-junctions as described in section 2.2.3. If the parallel resistance R_p is satisfyingly high and the serial resistance low — which is the case for this device — one can use the expression for V_{oc} derived from the ideal Shockley equation (see Eq. (2.13)) with making only a negligible error. The derivation of V_{oc} with respect to the logarithm of the photocurrent $\ln(j_{ph})$ is then given by

$$\frac{dV_{oc}}{d\ln(j_{ph})} = n_{id} \frac{k_B T}{q} \quad (6.2)$$

In inorganic semiconductors, pure band-to-band (Langevin) recombination results in an ideality factor n_{id} of one, whereas for pure trap-assisted recombination (SRH recombination) n_{id} is two. A combination of both recombination types results in n_{id} between one and two. In many articles, and also in this thesis, not V_{oc} vs. $\ln(j_{ph})$ is evaluated but V_{oc} vs. $\ln(P_L)$. In an ideal system with $I_{ph} \propto P_L^\kappa$ with $\kappa = 1$, both methods are equal, however, in the here measured solar cell κ is in the range of 0.95 for all degradation steps.

The light intensity dependent V_{oc} data for every degradation step are shown in Fig. 6.6. The fits for the extraction of n_{id} were performed in the range from 0.001 to 1.58 suns. As expected, n_{id} increases continuously with degradation time, the values are displayed in Fig. 6.7. In the case of the not degraded solar cell $n_{id} = 1.18$ increases to $n_{id} = 1.20$ after 30 h of dark degradation and $n_{id} = 1.23$ after additional 30 h degradation under illumination. This shows that the influence of recombination via trap states in comparison to Langevin recombination gets more pronounced with degradation time. This is accompanied by an increase of trap states at the DA interfaces, as recombination via trap states can only occur at the interface or at least in the vicinity of the interface as it is schematically sketched in Fig. 5.1. Charge carriers captured in trap states inside their specific phases, with a too large distance to DA interfaces and thus their recombination partners, do not increase trap assisted recombination but can only delay the recombination dynamics. This is due to the strong localization of the wave functions of both recombination partners, giving a negligible wave function overlap and therefore a not existing probability for tunneling of the trapped charge carrier directly to the partner, as can be seen by the Miller–Abrahams hopping rate (Eq. (2.2)).

The last point of this section is the question, why the open circuit voltage, as already men-

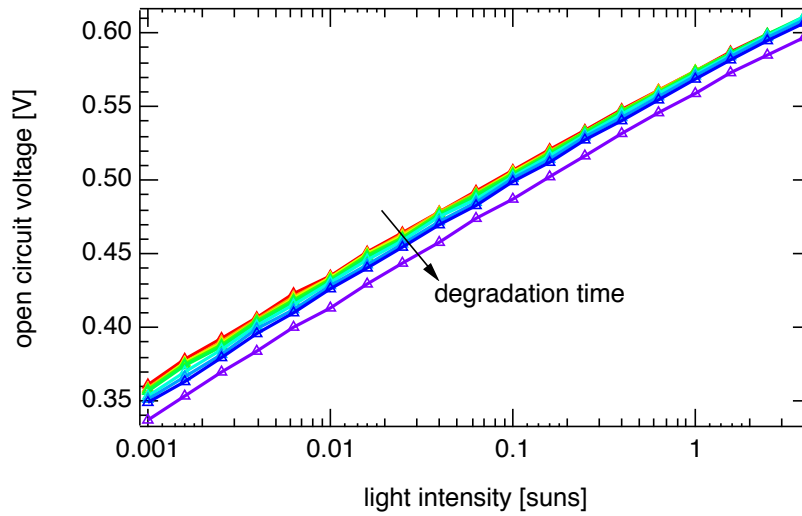


Figure 6.6.: Light intensity dependence of the open circuit voltage for all degradation steps.

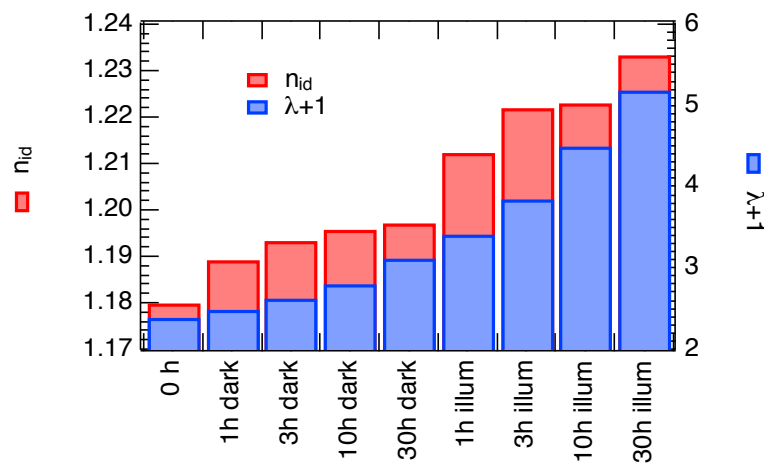


Figure 6.7.: Change of n_{id} with degradation time in comparison with the recombination order $\lambda + 1$. The increase of both parameters indicates the formation of trap states by oxygen induced degradation.

6. Influence of Trap States on the Open Circuit Voltage and the Recombination Dynamics in Organic Solar Cells

tioned above, is stable against oxygen degradation in the dark and decreases under simultaneous oxygen and light exposure. The most probable reasons therefor, that are discussed in literature are: a change in the effective band gap or a change of the metal work function due to oxidation of the contact [39]. The change of the charge carrier density stored in the device under open circuit conditions can be excluded to be the reason for the V_{oc} decrease as n at 1 sun is nearly constant for every degradation step and at 0.001 suns the charge carrier density even increases from $2.6 \times 10^{21} \text{ m}^{-3}$ for the not degraded cell by a factor of 4.6 to $1.2 \times 10^{22} \text{ m}^{-3}$ after 30 h of dark and illuminated oxygen degradation. For a constant E_g and N_c , when applying Eq. (2.18), the open circuit voltage should increase with an increasing charge carrier density, while in the performed investigations V_{oc} decreased at the same time from 0.36 to 0.34 V at 0.001 suns.

To distinguish, if a degradation of the metal electrode or the active layer is responsible for the V_{oc} decrease under illumination, temperature dependent measurements of V_{oc} for different illumination levels were performed on another solar cell, for the not degraded solar cell as well as after 39 h of synthetic air exposure under simultaneous illumination ($P_L = 1$ sun). The results for $P_L=1$ and 0.01 suns is shown in Fig. 6.8(a). The solar cell was prepared the same way as the above discussed one, except for the ITO, which was treated with an oxygen plasma before spin coating the PEDOT:PSS on top of it. Nevertheless, the solar cell parameters were similar to the solar cell without plasma treatment. Despite the saturation regime of V_{oc} is not completely reached for the investigated temperature range from 300 to 50 K, the measurements are important and useful since the focus of the further discussion is set on the temperature dependent difference ΔV_{oc} between the not degraded and degraded solar cell, which is displayed in Fig. 6.8(b). At 300 K, ΔV_{oc} is 49 mV for $P_L=1$ sun illumination and decreases to 41 mV at 250 K and increases again to 69 mV at 50 K. The same trend can be observed at 0.01 suns illumination level with only slightly different values. This result can be explained by at least

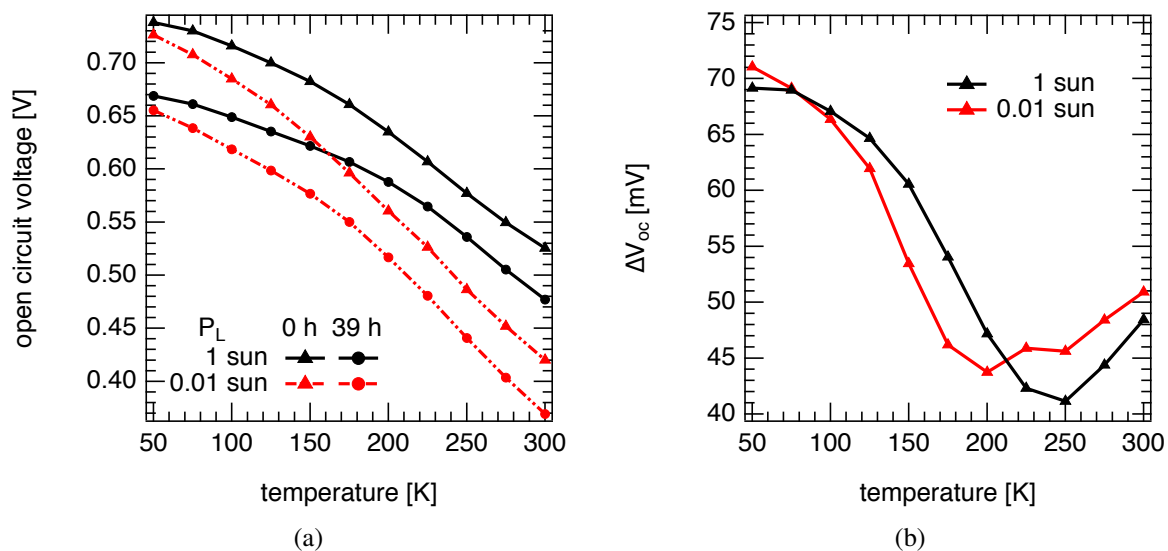


Figure 6.8.: The temperature dependence of the open circuit voltage for not degraded (0 h) and 39 h oxygen (plus simultaneous illumination) degraded P3HT:PC₆₁BM solar cells under 1 and 0.01 suns illumination (a). The difference between V_{oc} of the degraded and not degraded solar cells for the respective illumination levels (b).

two different mechanisms influencing the open circuit voltage, one that increases and one that decreases V_{oc} , both with different temperature dependencies.

In the following a possible explanation is presented, where only a degradation of the active layer has to be taken into account, whereas the electrode is not influenced by the oxygen degradation. For a better understanding Fig. 6.9 shows on the left side schematically the Gaussian DOS of the HOMO level of the donor in the not degraded case, illustrated by the small number of intrinsic trap states. The effective band $E_{g,eff,nd}$ gap is given by the difference of the transport energies of the LUMO ($E_{tr,LUMO}$) and the HOMO ($E_{tr,nd}$). The effective energy barrier between HOMO and the metal work function is Φ_{nd} . After degradation, the disorder σ_d in the HOMO level increases because of an increase of trap states, leading to a different transport energy $E_{tr,d}$, which finally results in a decrease of the effective band gap $E_{g,eff,d}$ as well as the effective energy barrier Φ_d . For the sake of simplicity $E_{tr,LUMO}$ was assumed to be not influenced by degradation. Since at higher temperatures the influence of the energy barrier in P3HT:PC₆₁BM is almost negligible as shown in chapter 4 the effect of the reduction of the effective band gap is dominant which leads to the decrease of ΔV_{oc} . Reaching even lower temperatures, the effect of the effective energy barrier gets more important, which then leads to the increase of ΔV_{oc} . Whether or not this mechanism alone can explain completely the experimental behavior is not clarified. Maybe, with the aid of macroscopic simulations, the suggested theory can be confirmed. Additionally, a change of dipoles at the interface between active layer and contact, as it was mentioned shortly in chapter 4 has to be taken into account, to completely resolve the question what exactly leads to the change of V_{oc} after oxygen degradation under simultaneous illumination.

6. Influence of Trap States on the Open Circuit Voltage and the Recombination Dynamics in Organic Solar Cells

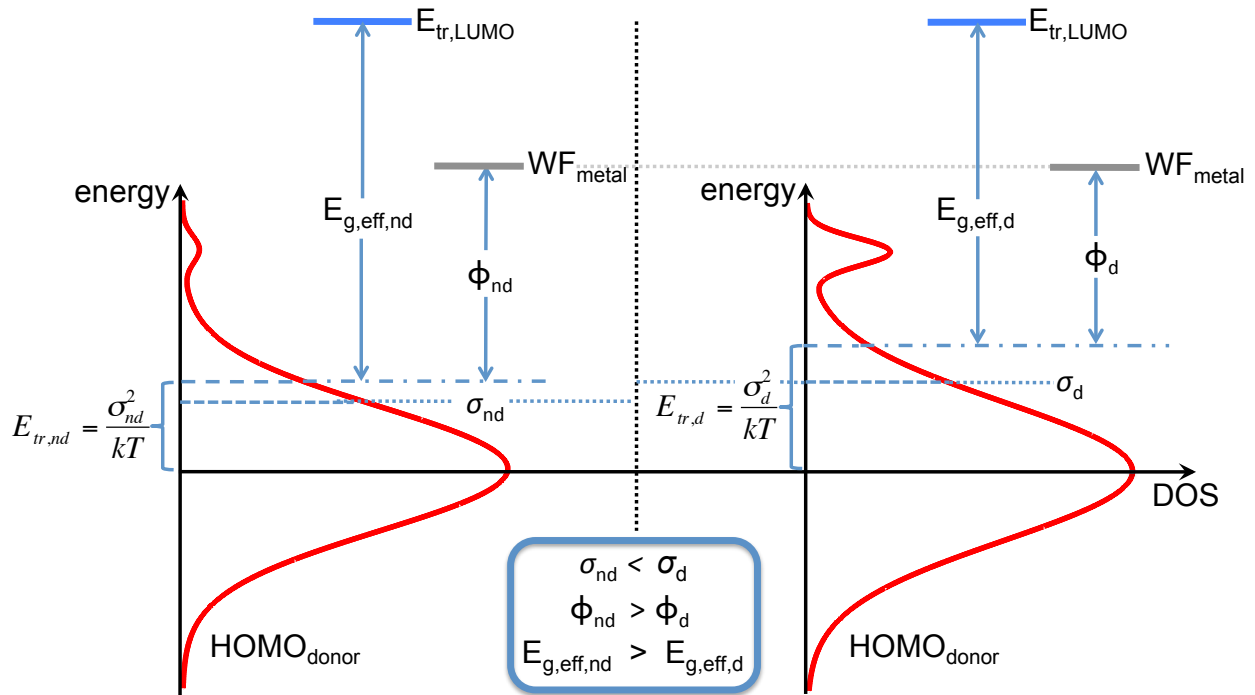


Figure 6.9.: Scheme to depict the possible mechanism explaining the V_{oc} behavior after degradation. Therefore, the Gaussian DOS of the HOMO level in a not degraded cell (left side, index nd) is compared with a degraded cell (right side, index d). The degradation is illustrated by the increased number of trap states on the right side, leading to an increase of the disorder ($\sigma_{nd} < \sigma_d$) and a shift of the transport energy E_{tr} in the HOMO level. This has a direct impact on the effective band gap as well as the effective energy barrier, which both influence the open circuit voltage.

6.2. Influence of Extrinsic Trap States on the Performance of Organic Solar Cells

6.2.1. Introduction

The second possibility to introduce trap states into the blend system is to add a second acceptor molecule with a significantly lower lying LUMO level. The influence of extrinsic traps on the solar cell performance was already investigated in MDMO-PPV:PC₆₁BM using TCNQ as additional traps [71]. Here, the authors showed that n_{id} increases with the incorporation of TCNQ, indicating an increase of the influence of trap assisted recombination (SRH). A similar study was performed on PCDTBT:PC₆₁BM blends by adding PC₈₄BM, where also a shift of n_{id} to higher values for the PCDTBT:PC₆₁BM:PC₈₄BM was observed. Additionally, the recombination order was obtained by differential resistance analysis, that provided an evolution from bimolecular to trap assisted recombination by incorporation of additional traps [61].

In the presented work, the well known P3HT:PC₆₁BM blend system was used together with TCNQ as guest molecule. As the LUMO level of TCNQ (-4.5 eV) is significantly lower than of PC₆₁BM (-3.7 eV), TCNQ should act as an extrinsic electron trap [71]. The results will substantiate the statements of chapter 5 and section 6.1, where the apparent recombination order was attributed to trap states.

6.2.2. Experimental

The solar cells were prepared in principle as described in section 3.2, namely: a reference solar cell P3HT:PC₆₁BM = 1:0.8 without any TCNQ (PC₆₁BM:TCNQ=1:0), one with one weight percent (wt%) TCNQ with respect to the PC₆₁BM content (PC₆₁BM:TCNQ=0.99:0.01) and one with 5 wt% TCNQ (PC₆₁BM:TCNQ=0.95:0.05). TCNQ was dissolved in chlorobenzene (3 mg/ml) at 80°C. The active layer thicknesses were in the range of 230-260 nm. After a thermal annealing of the active layer of 10 min at 130°C the final Ca/Al electrode was thermally evaporated.

The charge extraction measurements were performed in the cryostate as described in section 3.1, the light intensity was varied from 0.001 to 2.51 suns. The open circuit voltage transient was recorded using an illumination level of 1 sun.

6.2.3. Results and Discussion

To check if the TCNQ molecules were successfully incorporated into the P3HT:PC₆₁BM matrix, AFM¹ measurements were performed to examine if TCNQ forms large crystals and therefore doesn't act as trap. In some regions of the substrates, crystals were visible on the film containing 5 wt% TCNQ, but not throughout the complete device. Fig. 6.10(d) displays the surface of such a spot over an area of 90 × 90 μm. In most regions of the substrate no such crystals were visible. The surface of the blend without (Fig. 6.10(a)) and with 1 wt% (Fig. 6.10(b)) TCNQ showed the same structure and roughness (RMS²=11-13 nm). The surface of the film containing 5 wt% TCNQ but no visible crystals (Fig. 6.10(c)) showed a much smaller RMS

¹Atomic Force Microscope, Veeco Dimension Icon, tapping mode

²root mean squared

6. Influence of Trap States on the Open Circuit Voltage and the Recombination Dynamics in Organic Solar Cells

roughness of 6 nm, which could be an indication that TCNQ disturbs the annealing process leading to a different morphology in the blend influencing in consequence the solar cell parameters. It was reported for P3HT:PC₆₁BM solar cells that annealing at 110 °C leads to an increased roughness of the active layer, an improved j_{sc} and FF , a decreased V_{oc} but overall higher efficiency in comparison to the untreated solar cell [62].

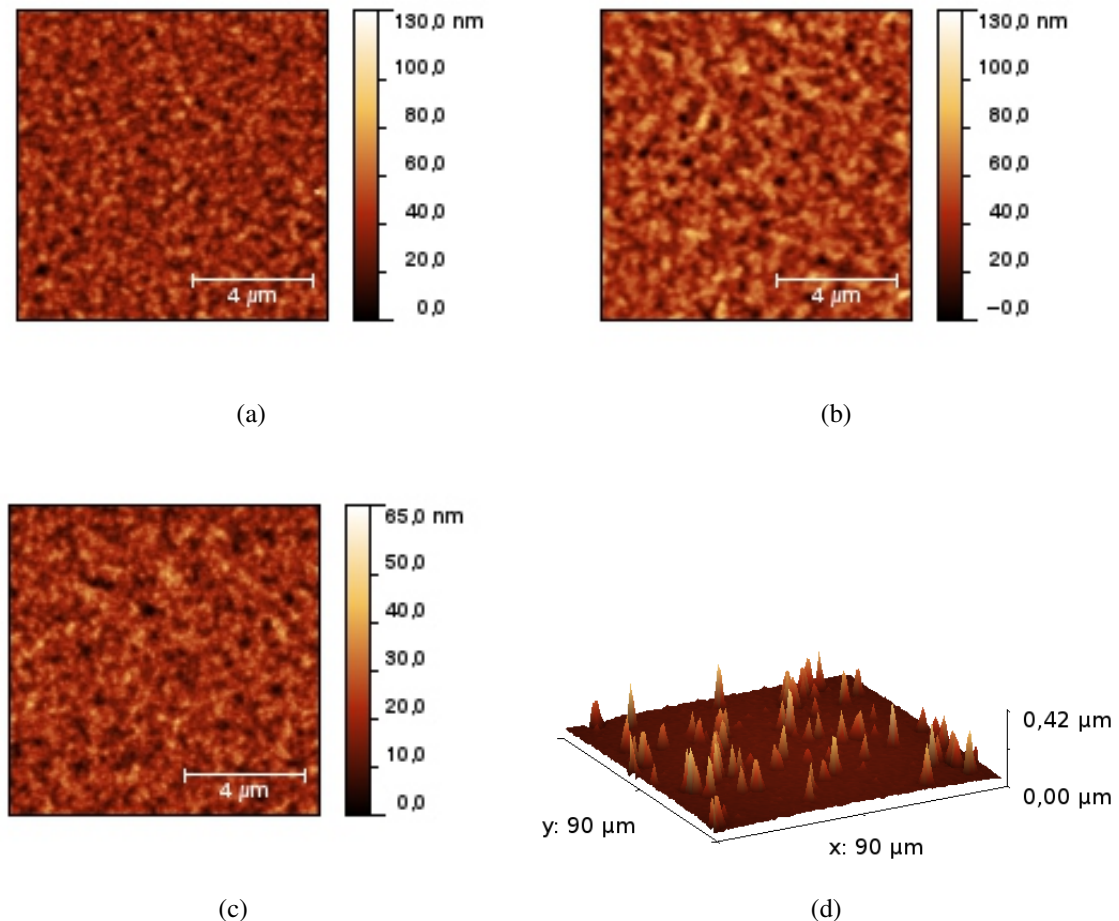


Figure 6.10.: Surface (AFM) images ($10 \times 10 \mu\text{m}$) of P3HT:acceptor=1:0.8 films with the acceptor being (a) only PC₆₁BM (b) a PC₆₁BM:TCNQ=0.99:0.01 blend and (c) a PC₆₁BM:TCNQ=0.95:0.05 blend, at which small crystals were visible at some spots on the substrate, shown by a $90 \times 90 \mu\text{m}$ 3d plot (d).

As a second method to find out if TCNQ crystals are existent in the active layer, which are not visible under the AFM, as it is not possible to scan the hole macroscopic sample by AFM, additional X-ray diffraction (XRD¹) measurements were performed for both films containing TCNQ. The results of the scans are shown in Fig. 6.11, where for the PC₆₁BM:TCNQ=0.99:0.01 solar cell, only the signature indicating a crystalline phase of P3HT (compare to Fig. 3.8) can be observed. No additional signatures indicating TCNQ crystals are visible, whereas for the PC₆₁BM:TCNQ=0.95:0.05 additional signatures show up. This por-

¹GE Sensing & Inspection Technologies, XRD 3003 TT

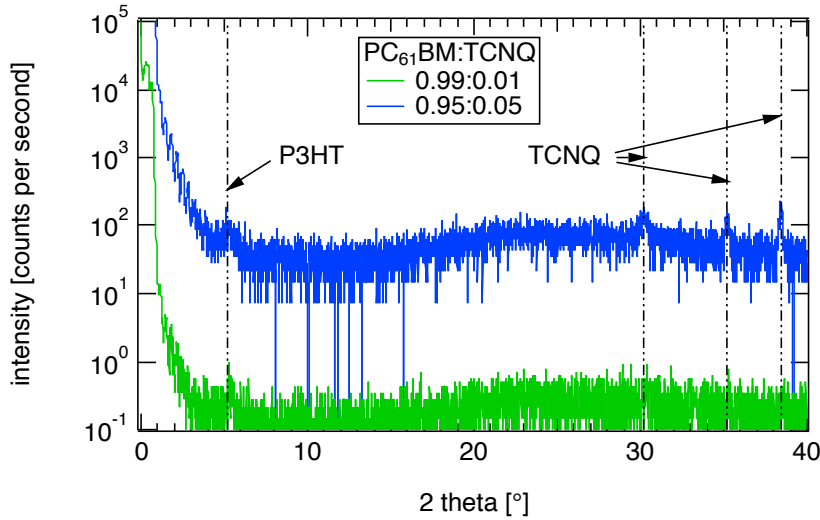


Figure 6.11.: XRD spectra of P3HT:PC₆₁BM:TCNQ films with a PC₆₁BM:TCNQ ratio of 0.99:0.01 and 0.95:0.05. The first peak can be ascribed to P3HT:PC₆₁BM by comparison with the XRD spectra of pure P3HT:PC₆₁BM films (Fig. 3.8). The additional peaks can be attributed to TCNQ.

tends, that in the case of the 1 wt%, the TCNQ seems to be incorporated as single molecules in the active layer, whereas in the 5 wt% TCNQ solar cell, parts of the TCNQ already form crystals, which do not act as trap states. Thus, the following study of the influence of extrinsic trap states on the solar cell characteristics and the recombination dynamics is of a qualitative nature, not quantitative.

The results of representative IV-curves in the dark and under 1 sun illumination using the solar simulator are shown in Fig. 6.12(a). The incorporation of extrinsic traps affect all photovoltaic parameters j_{sc} , V_{oc} and FF , listed in table 6.3. The most influenced parameter is the short circuit current density, which decreases from 8.5 mA/cm² to 91 % (PC₆₁BM:TCNQ=0.99:0.01) and 64 % (PC₆₁BM:TCNQ=0.95:0.05), whereas the V_{oc}/FF decreases only to 98/93 % (PC₆₁BM:TCNQ=0.99:0.01) and 93/86 % (PC₆₁BM:TCNQ=0.95:0.05) in respect to the P3HT:PC₆₁BM device. This behavior is similar to the above mentioned studies [61, 71] and also to the degradation mechanism under illumination (section 6.1). A part of the behavior of the 5 wt% TCNQ solar cell (decrease of j_{sc} and FF compared to the reference P3HT:PC₆₁BM SC) could originate from the unfavorable morphology as mentioned above. Nevertheless, the decrease of V_{oc} can not be caused by this effect, but by the incorporation of additional extrinsic trap states.

PC ₆₁ BM:TCNQ	j_{sc} [mA/cm ²]	V_{oc} [V]	FF [%]	η [%]
1:0	8.5	570	73	3.5
0.99:0.01	7.7	560	67	2.9
0.95:0.05	5.4	535	62	1.8

Table 6.3.: Parameters extracted from the IV-characteristics (Fig. 6.12)(a).

6. Influence of Trap States on the Open Circuit Voltage and the Recombination Dynamics in Organic Solar Cells

Beside the AFM/XRD measurements, external quantum efficiency (EQE¹) measurements of all three devices (Fig. 6.12(b)) showed that at least in the PC₆₁BM:TCNQ=0.95:0.05 device TCNQ does not only act as trap states, but do also actively contribute to the photocurrent generation by absorption of photons and creation of excitons in the TCNQ, leading to charge carriers that can be transported to the electrodes. To emphasize this additional absorption the EQE was normalized to 520 nm, where P3HT:PC₆₁BM SC have their maximum EQE.

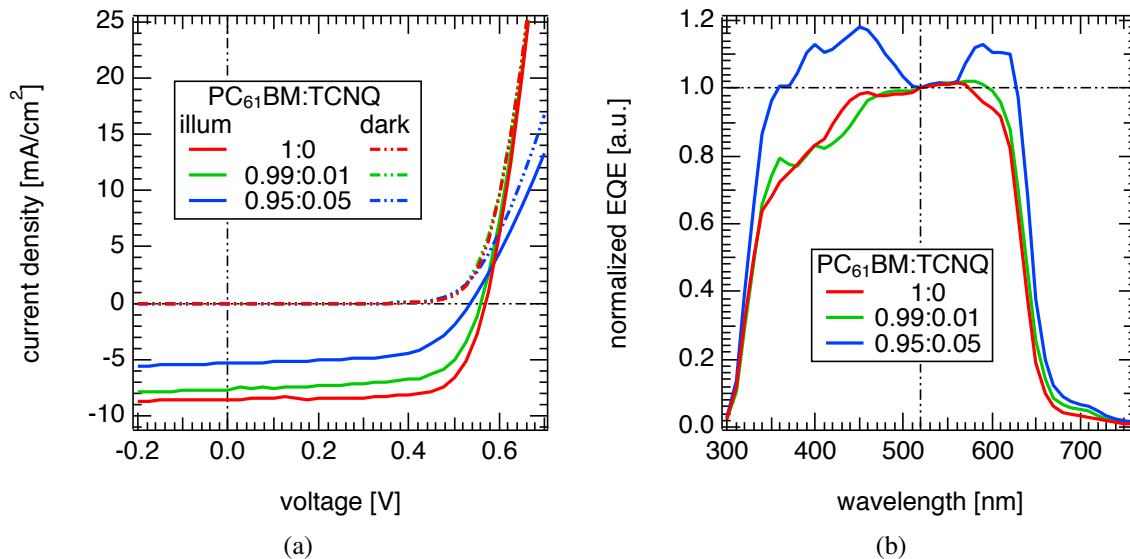


Figure 6.12.: IV-curves under 1 sun illumination for different concentrations of TCNQ (a) and the corresponding measurements of the external quantum efficiency (b).

As the device without TCNQ shows nearly the same IV-characteristics than the not degraded solar cell in section 6.1, the following measurements of the charge carrier density under open circuit conditions, as well as the open circuit transients and the light intensity dependence of the open circuit voltage were only measured for the two solar cells with extrinsic traps. The obtained data will be compared to the results of the not degraded cell in section 6.1.

Fig. 6.13 shows the charge carrier density under open circuit conditions for different open circuit voltages as obtained from charge extraction measurements under various light intensities. For the solar cell with a higher TCNQ content, the overall charge carrier density is slightly higher as for the one with PC₆₁BM:TCNQ=0.99:0.01 but still lower than for the P3HT:PC₆₁BM device (Fig. 6.2). Both curves do not show a power law behavior $n = n_0 \exp(c_n V_{oc})$ over the complete measured range, but mainly two different slopes c_n in the range of low and high open circuit voltages and a range of transition between them. For the further investigation of the recombination order, only the range of low charge carrier densities was analyzed. The respective fits are displayed in Fig. 6.13 as dash-dotted lines.

¹The EQE was measured in a self made setup consisting of a Xe lamp as a white light source which was spectrally split up by a monochromator and chopped by an optical chopper. The monochromatic light was then divided by a two branch fiber bundle, where one part of the light was focussed on a calibrated reference Si solar cell and the other focussed on test solar cell, located inside the glovebox system. The short circuit currents of both solar cells were measured with lock in amplifiers.

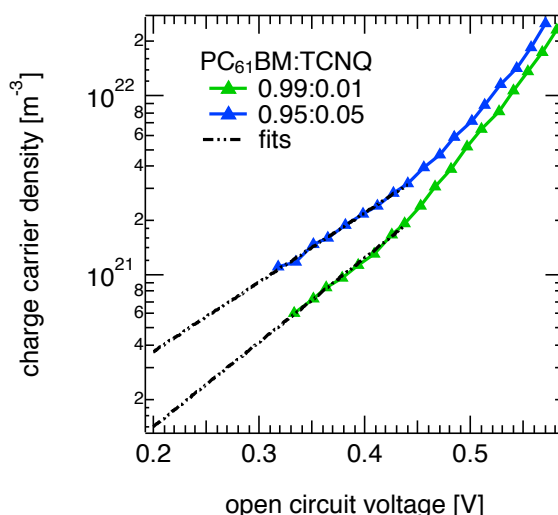


Figure 6.13.: The charge carrier density under open circuit conditions as obtained from charge extraction measurements under various illumination levels for the two solar cells with incorporated extrinsic trap states

The open circuit voltage transients (Fig.6.14(a)) were recorded after switching off the background light simulating 1 sun. Similar to Fig. 6.4(b) it was ensured that over the complete recorded time the V_{oc} values were measured correctly and were not influenced by a voltage drop at the internal resistance $R_{V_{oc}}$. In the transients two different time ranges can be observed for both solar cells with TCNQ molecules, as described for the degraded solar cell. As the $n(V_{oc})$ fit (Fig. 6.13) can only be performed for low open circuit voltages, just the decay of the charge carriers $n(t)$ in the longer time range can be reconstructed from $n(V_{oc})$ in combination with $V_{oc}(t)$. Therefore, only $\lambda_l + 1$ can be calculated from $n(t)$ (graph not shown). In the case of 1 wt% TCNQ $\lambda_l + 1$ is 3.07 and for the solar cell with 5 wt% TCNQ, the recombination order is even higher with a value of 3.65. In comparison with the $\lambda_l + 1$ value of 2.68 for the not degraded reference P3HT:PC₆₁BM solar cell (Tab. 6.2), the recombination order increases with a higher amount of extrinsic trap states.

To investigate the dominating recombination process of both solar cells with TCNQ, the light intensity dependence of the open circuit voltage (Fig. 6.14(b)) was used to calculate the ideality factor. It has to be mentioned first, that the solar cell with 5 wt% TCNQ exhibits a high parallel resistance R_p — higher than for the 1 wt% solar cell — implying that the single TCNQ crystals do not shorten the solar cell, which would result in low R_p and therefore a high influence on V_{oc} as explained in section 2.2.3. For the solar cell with 1 wt% TCNQ the ideality factor is 1.23 and 1.25 for the 5 wt% solar cell. For comparison, the P3HT:PC₆₁BM reference solar cell has a n_{id} of 1.18. This increase of the ideality factor with increasing TCNQ content implies that SRH recombination gets more important for higher trap contents in accordance to the results of degradation measurements.

In all these considerations, also in the degradation study, it is important that the investigated solar cells have no V_{oc} limitation by contact barriers since all measurements were performed under open circuit conditions. This implies that Eq. (2.18) as a link between V_{oc} and the polaron density has always to be valid. To confirm the importance of this statement, contact limited solar

6. Influence of Trap States on the Open Circuit Voltage and the Recombination Dynamics in Organic Solar Cells

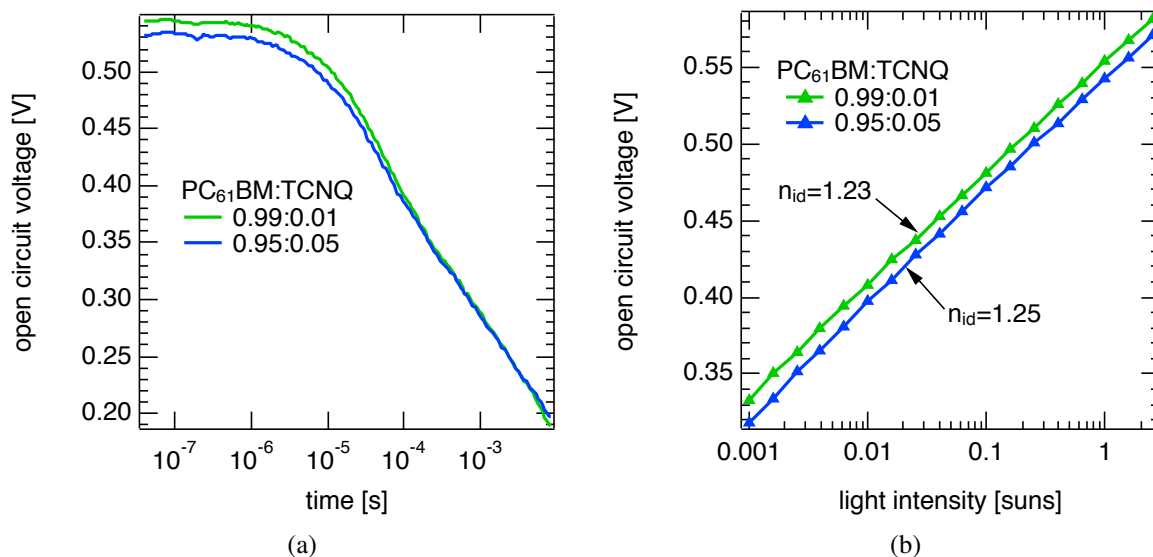


Figure 6.14.: Time evolution of the open circuit voltage for both solar cells with TCNQ traps after switching off the background light ($P_L=1$ sun) (a) as well as the light intensity dependence of the open circuit voltage (b).

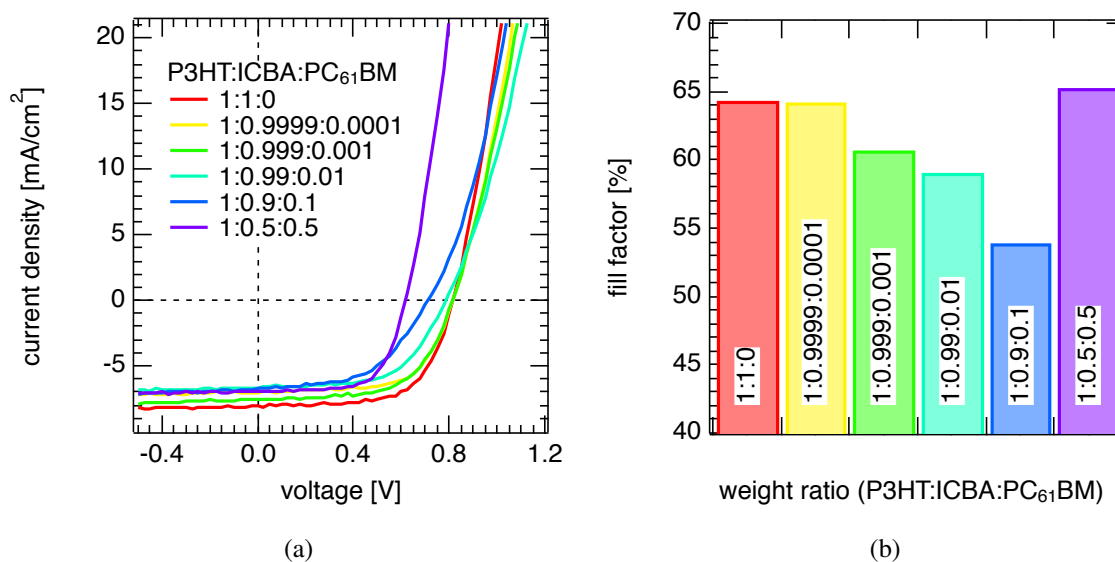


Figure 6.15.: (a) IV-curves under 1 sun illumination for different concentrations of PC₆₁BM acting as extrinsic traps in P3HT:ICBA solar cells and (b) the corresponding fill factors.

cells (P3HT:ICBA) with small contents of PC₆₁BM acting as extrinsic traps were fabricated and the same measurements were performed as shown above. As ICBA has a 0.17 eV higher LUMO level than PC₆₁BM [42, 119], this will inevitably result to a higher energy barrier Δ_e at the Ca/Al contact. Fig. 6.15(a) displays the IV-characteristics of the solar cells with different PC₆₁BM content, where a clear trend between solar cell performance and amount of trap states is visible, similar to the behavior of the solar cells with TCNQ as extrinsic traps.

All solar cells parameters — V_{oc} , j_{sc} and FF — are decreasing with increasing extrinsic trap content, which is shown in Fig. 6.15(b) for the FF in more detail. The fill factor was chosen, as it shows an interesting effect: for very high PC₆₁BM contents, here 50 % in comparison to ICBA, the PC₆₁BM molecules are not acting as trap anymore, but form their own percolating network which leads to a complete recovery of the FF . Beside the clear trend of the IV-curves, the recombination investigations didn't show a trend as for example the devices with TCNQ. Neither the recombination order determined from $n(t)$, taken from the combination of $n(V_{oc})$ and $V_{oc}(t)$, nor the ideality factor behaved as expected from theory explained in the chapters before. The reason is that limited contacts distort recombination measurements that are performed under open circuit conditions.

6.3. Conclusion

A strong influence of trap states on the performance of the solar cells and the recombination mechanisms was demonstrated if the solar cells were either exposed to oxygen or doped with TCNQ. All solar cell parameters decreased with an increasing amount of trap states, where the effect on the short circuit current density was the strongest. The existence of these additional trap states was confirmed by open circuit voltage transients in combination with charge carrier density measurements at open circuit voltage conditions, making it possible to receive information on the polaron decay in the solar cells. Both investigations showed that for longer degradation times or a higher TCNQ amount, the decay — especially for times longer than several hundred microseconds — is much slower. This effect is explained by a delayed release of charge carriers from trap states before they can recombine, as at least one charge carrier has to be mobile before the recombination process can take place (see chapter 5, Eq. (5.9), expressed by the terms $n_c p_t$ and $n_t p_c$). From these constructed $n(t)$ curves the apparent recombination order was determined to strengthen the assumption presented in chapter 5 that one reason for recombination orders higher than two is caused by trap states.

The increase of the ideality factor determined by the light intensity dependence of the open circuit voltage with increasing degradation time or TCNQ content is an additional indicator for the existence of trap states. Pure SRH recombination results in $n_{id} = 2$ and pure Langevin recombination in $n_{id} = 1$. The increase of n_{id} from 1.18 (not degraded P3HT:PC₆₁BM without TCNQ) to 1.23 (after 30 h of dark and additional 30 h of illuminated oxygen degradation) or 1.25 (5 % TCNQ) is caused by an increased influence of SRH recombination on the overall recombination, which is always a mixture of both recombination processes.

6. Influence of Trap States on the Open Circuit Voltage and the Recombination Dynamics in Organic Solar Cells

7. S-shaped IV-Characteristics as Result of a Reduced Surface Recombination Velocity and its Influence on the Open Circuit Voltage¹

7.1. Introduction

When one fabricates organic solar cells using new process parameters or materials (active material, electron/hole transport layer or metal contact) the resulting IV-curve under illumination does not always look like e.g. in Fig. 2.8, instead an s-shaped IV-characteristic can occur. Such a behavior was often described in literature [58, 96, 109, 111, 112] and was attributed to surface dipoles, unbalanced mobilities, traps or defects that create energy barriers and negatively influence the extraction of the photogenerated charge carriers. In this section a way to experimentally create s-shapes with varying strengths by an extended oxygen plasma treatment of the ITO glass substrate is shown. With the help of macroscopic simulations the origin of the s-shapes was investigated. Energy barriers as described in chapter 4 did not yield s-shaped IV-characteristics. Another parameter describing the quality of the interface, here the semiconductor/metal interface, is the surface recombination velocity. This mechanism can not only be used in the determination of recombination processes in semiconductors but can also describe the extraction (recombination) of charge carriers out of the active material into the metal. Assuming a reduced surface recombination velocity of holes at the anode could reproduce the experimentally obtained s-shaped curve with excellent agreement. To validate this approach, several experiments, namely light intensity dependent IV, transient photocurrent and open circuit voltage measurements were performed.

7.2. Experimental

All solar cells were prepared as described in section 3.2 with only small changes to create s-shapes in the IV-characteristics. After the cleaning procedure the ITO coated glass substrates were treated with atmosphere plasma, where it was important that the gas contained moisture. It has to be mentioned, that with dry air, as it was used for the degradation measurements in section 6.1, no s-shapes could be observed. To influence the strength of the s-shape, the plasma application time was varied. Furthermore, two different sets of plasma treated solar

¹Similar experimentally observed IV-curves under 1 sun illumination and corresponding macroscopic simulations are published by Wagenpfahl et al. [117], where the experimental work was done by myself and the theoretical and simulation part was performed by A. Wagenpfahl.

7. S-shaped IV-Characteristics as Result of a Reduced Surface Recombination Velocity and its Influence on the Open Circuit Voltage

cells were prepared: solar cells with and without PEDOT:PSS as interlayer between ITO and the active layer, a blend of P3HT:PC₆₁BM=1:0.8. The plasma treatment times for the solar cells with PEDOT:PSS were 2, 60, 300, 900, 1800 and 3600 s. The untreated cell was used as a reference. In the set without PEDOT:PSS, 0, 60, 300, 900, 1800 and 3600 s atmosphere plasma treatment time was used. Additionally a solar cell treated with 10 s of pure oxygen plasma was prepared for comparison. The thicknesses of the active layers were all in the range of 200 nm. As cathode, a Ca/Al electrode was thermally evaporated. The IV-curves under 1 sun AM1.5g spectrum were detected under the calibrated solar simulator in a nitrogen filled glovebox, the light intensity dependent IV-curves, as well as short circuit current and open circuit voltage transients were measured in the cryostate as described in section 3.1.

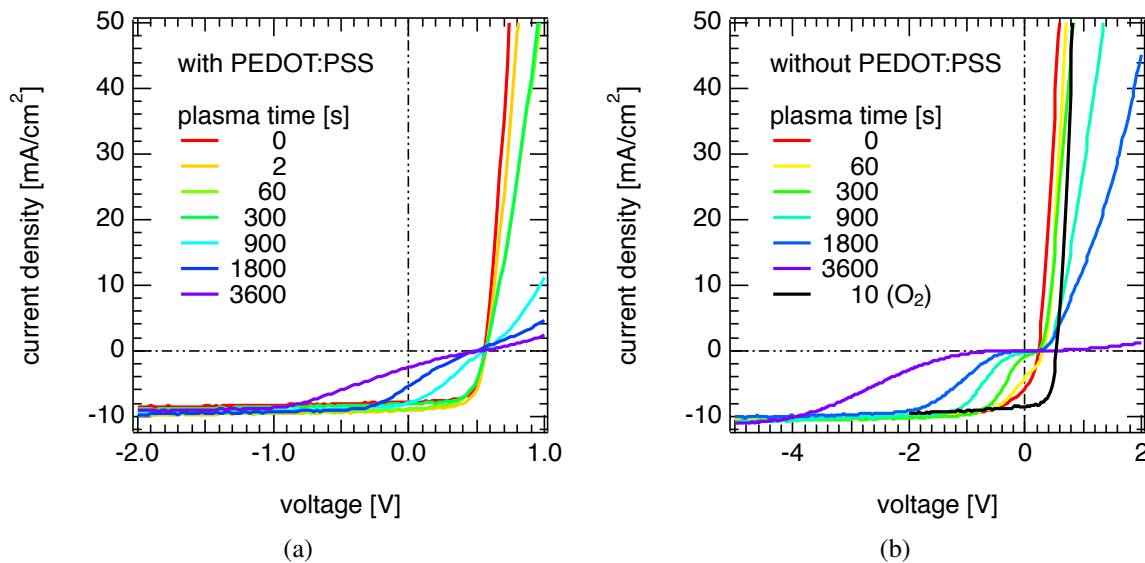


Figure 7.1.: IV-characteristics of s-shaped solar cells induced by an atmosphere plasma treatment of the ITO substrate for different times. Two different types of P3HT:PC₆₁BM solar cells were fabricated: with (a) and without (b) a PEDOT:PSS interlayer between ITO and the active layer. Additionally, in (b) an IV-characteristic is shown for a solar cell, where pure oxygen plasma was used for 10 s (black line).

7.3. Results and Discussion

Representative IV-characteristics of the prepared solar cells are shown in Fig. 7.1 ((a): with PEDOT:PSS, (b): without PEDOT:PSS). In both cases s-shapes were created with atmosphere plasma with increasing s-shape strength by increasing plasma time. The relevant solar cell parameters are summarized in Fig. 7.2 ((a): V_{oc} , (b): FF , (c): j_{sc} and (d): efficiency).

In the case of solar cells with PEDOT:PSS, short plasma times up to 300 s did not lead to s-shapes but only to a slight decrease of the efficiency. Increasing the plasma exposure time to 900 s and longer, s-shapes occurred, accompanied by a drop of FF and j_{sc} , whereas V_{oc} was not influenced.

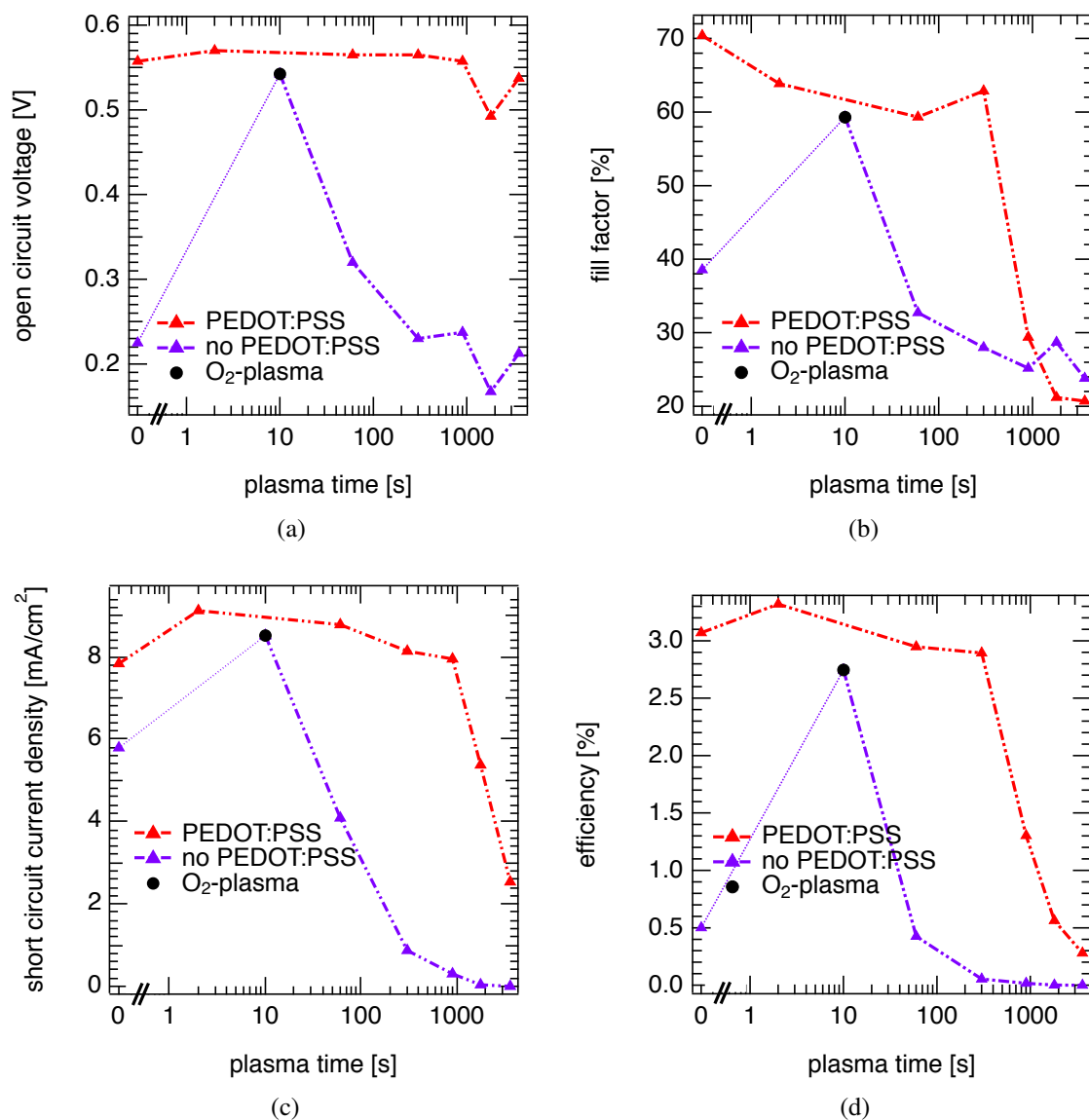


Figure 7.2.: Solar cell parameters ((a): V_{oc} , (b): FF , (c): j_{sc} and (d): efficiency) extracted from the IV-curves displayed in Fig. 7.1 in dependence of the plasma treatment time for solar cells with (red) and without (purple) PEDOT:PSS. The black circles indicate the parameters obtained from the solar cell fabricated on the 10 s oxygen plasma treated ITO substrate (without PEDOT:PSS).

7. S-shaped IV-Characteristics as Result of a Reduced Surface Recombination Velocity and its Influence on the Open Circuit Voltage

Solar cells without PEDOT:PSS behaved something different, as they showed already a low performance in the untreated case, where the fill factor only reached values below 40 %. At short plasma treatment times (60 s), an inflection point in the IV-characteristic turned up indicating the s-shaped behavior of the curve, accompanied by a decrease of FF and j_{sc} . The reason why V_{oc} increased in the case of solar cells without PEDOT:PSS, where it should drop with an increasing s-shape behavior, is that the untreated solar cell can not be taken as a reference in that case. In principle, the used plasma treatment does not only reduce the surface recombination velocity, but can also change the work function of the ITO [51] or have a beneficial surface cleaning effect [118]. Therefore, it is more reasonable to use the solar cell as reference, where a 10 s pure oxygen plasma treatment was applied to the ITO substrate. This plasma treatment provides the same cleaning effects as the atmosphere plasma, but does not lead to a reduced surface recombination velocity, which was proven by extended O₂-plasma treatments up to 600 s, where no changes in the IV-curves were observed (data not shown). Taking the oxygen treated device as reference, a clear trend for the set of solar cells without PEDOT:PSS gets visible: a decrease of all parameters with increasing plasma time, which is at least for V_{oc} in contrast to the data obtained from the solar cells with PEDOT:PSS.

To substantiate the claim that a reduced surface recombination velocity is the reason for the occurrence of the above described s-shaped IV-curves, macroscopic simulations were performed. To express the ability of a charge carrier to pass over from one junction to another, for example the hole on the HOMO of the donor to the electrode (PEDOT:PSS or ITO), the surface recombination rate J is defined by [40]

$$J = qS(n - n_{th}) \quad , \quad (7.1)$$

where S is the surface recombination velocity and n_{th} the thermally activated charge carrier density at the respective contact. Further information about the calculation of n_{th} and the background of the macroscopic simulation are given in [116, 117]. Since in a solar cell two contacts (cathode, anode) are needed as well as two different charge carrier species are present (electrons, holes), four different recombination velocities are defined. In an ideal device, all surface recombination velocities should be infinity or at least be considerable high. In this case, as depicted in Fig. 7.3 schematically on the left side, the charge carriers generated in the active material can be extracted fast enough from the active layer into the electrode. On the right side of Fig. 7.3, the case of a reduced surface recombination velocity is shown. Here the generated charge carriers are transported faster to the electrode as they can be extracted, leading to a pile up of charge carriers, resulting in a local space charge and as a final consequence to an s-shaped IV-curve.

The fixed simulation parameters used here were the same as summarized in table 4.2. Additionally, the temperature T was set to 300 K, the mobility $\mu_{n,p}$ of both, electrons and holes, to 10^{-8} m²/(Vs), and the injection barriers for electrons Φ_n and holes Φ_p to 0.0 and 0.1 eV, respectively. For the recombination mechanism in the bulk material pure Langevin recombination was assumed. To take into account that in the experiment only the properties of the anode were changed by the plasma treatment, the two surface recombination velocities concerning the cathode (S_n^c, S_p^c) were set to infinity, which was treated numerically with 10^{50} m/s. To explain both experimental data sets, with and without PEDOT:PSS, two different simulations were performed. In the first, the surface recombination velocity of electrons at the anode S_n^a was set to infinity, whereas the surface recombination velocity of holes at the anode S_p^a was varied. In the

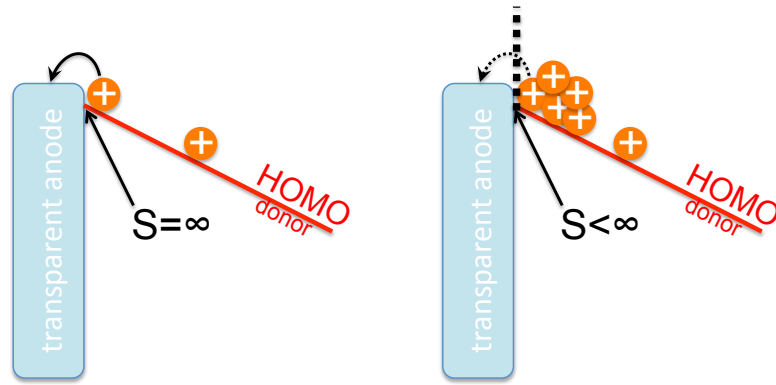


Figure 7.3.: Visualization of the surface recombination velocity S . On the left side, S is infinity or at least considerable high that all charge carriers can be extracted fast enough from the active layer into the electrode. On the right side the case of a reduced surface recombination velocity is depicted. Here the charge carriers can not be transferred fast enough into the electrode, leading to a pile up of charge carriers which in consequence leads to an s-shaped IV-characteristic.

second set, S_p^a was set to 10^{-9} m/s and S_n^a was varied.

Fig. 7.4(a) shows the simulated IV-curves with the first set of parameters. As expected, with decreasing S_p^a , the s-shape behavior gets more pronounced, as seen in the decreasing FF and j_{sc} , when S_p^a is lower than $\sim 10^{-4}$ m/s. In the range of 10^{-2} m/s $< S_p^a < \infty$, the solar cell performance is not influenced by the reduced S_p^a at all, at least for the used generation rate. Not so apparent in Fig. 7.4(a) is the trend of V_{oc} , which also decreased with reduced S_p^a . Therefore, Fig. 7.4(b) displays separately the dependence of the open circuit voltage on the surface recombination velocity S_p^a (red line). In the range of 10^{-2} m/s $< S_p^a < \infty$, V_{oc} was constant, and then decreased continuously with decreasing S_p^a . In principle, the simulated IV-curves are in a good agreement with the experimental results obtained from the solar cells without PEDOT:PSS, as in both cases all solar cell parameters decreased with an increased plasma treatment (experiment) or decreased S_p^a (simulation).

To explain the stabilization of V_{oc} (Fig. 7.2(a)) for the solar cells with PEDOT:PSS as interlayer, one has first to take into account the functionality of PEDOT:PSS. In literature it is mentioned, that PEDOT:PSS improves the injection/extraction of holes at the ITO contact [19, 84], leading to an overall better solar cell performance, as it was also observed here. This allows to draw the conclusion that S_p^a is higher for solar cells using a PEDOT:PSS interlayer. An additional indication therefore is, that s-shapes occur only at longer plasma treatments in the case of solar cells with PEDOT:PSS compared to solar cells without. Furthermore, PEDOT:PSS is a HTL and thus an electron blocking layer, which leads to a reduced surface recombination velocity of electrons at the anode S_n^a . Therefore, for the second set of macroscopic simulation parameters S_p^a was set to a reduced value of 10^{-9} m/s to create s-shapes and S_n^a was varied. Since the IV-characteristics are similar for all simulated S_n^a values (j_{sc} was constant for 10^{-11} m/s $< S_n^a < \infty$), these curves are not shown. In Fig. 7.4(b, blue line), the open circuit voltage in dependence of S_n^a is depicted. For $S_n^a > 10^2$ m/s the surface recombination velocity is still too high and V_{oc} is at the same level as for $S_p^a = 10^{-9}$ m/s and $S_n^a = \infty$. If S_n^a decreases, V_{oc} is approaching the values of a solar cell with not reduced surface recombination velocities (i.e.

7. S-shaped IV-Characteristics as Result of a Reduced Surface Recombination Velocity and its Influence on the Open Circuit Voltage

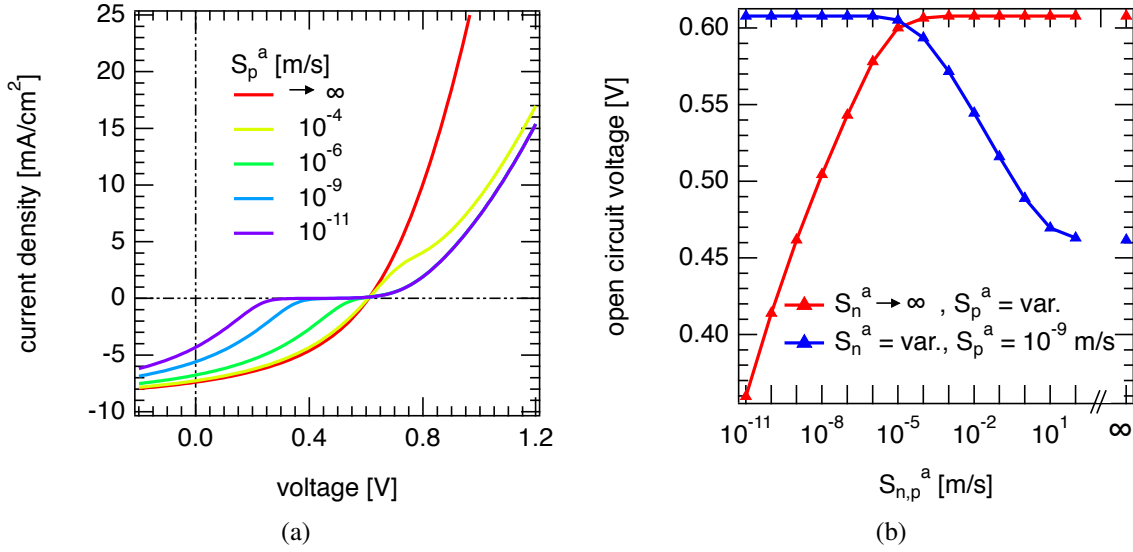


Figure 7.4.: (a) Simulated IV-characteristics showing the appearance of s-shape due to a reduced surface recombination rate for holes at the anode S_p^a . With decreasing S_p^a the s-shape gets more pronounced. (b) Dependence of V_{oc} on the surface recombination velocity. In the case of $S_n^a \rightarrow \infty$, the V_{oc} decreases with lower S_p^a (red curve). In addition to a lowered S_p^a ($=10^{-9}$ m/s) also S_n^a reduced to an adequate low level (here: 10^{-5} m/s), V_{oc} reaches again the same values as for unreduced $S_{n,p}^a$ (blue line).

$S_{n,p}^a \sim \infty$) but show an s-shaped IV-curve. Thus, the stabilization of V_{oc} for the plasma treated solar cells with PEDOT:PSS can be explained by an additionally reduced S_n^a . The reason for the higher V_{oc} is that the reduced S_n^a leads to an increase of the electron density n at the anode additionally to the high hole density p caused by the reduced S_p^a . From the Poisson equation, the actual electrical field is proportional to the difference of $p - n$ ¹. A higher n now reduces the difference and therefore lowers the formation of a space charge which decreases V_{oc} .

To experimentally substantiate the results of the macroscopic simulations and the approach of a reduced surface recombination velocity being responsible for the occurrence of an s-shape, IV-curves for different light intensities from 0.00025 to 2.5 suns were measured. The motive behind this approach is the following: If the reduced surface recombination velocity, which figuratively speaking limits the amount of charge carriers that can be extracted into the electrode, is responsible for the s-shape, then the s-shape should vanish if less charge carriers were generated at lower light intensity. Fig. 7.5 shows the FF as well as the V_{oc} , extracted from the IV-curves in dependence of the light illumination level for two solar cells (0 and 900 s plasma treatment) with a PEDOT:PSS interlayer.

First of all, the FF behavior of the 0 s plasma treated reference device has to be explained, before the solar cell with s-shaped IV-curve will be discussed. In principle, the FF is mainly influenced by the recombination of the generated charge carriers. An IV-curve in the voltage range from 0 to ~ 0.4 V, where the slope of dJ/dV is still low, is dominated by a first order

¹ $\vec{\nabla}E(x) = \frac{\rho(x)}{\epsilon}$, $\rho \propto (p - n)$, where ρ is the charge carrier density

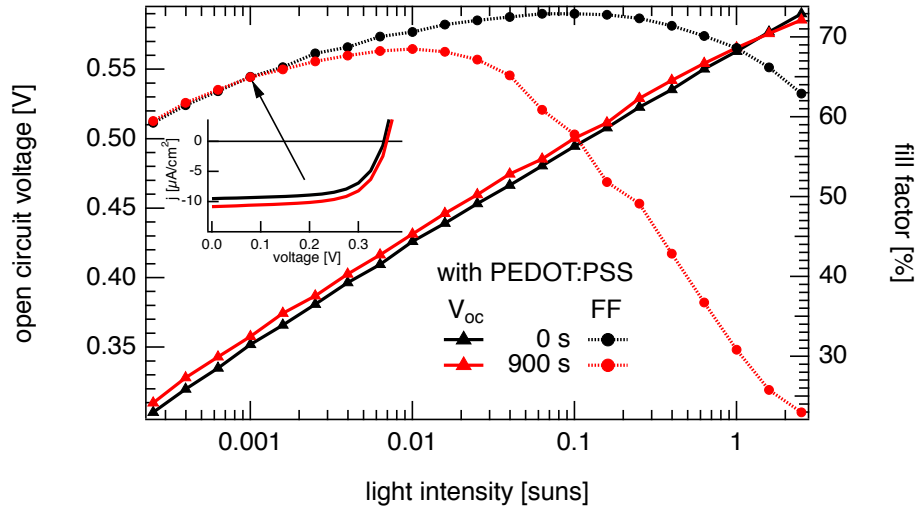


Figure 7.5.: Light intensity dependence of the open circuit voltage and the fill factor for solar cells (0 and 900 s plasma treatment) with a PEDOT:PSS interlayer. For high light intensities (see IV-curves Fig. 7.1(a)) the 900 s plasma treated solar cell has a low fill factor originating from the s-shape. For low light intensities, when less charge carriers are generated, the s-shape vanishes which can be seen by an increase of the FF with lower P_L until it reaches the values of the not plasma treated solar cell. The reason therefore is, that the reduced surface recombination velocity is then still high enough to prevent the pile up of charges at the electrode. In the inset, the IV-curves of both solar cells under 0.001 suns illumination are displayed. V_{oc} shows the same P_L dependence for both solar cells, which can be explained by the reduced S_n^a .

recombination kinetics, whereas around V_{oc} the dominating recombination process is of the second order (Langevin) [23]. In the range of high light intensities the FF was shown to be dominated completely by Langevin recombination [70, 99]. This mechanism can explain the increase of FF with decreasing P_L down to 0.063 suns, as under lower light intensities lower charge carrier densities are present in the device, resulting in lower Langevin recombination rate. For lower light intensities, first order recombination processes get more important leading to a decrease of FF . In macroscopic simulations with varying generation rates the two $FF(P_L)$ ranges could be reproduced by adding a SRH (first order) recombination process to the Langevin recombination. Where in the case of pure Langevin recombination the FF was continuously increasing with lower generation rate, the introduction of SRH recombination in addition to Langevin recombination led to a decrease of FF for lower generation rates.

Before comparing the P_L dependence of the FF of the solar cells with and without s-shaped IV-curve it has to be pointed out that the active layers of both solar cells have equal properties (morphology, thickness,..) and therefore the same underlying recombination mechanisms of photogenerated charge carriers, which can be seen in the equal $V_{oc}(P_L)$ behavior. Nevertheless, a different $FF(P_L)$ trend can be observed. As explained above when discussing the IV-curves under 1 sun illumination, the reduced surface recombination rate leads to a pile up of charge carriers resulting in a space charge influencing strongly the FF of the device. By reducing the

7. S-shaped IV-Characteristics as Result of a Reduced Surface Recombination Velocity and its Influence on the Open Circuit Voltage

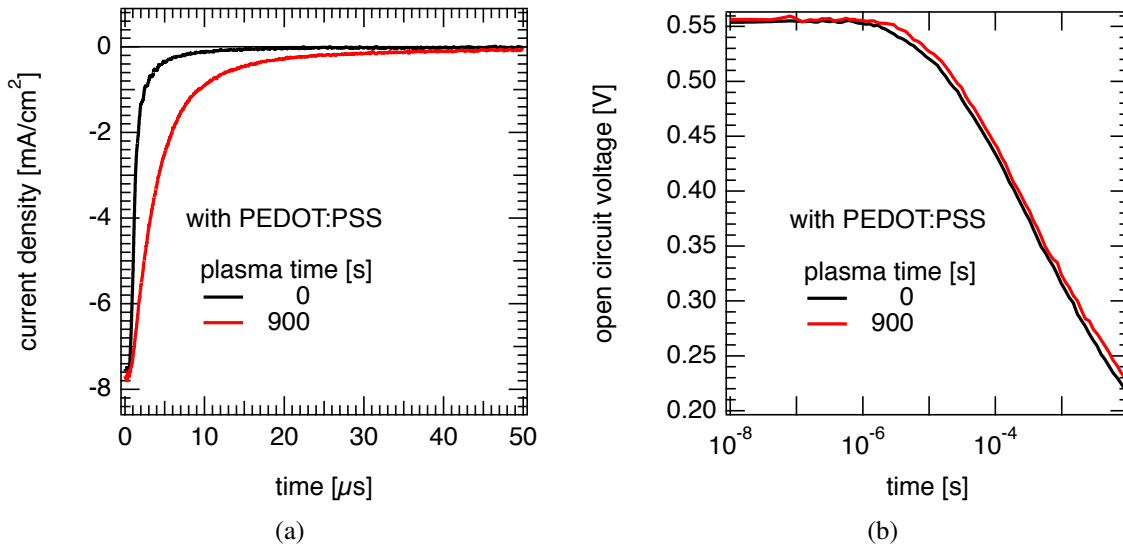


Figure 7.6.: Photocurrent j_{sc} (a) and open circuit voltage V_{oc} (b) transients of 0 s (no s-shape) and 900 s (s-shape) ITO plasma treated solar cells using PEDOT:PSS as interlayer. Whereas $V_{oc}(t)$ is unaffected by the reduced surface recombination velocity, $j_{sc}(t)$ differs despite equal steady state j_{sc} , visible at $t = 0$ s. Details are given in the text.

light intensity and therefore the generation of charge carriers, less charge carriers are piled up, the space charge is lower and the FF is increasing. This effect is still superimposed by the effects of the recombination processes, as for example the reduction of bimolecular recombination which is also partly responsible for the FF increase with decreasing P_L in the high light intensity range. In the case of the solar cell with s-shaped IV-curve the maximum FF is reached at 0.01 suns, which is lower than for the solar cell without s-shaped IV-curve. Under this condition, the fill factor of both solar cells are nearly equal. For light intensities of 0.001 suns or lower, the FF of both solar cells is the same, indicating that less charge carriers are generated than can be extracted despite the reduced surface recombination velocity without being piled. Under these conditions the fill factor is only influenced by the recombination mechanisms of charge carriers in the active layer which are equal for both devices. The inset in Fig. 7.5 shows the IV-curves of both solar cells under 0.001 suns illumination, where the s-shape has vanished in the solar cell that exhibited a s-shaped IV-curve under higher light intensities.

The similar trend was observed for the solar cells without PEDOT:PSS. Here, the reference solar cell (10 s oxygen treated), showed the same trend for $FF(P_L)$ and $V_{oc}(P_L)$ as the solar cell without s-shaped IV-curve with PEDOT:PSS. For the solar cell with a less distinct s-shape (60 s plasma treated), the FF was increasing over the whole light intensity range from 2.5 suns ($FF=36\%$) to 0.00025 suns ($FF=56\%$), but did not reach completely the same FF as the reference solar cell (data not shown). Since in the solar cells without PEDOT:PSS, V_{oc} was not stabilized by a reduced S_n^a , the light intensity dependent V_{oc} did not show a linear increase with increasing P_L (in the V_{oc} vs. $\ln(P_L)$ plot) for the solar cell exhibiting an s-shape, but a constant V_{oc} , whereas the reference solar cell without PEDOT:PSS showed the typical linear increase.

A last experimental hint for the applicability of the theory of a reduced surface recombination being responsible for s-shaped IV-characteristics was the measurement of the transient

photocurrent as it was performed in chapter 5 to calculate the charge carrier density under short circuit conditions. Fig. 7.6(a) shows the transients of the 0 and 900 s plasma treated solar cells with PEDOT:PSS switching off the light source with $P_L=1$ sun. Both solar cells showed similar j_{sc} under illumination, which is the value at $t=0$ s, when the light was switched off, despite the s-shaped behavior in the 900 s plasma treated solar cell. Interestingly, in the case of the solar cell with the reduced surface recombination velocity, the decrease of the photocurrent was much slower than for the solar cell without s-shaped IV-curve. As consequence, the charge carrier density under short circuit conditions was much higher for the solar cell with s-shaped IV-curve as for the 0 s plasma treated one. This can be understood referring to Eq. (7.1). In the case of a reduced surface recombination velocity S , the number of charges near the interface n has to be increased to assure the same surface recombination rate J , which was equal for both solar cells due to equal short circuit currents under steady state conditions.

The identical behavior of the open circuit voltage transients (Fig. 7.6(b)) for the same two solar cells show, that under open circuit conditions no space charge is apparent in the active layer and $V_{oc}(t)$ is only determined by recombination mechanisms of the charge carriers inside the active layer. For the solar cells with s-shaped IV-curve fabricated without PEDOT:PSS, this was not the case. Here V_{oc} was nearly constant in the measured time range, as V_{oc} was mainly determined by the interface properties (data not shown).

7.4. Conclusion

In this section the experimental possibility to reproducibly create solar cells with different pronounced s-shapes was described first as a basis for various experiments and theoretical considerations. Using extended ambient air plasma treatments of the ITO/glass substrates with different treatment times led to several solar cells with s-shaped IV-curve. Two sets of solar cells were fabricated, one without using PEDOT:PSS as interlayer between the ITO and the active layer, and one using PEDOT:PSS. The first set resulted in solar cells with s-shaped IV-curve, where all solar cell parameters were decreasing with increasing plasma treatment time, which was attributed to a reduced surface recombination velocity of holes at the anode S_p^a . A reduced S_p^a can cause a pile up of holes at the anode because they can not be extracted fast enough, leading to a space charge and as a last consequence to s-shaped IV-curves. This assumption was confirmed by macroscopic simulations. The second set of devices using PEDOT:PSS resulted also in solar cells exhibiting s-shaped IV-curves, but only for longer plasma treatment times ($t \geq 900$ s), where again the fill factor and the short circuit current decreased with increasing s-shape strength. The open circuit voltage was stabilized by the PEDOT:PSS interlayer instead. This effect was attributed to the electron blocking properties of PEDOT:PSS, which result in a reduced surface recombination velocity of electrons at the anode. This reduces the space charge at the anode at V_{oc} . Therefore the V_{oc} in solar cells with PEDOT:PSS remains unaffected. This effect was also validated with macroscopic simulations.

To substantiate this scenario, light intensity dependent IV-curves were measured. It could be shown that under low light intensities, the reduced surface recombination velocity was still high enough to extract the photogenerated charge carriers without being piled up, resulting in not s-shaped IV-curves for solar cells that showed s-shape IV-curves under e.g. 1 sun illumination. From transient photocurrent measurements it could also be demonstrated qualitatively that in solar cells with a lower surface recombination velocity, the charge carrier density in the device

7. S-shaped IV-Characteristics as Result of a Reduced Surface Recombination Velocity and its Influence on the Open Circuit Voltage

has to be higher than in a solar cell with a higher surface recombination velocity to ensure the same surface recombination rate, meaning the same current. $V_{oc}(t)$ as well as $V_{oc}(P_L)$ measurements for solar cells with PEDOT:PSS could also solidify the assumption that PEDOT:PSS as an electron blocker eliminates the space charge under open circuit conditions and V_{oc} is only dependent on the intrinsic properties of the active layer, e.g. the recombination mechanisms.

As a last point in this section a second possibility to produce solar cells with s-shaped IV-curve is briefly mentioned. Using the fact that PEDOT:PSS is an acid in water (pH=1.2–2.2 at 20 °C), PEDOT:PSS can etch the ITO. Therefore, ITO/glass substrates were spincoated with PEDOT:PSS and stored for several days in humid atmosphere before they were heated at 130 °C in the glovebox followed by the standard solar cell fabrication steps. Fig. 7.7 shows P3HT:PC₆₁BM solar cells where the PEDOT:PSS coated ITO/glass substrates were stored up to 30 days. For the 30 days stored device, a clear s-shape can be observed. In this case, the electron blocking properties of the PEDOT:PSS seem to be reduced, maybe by etching products of the ITO in the PEDOT:PSS layer, since V_{oc} is lower than for the solar cells without s-shape.

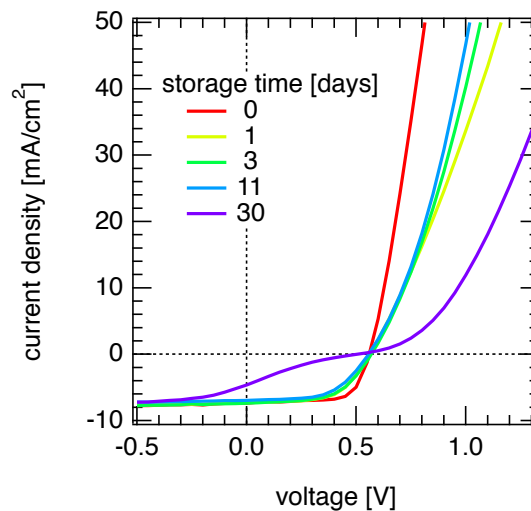


Figure 7.7.: IV-characteristics of solar cells induced by an ITO etching process due to the acid PEDOT:PSS under humid atmosphere. The solar cell where the PEDOT:PSS/ITO/glass substrate was stored for 30 days shows a clear s-shaped IV-curve.

8. Summary

The focus of the presented work was studying recombination mechanisms occurring in organic solar cells, as well as their impact on one of their most important parameters — the open circuit voltage. Beforehand, the fundamental working principles of organic solar cells were summarized, with a special attention to the recombination mechanisms and the open circuit voltage in general. After the explanation of the measurement technique called *charge extraction*, which is often used in the framework of this theses, the manufacturing process of organic solar cells was briefly introduced as well as the thereby used materials.

Firstly, the relationship between open circuit voltage and the respective charge carrier density in the active layer under open circuit conditions was analyzed. Eq. 2.18 is used to describe the open circuit voltage, whose validity was proven with the aid of fits to the measured data. Thereby, it was emphasized that the equation is only valid under special conditions. In the case of the often used reference system P3HT:PC₆₁BM, which was also used here, the fits were in agreement with the measurement data only in the range of high temperatures, i.e. 150 to 300 K, where the open circuit increased linear with decreasing temperature. At lower temperatures, the experiment showed a saturation of the open circuit voltage. Here, even under the assumption that the fit parameters effective density of states and band gap are temperature independent, a falling charge carrier density with lower temperatures, as it was observed, would result in a slower increase of the open circuit voltage with decreasing temperature according to the equation. In the temperature range from 50 to 150 K a V_{oc} saturation takes place, which stands in no direct relationship to the intrinsic properties of the active layer. This effect is due to injection energy barriers at the contacts, which was ascertained by macroscopic simulations. Furthermore, it was observed that the open circuit voltage in the case of saturation is equivalent to the so called built-in potential. The difference between the saturated open circuit voltage and the voltage given by the extrapolation of the linear open circuit voltage range to 0 K, corresponds thereby to the sum of the energy barriers at both contacts.

With the knowledge that the open circuit voltage is directly related to the corresponding charge carrier density in not contact limited solar cells, it was possible to consider another hotly debated topic in OPV: the recombination of charge carriers in the active layer. It was reported in various publications that the recombination rate is proportional to the charge carrier density with an exponent higher than two, whereby the exponent is often referred to as recombination order. The recombination mechanisms Shockley-Read-Hall (SRH) or Langevin would only result in recombination orders of 1 or 2, respectively. When both take place simultaneously, a value between 1 and 2 is expected. Two main explanations exist in literature about this phenomena, where both assume that the recombination is mainly of Langevin type. One is based on the approach that there are trap states for the respective charge carriers in separated phases, i.e. electrons in the acceptor phase and holes in the donor phase, which leads to a delayed recombination of the charge carriers at the interface of both phases and finally to an apparent recombination order higher than 2. The other theory includes the higher charge carrier density

8. Summary

dependence of the recombination rate into the so called recombination prefactor. The charge carrier density dependence of this factor is then explained by the charge carrier density dependence of the mobility. To resolve which theory is to favor, the charge carrier density dependence of the mobility and the recombination prefactor were measured separately. Therefore, the reference system P3HT:PC₆₁BM as well as PTB7:PC₇₁BM, the commercially available material system reaching the highest overall efficiency, were characterized by temperature and illumination dependent current-voltage and charge extraction measurements. It was found that for the system P3HT:PC₆₁BM at room temperature the charge carrier density dependence of the mobility was nearly matching completely the charge carrier density dependence of the recombination prefactor. Nevertheless, at lower temperature the discrepancy between both charge carrier density dependencies became obvious, which substantiates the idea of trap states in a phase separated system. In the material system PTB7:PC₇₁BM the increased recombination order could not be explained by the charge carrier density dependent mobility even at room temperature. As conclusion, it can be stated that both theories have their justification and their respective impact is strongly dependent on the temperature and the material system. As the charge carrier density dependence of the mobility has its origin also in trap states, it has to be mentioned that recombination orders higher than 2 should be an inherent property of disordered semiconductors.

After making out the importance of trap states on the recombination of charge carriers in organic solar cells, additional trap states were incorporated into the solar cells to investigate their impact on the IV-characteristics as well as recombination order and type. To achieve this, a solar cell was exposed to synthetic air (in the dark and under illumination), leading to an increase of the trap state concentration. Furthermore solar cells were fabricated, in which TCNQ was added in small concentrations to the active layer consisting of P3HT:PC₆₁BM. This molecules act as electron traps because of their lower LUMO level. The oxygen degraded solar cell behaved similar to already reported results from literature in terms of IV-characteristics. While the open circuit voltage was not influenced in the case of degradation in the dark, the fill factor was even increasing slightly, but both decrease when it comes to oxygen degradation under simultaneous illumination. The strongest impact of degradation could be seen on the short circuit current density, which decrease in the dark as well as under illumination. The recombination order was determined by a combination of open circuit voltage transients and the dependence of the charge carrier density on the open circuit voltage. Thereby, a continuous increase of the recombination order from 2.4 to more than 5 was observed with higher degradation times. To give a statement about the dominating recombination type, the ideality factor was determined from the illumination dependence of the open circuit voltage. For pure SRH recombination, that means recombination directly through trap states, one would expect a theoretical value for the ideality factor of 1, for Langevin recombination of 2 and when both types appear at the same time, a value between 1 and 2. As with increasing degradation time, the number of traps in the active layer is increasing, it is expected that the ideality factor is also increasing, meaning a higher impact of Shockley-Read-Hall recombination in relation to Langevin recombination. This theoretical expectation was confirmed by the measurements. A similar picture was revealed for the solar cells using TCNQ molecules as extrinsic traps. In this measurement series all IV parameters were decreasing with increasing TCNQ content, whereas the strongest impact was again on the short circuit current density. The recombination investigations yielded also a consistent picture concerning the influence of trap states, as it was observed in the oxygen

degraded solar cell. The recombination order as well as the ideality factor was increasing with higher TCNQ content. Therefore, it can be finally concluded that traps have a strong impact on the IV-characteristics and thus the efficiency of organic solar cells.

Finally, a phenomenon called s-shaped IV-curves was investigated, which can occur when one for example changes the contacts of the solar cells. As such solar cells have a strongly reduced efficiency it is important to understand the underlying physical mechanism. In the framework of this thesis, a reduced surface recombination velocity was identified as origin. This initial assumption was backed up by experimental results and macroscopic simulations. To achieve this, the reproducible preparation of s-shaped solar cells was the first step. This was done by a special plasma treatment of the ITO contact. The measured IV-curves of such solar cells were then reproduced by macroscopic simulations, where the surface recombination velocity was reduced. Hereby, it has to be distinguished between the surface recombination of majority and minority charge carriers at the respective contacts. The theory could even be experimentally confirmed by illumination level dependent IV-curves as well as short circuit current density and open circuit voltage transients.

Thus, this thesis presents a detailed study of the charge density dependence of the open circuit voltage as well as the recombination mechanisms in organic solar cells and the influence of trap states on these.

9. Zusammenfassung

Im Fokus der vorliegenden Arbeit lagen die Rekombinationsmechanismen welche in organischen Solarzellen vorkommen, sowie deren Einfluss auf eine der wichtigsten charakteristischen Kenngrößen dieser - der Leerlaufspannung. Vorab wurde die prinzipielle Funktionsweise organischer Solarzellen zusammengefasst und hierbei gesondert ein Hauptaugenmerk auf die Rekombinationsmechanismen und die Leerlaufspannung gelegt. Nach der Erläuterung der Messmethode der Ladungsträgerextraktion, welche im Rahmen der Solarzellencharakterisierung häufig angewendet wurde, wurde noch kurz auf das Standardherstellungsverfahren der Solarzellen eingegangen, sowie die dabei verwendeten Materialien vorgestellt.

Zuerst wurde der Zusammenhang zwischen Leerlaufspannung und zugehöriger Ladungsträgerdichte in der aktiven Schicht unter Leerlaufbedingungen untersucht. Gleichung 2.18 wird zur Beschreibung der Leerlaufspannung verwendet, deren Gültigkeit mit Hilfe von Fits an die Messdaten überprüft wurde. Dabei stellte sich heraus, dass die Gleichung nur für bestimmte Rahmenbedingungen gültig ist. Im Fall des häufig verwendeten Referenzsystems P3HT:PC₆₁BM, welches auch hier benutzt wurde, stimmten die Fits nur im Bereich höherer Temperaturen, in denen die Leerlaufspannung linear mit tieferen Temperaturen steigt, d.h. von 150 bis 300 K, mit den Messwerten überein. Im Bereich tieferer Temperaturen stellte sich experimentell eine Sättigung der Leerlaufspannung ein. Hier würde man unter der Annahme, dass die Fitparameter effektive Zustandsdichte und Bandlücke temperaturunabhängig sind, trotz der gemessenen fallenden Ladungsträgerdichten bei tieferen Temperaturen laut Gleichung nur einen geringeren Anstieg der Leerlaufspannung mit kleineren Temperaturen erwarten. Im Temperaturbereich von 50 bis 150 K kommt es zu einer Sättigung von V_{oc} die in keinem direktem Zusammenhang zu den intrinsischen Eigenschaften der aktiven Schicht steht. Dabei handelt es sich um Energiebarrieren an den Kontakten, was mit Hilfe von makroskopischen Simulationen nachgewiesen werden konnte. Weiterhin wurde festgestellt, dass die Leerlaufspannung im Sättigungsfall genau dem sogenannten eingebauten Potential (engl. *Built-In Potential*) entspricht. Die Differenz zwischen dem eingebauten Potential und der Bandlücke, welchen man häufig aus der Extrapolation des linearen Leerlaufspannungsbereichs auf $T=0$ K abliest, entspricht dabei der Summe der Energiebarrieren an beiden Kontakten.

Mit der Erkenntnis, dass für nicht kontaktlimitierte Solarzellen ein direkter Zusammenhang zwischen der Leerlaufspannung und der zugehörigen Ladungsträgerdichte besteht war es möglich sich einem anderen heiß diskutiertem Thema der OPV zu widmen: der Rekombination von generierten Ladungsträgern in der aktiven Schicht. In mehreren Publikationen wurde berichtet, dass die Rekombinationsrate proportional zur Ladungsträgerdichte mit einem Exponenten größer zwei ist, wobei der Exponent oftmals Rekombinationsordnung genannt wird. Die Rekombinationsmechanismen nach Shockley-Read-Hall (SRH) bzw. Langevin würden allerdings nur Rekombinationsordnungen von 1 bzw. 2 oder bei einem gleichzeitigen Vorkommen beider Typen einen Wert zwischen 1 und 2 erwarten lassen. Zu diesem Phänomen existieren zwei Erklärungen in der Literatur, die darauf beruhen, dass die Rekomb-

9. Zusammenfassung

bination hauptsächlich vom Typ Langevinrekombination ist. Die eine basiert auf dem Ansatz, dass es Fallenzustände für entsprechende Ladungsträger in separaten Phasen gibt, d.h. Elektronen in Akzeptorphasen und Löcher in Donatorphasen, was in einer verzögerten Rekombination der Ladungsträger an der Grenzfläche beider Phasen führt und damit zu einer höheren Rekombinationsordnung als 2. Die andere Theorie steckt die erhöhte Ladungsträgerdichteabhängigkeit der Rekombinationsrate in den sogenannten Rekombinationsvorfaktor. Die Ladungsträgerdichteabhängigkeit dieses Faktors wird dann mit der Abhängigkeit der Mobilität von der Ladungsträgerdichte erklärt. Um Aufschluss zu erhalten, welche Theorie zu favorisieren ist, wurde sowohl die Ladungsträgerdichteabhängigkeit der Mobilität als auch des Rekombinationsvorfaktors gemessen. Dazu wurden am Referenzsystem P3HT:PC₆₁BM als auch an PTB7:PC₇₁BM, das kommerzielle erhältliche Materialsystem welches die höchste Effizienz liefert, Ladungsextraktionsmessungen sowie Strom-Spannungskennlinien für verschiedene Temperaturen und Beleuchtungsstärken durchgeführt. Es konnte gezeigt werden, dass für das System P3HT:PC₆₁BM bei Raumtemperatur die Ladungsträgerdichteabhängigkeit der Mobilität fast komplett derer des Rekombinationsvorfaktors entspricht. Für tiefere Temperaturen wird allerdings die Diskrepanz zwischen den Ladungsträgerdichteabhängigkeiten immer größer, welches dort immer stärker die Theorie der Störstellen im phasenseparierten System untermauert. Im Materialsystem PTB7:PC₇₁BM ist schon für Raumtemperatur die erhöhte Rekombinationsordnung nicht durch die Ladungsträgerdichteabhängigkeit der Mobilität zu erklären. Als Schlussfolgerung kann man festhalten, dass beide Theorien ihre Berechtigung haben und deren jeweiliger Einfluss stark von der Temperatur und dem Materialsystem abhängig ist. Da auch die Ladungsträgerdichteabhängigkeit der Mobilität ihren Ursprung in Störstellen hat, ist zu erwähnen, dass Rekombinationsordnungen größer 2 in allen ungeordneten Halbleitern vorkommen sollten.

Nach diesen Erkenntnissen wurden zusätzliche Störstellen in Solarzellen eingebaut um deren Einfluss auf die charakteristischen Kenngrößen sowie Rekombinationsordnung und -typ zu untersuchen. Um das zu erreichen wurde eine Solarzelle synthetischer Luft ausgesetzt (im Dunkeln und unter Beleuchtung), was zu einer Erhöhung der Störstellenkonzentration führt bzw. Solarzellen hergestellt, bei denen in die aktive Schicht aus P3HT:PC₆₁BM zusätzlich in geringen Konzentrationen TCNQ beigefügt wurde. Diese Moleküle fungieren wegen ihrer niedrigeren LUMO Levels als Elektronenstörstellen. Bei der sauerstoffdegradierten Solarzelle verhielten sich die charakteristischen Kenngrößen ähnlich zu in der Literatur berichteten Ergebnissen. Während die Leerlaufspannung im Falle von Dunkeldegradation nicht beeinflusst wird, nimmt der Füllfaktor sogar leicht zu, beide sinken allerdings im Falle von Sauerstoffdegradation unter Beleuchtung. Am stärksten wird die Kurzschlussstromdichte beeinflusst, welche sowohl bei Dunkel- als auch Helldegradation abnimmt. Die Rekombinationsordnung wurde hierfür aus einer Kombination von Leerlaufspannungstransienten und Messungen der Abhängigkeit der Ladungsträgerdichte von der Leerlaufspannung bestimmt. Dabei konnte mit erhöhter Degradation ein kontinuierlicher Anstieg der Rekombinationsordnung von 2.4 auf mehr als 5 beobachtet werden. Um eine Aussage über den Rekombinationstyp zu treffen wurde der Idealitätsfaktor aus der Abhängigkeit der Leerlaufspannung von der Beleuchtungsstärke bestimmt. Bei reiner SRH Rekombination, also Rekombination direkt über Störstellen, erwartet man einen theoretischen Idealitätsfaktor von 2, bei Langevin Rekombination einen Wert von 1, kommen beide Typen in einem System gleichzeitig vor, einen Wert zwischen 1 und 2. Da mit steigender Degradationsdauer die Anzahl der Störstellen in der aktiven Schicht steigt, wurde erwartet, dass der Ide-

alitätsfaktor mit zunehmender Degradationszeit steigt, was einen erhöhten Einfluss von SRH-Rekombination in Relation zur Langevin Rekombination bedeutet. Dieses theoretisch erwartete Ergebnis konnte Anhand der Messungen bestätigt werden. Ein ähnliches Bild ergab sich für die Solarzellen mit TCNQ als extrinsische Störstellen. In dieser Messreihe sanken alle charakteristischen Kenngrößen mit erhöhter TCNQ Konzentration, wobei der stärkste Einfluss auch hier bei der Kurzschlussstromdichte festzustellen war. In den Rekombinationsuntersuchungen ergab sich ein zur sauerstoffdegradierten Zelle konsistentes Bild. Sowohl die Rekombinationsordnung stieg mit höherem TCNQ Gehalt, als auch der Idealitätsfaktor. Zusammenfassend kann also behauptet werden, dass Störstellen einen großen Einfluss auf die charakteristischen Kenngrößen und damit auf die Effizienz von organischen Solarzellen haben.

Zuletzt wurde ein Phänomen untersucht, welches zu Tage treten kann, wenn man z.B. die Kontakte der Solarzellen verändert. Dabei handelt es sich um s-förmige Strom-Spannung Kennlinien die bei der Vermessung von Solarzellen unter Beleuchtung auftreten. Da solche Solarzellen eine stark verringerte Effizienz besitzen, ist es wichtig den dahinterstehenden physikalischen Mechanismus zu identifizieren. Im Rahmen dieser Arbeit konnte eine reduzierte Oberflächenrekombinationsgeschwindigkeit als Ursache ausgemacht werden. Diese anfängliche Annahme konnte sowohl experimentell als auch anhand von Simulationen gestützt werden. Um das zu erreichen, war das reproduzierbare Herstellen solcher Solarzellen unerlässlich, was mit einer speziellen Plasmabehandlung des ITO Kontaktes erreicht wurde. Die gemessenen IV-Kennlinien solcher Solarzellen konnten anhand von makroskopischen Simulationen nachgebildet werden, indem darin die Oberflächenrekombinationsgeschwindigkeit reduziert wurde, wobei man dabei die Oberflächenrekombination von Majoritäts bzw. Minorität-ladungsträgern an den entsprechenden Kontakten unterscheiden muss. Experimentell untermauert werden konnte die Theorie anhand von lichtleistungsabhängigen IV-Kurven bzw. Transienten der Kurzschlussstromdichte und der Leerlaufspannung.

Somit behandelt diese Arbeit eine ausführliche Untersuchung über die Ladungsträgerdichteabhängigkeit der Leerlaufspannung sowie der Rekombinationsmechanismen in organischen Solarzellen und den Einfluss von Störstellen auf diese.

Bibliography

- [1] G. J. Adriaenssens and V. I. Arkhipov. Exciton Formation, Relaxation, and Decay in PCDTBT. *Solid State Commun.*, 103:541, 1997.
- [2] T. Agostinelli, S. Lilliu, J. G. Labram, M. Campoy-Quiles, M. Hampton, E. Pires, J. Rawle, O. Bikondoa, D. D. C. Bradley, T. D. Anthopoulos, J. Nelson, and J. E. Macdonald. Real-time investigation of crystallization and phase-segregation dynamics in p3ht:pcbm solar cells during thermal annealing. *Adv. Funct. Mater.*, 21:1701, 2011.
- [3] V. I. Arkhipov. Charge transport in doped disordered organic materials. University Lecture, 2004.
- [4] C. Arndt. Untersuchung von angeregten Zuständen in Bulk-Heterojunction Polymer/Fulleren-Solarzellen. Master's thesis, TU Ilmenau, 2003.
- [5] N. Banerji, S. Cowan, M. Leclerc, E. Vauthey, and A. J. Heeger. Exciton Formation, Relaxation, and Decay in PCDTBT. *J. Am. Chem. Soc.*, 132:17459, 2010.
- [6] N. Banerji, S. Cowan, E. Vauthey, and A. J. Heeger. Ultrafast Relaxation of the Poly(3-hexylthiophene) Emission Spectrum. *J. Phys. Chem. C*, 115:9726, 2011.
- [7] S. D. Baranovskii, H. Cordes, F. Hensel, and G. Leising. Charge-carrier transport in disordered organic solids. *Phys. Rev. B*, 62:7934, 2000.
- [8] H. Bässler. Charge Transport in Disordered Organic Photoconductors. *phys. stat. sol. (b)*, 175:15, 1993.
- [9] A. Baumann, J. Lorrman, C. Deibel, and V. Dyakonov. Bipolar charge transport in poly(3-hexylthiophene)/methanofullerene blends: A ratio dependent study. *Appl. Phys. Lett.*, 93:252104, 2008.
- [10] A. Baumann, T. J. Savenije, D. H. K. Murthy, M. Heeney, V. Dyakonov, and C. Deibel. Influence of phase segregation on recombination dynamics in organic bulk-heterojunction solar cells. *Adv. Funct. Mater.*, 21:1687, 2011.
- [11] J. C. Blakesley and N. C. Greenham. Charge transfer at polymer-electrode interfaces: The effect of energetic disorder and thermal injection on band bending and open-circuit voltage. *J. Appl. Phys.*, 106:034507, 2009.
- [12] J. C. Blakesley and D. Neher. Relationship between energetic disorder and open-circuit voltage in bulk heterojunction organic solar cells. *Phys. Rev. B*, 84:075210, 2011.

- [13] P. Bouit, D. Rauh, S. Neugebauer, J. L. Delgado, E. D. Piazza, S. Rigaut, O. Maury, C. Andraud, V. Dyakonov, and N. Martin. A "Cyanine-Cyanine" salt exhibiting photovoltaic properties. *Org. Lett.*, 11:4806, 2009.
- [14] C. Brabec, V. Dyakonov, and U. Scherf, editors. *Organic Photovoltaics*. Wiley-VCH, 2008.
- [15] C. J. Brabec, A. Cravino, D. Meissner, N. S. Sariciftci, T. Fromherz, M. T. Rispens, L. Sanchez, and J. C. Hummelen. Origin of the Open Circuit Voltage of Plastic Solar Cells. *Adv. Funct. Mater.*, 11:374, 2001.
- [16] C. J. Brabec, S. Gowrisanker, J. J. M. Halls, D. Laird, S. Jia, and S. P. Williams. Polymer-Fullerene Bulk-Heterojunction Solar Cells. *J. Phys. Chem. C*, 22:3839, 2010.
- [17] C. L. Braun. Electric field assisted dissociation of charge transfer states as a mechanism of photocarrier production. *J. Chem. Phys.*, 80:4157, 1984.
- [18] J.-L. Bredas, J. Norton, J. Cornil, and V. Coropceanu. Molecular Understanding of Organic Solar Cells: The Challenges. *Accounts of Chemical Research*, 42:1691, 2009.
- [19] T. M. Brown, J. S. Kim, R. H. Friend, F. Cacialli, R. Daik, and W. J. Feast. Built-in field electroabsorption spectroscopy of polymer light-emitting diodes incorporating a doped poly(3,4-ethylene dioxythiophene) hole injection layer. *Appl. Phys. Lett.*, 75:1679, 1999.
- [20] D. Cheyuns, J. Poortmans, P. Heremans, C. Deibel, S. Verlaak, B. P. Rand, and J. Genoe. Analytical model for the open-circuit voltage and its associated resistance in organic planar heterojunction solar cells. *Phys. Rev. B*, 77:165332, 2008.
- [21] S. A. Choulis, Y. Kim, J. Nelson, D. D. C. Bradley, M. Giles, M. Shkunov, and I. McCulloch. High ambipolar and balanced carrier mobility in regioregular poly(3-hexylthiophene). *Appl. Phys. Lett.*, 85:3890, 2004.
- [22] T. M. Clarke, F. C. Jamieson, and J. R. Durrant. Transient Absorption Studies of Bimolecular Recombination Dynamics in Polythiophene/Fullerene Blend Films. *J. Phys. Chem. C*, 113:20934, 2009.
- [23] S. R. Cowan, A. Roy, and A. J. Heeger. Recombination in polymer-fullerene bulk heterojunction solar cells. *Phys. Rev. B*, 82:245207, 2010.
- [24] M. T. Dang, L. Hirsch, and G. Wantz. P3HT:PCBM, Best Seller in Polymer Photovoltaic Research. *Adv. Mater.*, 23:3597, 2011.
- [25] C. Deibel, A. Baumann, and V. Dyakonov. Polaron recombination in pristine and annealed bulk heterojunction solar cells. *Appl. Phys. Lett.*, 93:163303, 2008.
- [26] C. Deibel and V. Dyakonov. Polymer-Fullerene Bulk Heterojunction Solar Cells (Review Paper). *Rep. Prog. Phys.*, 73:096401, 2009.
- [27] C. Deibel, D. Mack, J. Gorenflot, A. Schöll, S. Krause, F. Reinert, D. Rauh, and V. Dyakonov. Energetics of excited states in the conjugated polymer poly(3-hexylthiophene). *Phys. Rev. B*, 81:085202, 2010.

- [28] C. Deibel, T. Strobel, and V. Dyakonov. Origin of the Efficient Polaron-Pair Dissociation in Polymer-Fullerene Blends. *Phys. Rev. Lett.*, 103:036402, 2009.
- [29] C. Deibel, T. Strobel, and V. Dyakonov. Role of the Charge Transfer State in Organic Donor-Acceptor Solar Cells. *Adv. Mater.*, 22:4097, 2010.
- [30] C. Deibel, A. Wagenpfahl, and V. Dyakonov. Influence of charge carrier mobility on the performance of organic solar cells. *phys. stat. sol. (RRL)*, 2:175, 2008.
- [31] C. Deibel, A. Wagenpfahl, and V. Dyakonov. Origin of reduced polaron recombination in organic semiconductor devices. *Phys. Rev. B*, 80:075203, 2009.
- [32] J. L. Delgado, E. Espildora, M. Liedtke, A. Sperlich, D. Rauh, A. Baumann, C. Deibel, V. Dyakonov, and N. Martin. Fullerene Dimers (C60/C70) for Energy Harvesting. *Chem. Eur. J.*, 15:13747, 2009.
- [33] V. Dyakonov. The polymer–fullerene interpenetrating network: one route to a solar cell approach. *Physica E*, 14:53, 2002.
- [34] M. A. Faist, P. E. Keivanidis, S. Foster, P. H. Wöbkenberg, T. D. Anthopoulos, D. D. C. Bradley, J. R. Durrant, and J. Nelson. Effect of Multiple Adduct Fullerenes on Charge Generation and Transport in Photovoltaic Blends with Poly(3-hexylthiophene-2,5-diyl). *J. Polym. Sci. Part B: Polym. Phys.*, 49:45, 2011.
- [35] A. Foertig, A. Baumann, D. Rauh, V. Dyakonov, and C. Deibel. Charge carrier concentration and temperature dependent recombination in polymer-fullerene solar cells. *Appl. Phys. Lett.*, 95:052104, 2009.
- [36] J. M. Frost, M. A. Faist, and J. Nelson. Energetic Disorder in Higher Fullerene Adducts: A Quantum Chemical and Voltammetric Study. *Adv. Mater.*, 22:4881, 2010.
- [37] I. R. Gould, D. Noukakis, L. Gomes-Jahn, R. H. Young, J. L. Goodman, and S. Farid. Radiative and nonradiative electron transfer in contact radical-ion pairs. *Chem. Phys.*, 176:439, 1993.
- [38] M. A. Green, K. Emery, Y. Hishikawa, W. Warta, and E. D. Dunlop. Solar cell efficiency tables (Version 41). *Prog. Photovolt: Res. Appl.*, 21:1, 2012.
- [39] N. Grossiord, J. M. Kroon, R. Andriessen, and P. W. Blom. Degradation mechanisms in organic photovoltaic devices. *Org. Electron.*, 13:432, 2012.
- [40] A. S. Grove, editor. *Physics and Technology of Semiconductor Devices*. Wiley, New York, 1967.
- [41] Z.-L. Guan, J. B. Kim, H. Wang, C. Jaye, and D. A. F. Y.-L. Loob. Direct determination of the electronic structure of the poly(3-hexylthiophene):phenyl-[6,6]-C61 butyric acid methyl ester blend. *Org. Electron.*, 11:1779, 2010.
- [42] Y. He, H.-Y. Chen, J. Hou, and Y. Li. Indene-C₆₀ Bisadduct: A New Acceptor for High-Performance Polymer Solar Cells. *J. Am. Chem. Soc.*, 132:1377, 2010.

- [43] Z. He, C. Zhong, X. Huang, W.-Y. Wong, H. Wu, L. Chen, S. Su, and Y. Cao. Simultaneous Enhancement of Open-Circuit Voltage, Short-Circuit Current Density, and Fill Factor in Polymer Solar Cells. *Adv. Mater.*, 23:4636, 2011.
- [44] I. G. Hill, A. Rajagopal, and A. Kahn. Energy-level alignment at interfaces between metals and the organic semiconductor 4,4'-N,N'-dicarbazolyl-biphenyl. *J. Appl. Phys.*, 84:3236, 1998.
- [45] http://www.erneuerbare-energien.de/erneuerbare_energien/windenergie/kurzinfo/doc/4642.php. last accessed January 2013.
- [46] <http://www.kernenergie.de/kernenergie/themen/kernkraftwerke/kernkraftwerke-in-deutschland.php>. last accessed January 2013.
- [47] <http://www.riekemetals.com/component/riekemvc/?view=compound&id=9617>. last accessed January 2013.
- [48] I.-W. Hwang, D. Moses, and A. J. Heeger. Photoinduced Carrier Generation in P3HT/PCBM Bulk Heterojunction Materials. *J. Phys. Chem. B*, 112:4350, 2008.
- [49] G. Juška, K. Arlauskas, J. Stuchlik, and R. Österbacka. Non-Langevin bimolecular recombination in low-mobility materials. *J. Non-Cryst. Sol.*, 352:1167, 2006.
- [50] G. Juška, K. Genevičius, N. Nekrašas, G. Sliaužys, and G. Dennler. Trimolecular recombination in polythiophene: fullerene bulk heterojunction solar cells. *Appl. Phys. Lett.*, 93:143303, 2008.
- [51] J. S. Kim, M. Granström, R. H. Friend, N. Johansson, W. R. Salaneck, R. Daik, W. J. Feast, and F. Cacialli. Indium-tin oxide treatments for single- and double-layer polymeric light-emitting diodes: The relation between the anode physical, chemical, and morphological properties and the device performance. *J. Appl. Phys.*, 84:6859, 1998.
- [52] T. Kirchartz, B. E. Pieters, J. Kirkpatrick, U. Rau, and J. Nelson. Recombination via tail states in polythiophene:fullerene solar cells. *Phys. Rev. B*, 83:115209, 2011.
- [53] J. Kniepert, M. Schubert, J. C. Blakesley, and D. Neher. Photogeneration and Recombination in P3HT/PCBM Solar Cells Probed by Time-Delayed Collection Field Experiments. *Phys. Chem. Lett.*, 2:700, 2011.
- [54] L. J. A. Koster, V. D. Mihailechi, R. Ramaker, and P. W. M. Blom. Device model for the operation of polymer/fullerene bulk heterojunction solar cells. *Phys. Rev. B*, 72:085205, 2005.
- [55] L. J. A. Koster, V. D. Mihailechi, R. Ramaker, and P. W. M. Blom. Light intensity dependence of open-circuit voltage of polymer:fullerene solar cells. *Appl. Phys. Lett.*, 86:123509, 2005.
- [56] L. J. A. Koster, E. C. P. Smits, V. D. Mihailechi, and P. W. M. Blom. Bimolecular recombination in polymer/fullerene bulk heterojunction solar cells. *Appl. Phys. Lett.*, 88:052104, 2006.

- [57] J. E. Kroeze, T. J. Savenije, M. J. W. Vermeulen, and J. M. Warman. Contactless Determination of the Photoconductivity Action Spectrum, Exciton Diffusion Length, and Charge Separation Efficiency in Polythiophene-Sensitized TiO₂ Bilayers. *J. Phys. Chem. B*, 107:7696, 2003.
- [58] A. Kumar, S. Sista, and Y. Yang. Dipole induced anomalous S-shape I-V curves in polymer solar cells. *J. Appl. Phys.*, 105:094512, 2009.
- [59] P. Langevin. Recombinaison et mobilités des ions dans les gaz. *Ann. Chim. Phys.*, 28:433, 1903.
- [60] M. Lenes, G.-J. A. H. Wetzelaer, F. B. Kooistra, S. C. Veestra, J. C. Hummelen, and P. W. M. Blom. Fullerene Bisadducts for Enhanced Open-Circuit Voltages and Efficiencies in Polymer Solar Cells. *Adv. Mater.*, 20:2116, 2008.
- [61] W. L. Leong, S. R. Cowan, and A. J. Heeger. Differential Resistance Analysis of Charge Carrier Losses in Organic Bulk Heterojunction Solar Cells: Observing the Transition from Bimolecular to Trap-Assisted Recombination and Quantifying the Order of Recombination. *Adv. Energy. Mater.*, 1:517, 2011.
- [62] G. Li, V. Shrotriya, Y. Yao, and Y. Yang. Investigation of annealing effects and film thickness dependence of polymer solar cells based on poly(3-hexylthiophene). *J. Appl. Phys.*, 98:043704, 2005.
- [63] Y. Liang, Z. Xu, S.-T. T. J. Xia, Y. Wu, G. Li, C. Ray, and L. Yu. For the Bright Future—Bulk Heterojunction Polymer Solar Cells with Power Conversion Efficiency of 7.4%. *Adv. Mater.*, 22:E135, 2010.
- [64] Y. Liang and L. Yu. A New Class of Semiconducting Polymers for Bulk Heterojunction Solar Cells with Exceptionally High Performance. *Accounts Chem. Res.*, 43:1227, 2010.
- [65] M. Liedtke, A. Sperlich, H. Kraus, A. Baumann, C. Deibel, M. J. M. Wirix, J. Loos, C. M. Cardona, and V. Dyakonov. Triplet Exciton Generation in Bulk-Heterojunction Solar Cells Based on Endohedral Fullerenes. *J. Am. Chem. Soc.*, 133:9088, 2011.
- [66] M. Limpinsel, A. Wagenpfahl, M. Mingeback, C. Deibel, and V. Dyakonov. Photocurrent in bulk heterojunction solar cells. *Phys. Rev. B*, 81:085203, 2010.
- [67] J. Liu, Y. Shi, and Y. Yang. Solvation-Induced Morphology Effects on the Performance of Polymer-Based Photovoltaic Devices. *Adv. Funct. Mater.*, 11:420, 2001.
- [68] L. Liu and G. Li. Modeling and Simulation of Organic Solar Cells. *IEEE Nanotech. Mat. a. Dev. Conf.*, page 334, 2010.
- [69] L. Lüer, H.-J. Egelhaaf, D. Oelkrug, G. Cerullo, G. Lanzani, B.-H. Huisman, and D. de Leeuw. Oxygen-induced quenching of photoexcited states in polythiophene films. *Org. Electr.*, 5:83, 2004.
- [70] R. C. I. MacKenzie, T. Kirchartz, G. F. A. Dibb, and J. Nelson. Modeling Nongeminate Recombination in P3HT:PCBM Solar Cells. *J. Phys. Chem. C*, 115:9806, 2011.

- [71] M. M. Mandoc, F. B. Kooistra, J. C. Hummelen, B. de Boer, and P. W. M. Blom. Effect of traps on the performance of bulk heterojunction organic solar cells. *Appl. Phys. Lett.*, 91:263505, 2007.
- [72] R. Marcus. Relation between Charge Transfer Absorption and Fluorescence Spectra and the Inverted Region. *J. Phys. Chem.*, 93:3078, 1989.
- [73] A. Maurano, R. Hamilton, C. G. Shuttle, A. M. Ballantyne, J. Nelson, B. O'Regan, W. Zhang, I. McCulloch, H. Azimi, M. Morana, C. J. Brabec, and J. R. Durrant. Recombination Dynamics as a Key Determinant of Open Circuit Voltage in Organic Bulk Heterojunction Solar Cells: A Comparison of Four Different Donor Polymers. *Adv. Mater.*, 22:4987, 2010.
- [74] V. D. Mihailesti, P. W. M. Blom, J. C. Hummelen, and M. T. Rispens. Cathode dependence of the open-circuit voltage of polymer:fullerene bulk heterojunction solar cells. *J. Appl. Phys.*, 94:6849, 2003.
- [75] V. D. Mihailesti, J. K. J. van Duren, P. W. M. Blom, J. C. Hummelen, R. A. J. Janssen, J. M. Kroon, M. T. Rispens, W. J. H. Verhees, and M. M. Wienk. Electron transport in a methanofullerene. *Adv. Funct. Mater.*, 13:43, 2003.
- [76] A. Miller and E. Abrahams. Impurity Conduction at Low Concentrations. *Phys. Rev.*, 120:745, 1960.
- [77] D. Monroe. Hopping in exponential band tails. *Phys. Rev. Lett.*, 54:146, 1985.
- [78] I. Montanari, A. F. Nogueira, J. Nelson, J. R. Durrant, C. Winder, M. A. Loi, N. S. Sariciftci, and C. Brabec. Transient optical studies of charge recombination dynamics in a polymer/fullerene composite at room temperature. *Appl. Phys. Lett.*, 81:3001, 2002.
- [79] J. Nelson. Diffusion-limited recombination in polymer-fullerene blends and its influence on photocurrent collection. *Phys. Rev. B*, 67:155209, 2003.
- [80] J. Noolandi. Multiple-trapping model of anomalous transit-time dispersion in α -Se. *Phys. Rev. B*, 16:4466, 1977.
- [81] H. Ohkita, S. Cook, Y. Astuti, W. Duffy, S. Tierney, W. Zhang, M. Heeney, I. McCulloch, J. Nelson, D. D. C. Bradley, and J. R. Durrant. Charge Carrier Formation in Polythiophene/Fullerene Blend Films Studied by Transient Absorption Spectroscopy. *J. Am. Chem. Soc.*, 130:3030, 2008.
- [82] L. Onsager. Initial recombination of ions. *Phys. Rev.*, 54:554, 1938.
- [83] W. F. Pasveer, J. Cottaar, C. Tanase, R. Coehoorn, P. A. Bobbert, P. W. M. Blom, D. M. de Leeuw, and M. A. J. Michels. Unified Description of Charge-Carrier Mobilities in Disordered Semiconducting Polymers. *Phys. Rev. Lett.*, 94:206601, 2005.
- [84] L. S. C. Pingree, B. A. MacLeod, and D. S. Ginger. The Changing Face of PEDOT:PSS Films: Substrate, Bias, and Processing Effects on Vertical Charge Transport. *J. Phys. Chem. C*, 112:7922, 2008.

- [85] M. Pope and C. E. Swenberg, editors. *Electronic Processes in Organic Crystals and Polymers*. Oxford University Press, 2nd edition, 1999.
- [86] V. Quaschnig. *Regenerative Energiesysteme*. Hanser Verlag München, 6th edition, 2009.
- [87] C. M. Ramsdale, J. A. Barker, A. C. Arias, J. D. MacKenzie, R. H. Friend, and N. C. Greenham. The origin of the open-circuit voltage in polyfluorene-based photovoltaic devices. *J. Appl. Phys.*, 92:4266, 2002.
- [88] U. Rau. Reciprocity relation between photovoltaic quantum efficiency and electroluminescent emission of solar cells. *Phys. Rev. B*, 76:085303, 2007.
- [89] D. Rauh, C. Deibel, and V. Dyakonov. Charge Density Dependent Nongeminate Recombination in Organic Bulk Heterojunction Solar Cells. *Adv. Funct. Mater.*, 22:3371, 2012.
- [90] D. Rauh, A. Wagenpfahl, C. Deibel, and V. Dyakonov. Relation of open circuit voltage to charge carrier density in organic bulk heterojunction solar cells. *Appl. Phys. Lett.*, 98:133301, 2011.
- [91] J. Schafferhans, A. Baumann, C. Deibel, and V. Dyakonov. Trap distribution and the impact of oxygen-induced traps on the charge transport in poly(3-hexylthiophene). *Appl. Phys. Lett.*, 93:093303, 2008.
- [92] J. Schafferhans, A. Baumann, A. Wagenpfahl, C. Deibel, and V. Dyakonov. Oxygen doping of P3HT:PCBM blends: Influence on trap states, charge carrier mobility and solar cell performance. *Org. Electr.*, 11:1693, 2010.
- [93] J. Schafferhans, C. Deibel, and V. Dyakonov. Electronic Trap States in Methanofullerenes. *Adv. Energy Mater.*, 1:655, 2011.
- [94] M. C. Scharber, D. Mühlbacher, M. Koppe, P. Denk, C. Waldauf, A. J. Heeger, and C. J. Brabec. Design Rules for Donors in Bulk-Heterojunction Solar Cells – Towards 10 % Energy-Conversion Efficiency. *Adv. Mater.*, 18:789, 2006.
- [95] P. Schilinsky, C. Waldauf, and C. J. Brabec. Recombination and loss analysis in polythiophene based bulk heterojunction photodetectors. *Appl. Phys. Lett.*, 81:3885, 2002.
- [96] K. Schulze, C. Uhrich, R. Schüppel, K. Leo, M. Pfeiffer, E. Brier, E. Reinold, and P. Bäuerle. Efficient Vacuum-Deposited Organic Solar Cells Based on a New Low-Bandgap Oligothiophene and Fullerene C₆₀. *Adv. Mater.*, 18:2872, 2006.
- [97] P. E. Shaw, A. Ruseckas, and I. D. W. Samuel. Exciton Diffusion Measurements in Poly(3-hexylthiophene). *Adv. Mater.*, 20:3516, 2008.
- [98] C. G. Shuttle, R. Hamilton, J. Nelson, B. C. O'Regan, and J. R. Durrant. Measurement of Charge-Density Dependence of Carrier Mobility in an Organic Semiconductor Blend. *Adv. Funct. Mater.*, 20:698, 2010.

- [99] C. G. Shuttle, R. Hamilton, B. C. O'Regan, J. Nelson, and J. R. Durrant. Charge-density-based analysis of the current-voltage response of polythiophene/fullerene photovoltaic devices. *Proc. Natl. Aca. Sci.*, 107:16448, 2010.
- [100] C. G. Shuttle, B. O'Regan, A. M. Ballantyne, J. Nelson, D. D. C. Bradley, J. de Mello, and J. R. Durrant. Experimental determination of the rate law for charge carrier decay in a polythiophene: fullerene solar cell. *Appl. Phys. Lett.*, 92:093311, 2008.
- [101] C. G. Shuttle, N. D. Treat, J. D. Douglas, J. M. J. Fréchet, and M. L. Chabinyc. Deep Energetic Trap States in Organic Photovoltaic Devices. *Adv. Energy Mater.*, 2:111, 2011.
- [102] H. Sirringhaus, N. Tessler, and R. H. Friend. Integrated Optoelectronic Devices Based on Conjugated Polymers. *Science*, 280:1741, 1998.
- [103] P. Stallinga. Electronic Transport in Organic Materials: Comparison of Band Theory with Percolation/(Variable Range) Hopping Theory. *Adv. Mater.*, 23:3356, 2011.
- [104] R. A. Street, S. Cowan, and A. J. Heeger. Experimental test for geminate recombination applied to organic solar cells. *Phys. Rev. B*, 82:121301(R), 2010.
- [105] T. Strobel, C. Deibel, and V. Dyakonov. Role of Polaron Pair Diffusion and Surface Losses in Organic Semiconductor Devices. *Phys. Rev. Lett.*, 105:266602, 2010.
- [106] T. Stübinger and W. Brütting. Exciton diffusion and optical interference in organic donor–acceptor photovoltaic cells. *J. Appl. Phys.*, 90:3632, 2001.
- [107] C. Tanase, E. J. Meijer, P. M. Blom, and D. M. de Leeuw. Unification of the Hole Transport in Polymeric Field-Effect Transistors and Light-Emitting Diodes. *Phys. Rev. Lett.*, 91:216601, 2003.
- [108] N. Tessler, Y. Preezant, N. Rappaport, and Y. Roichman. Charge Transport in Disordered Organic Materials and Its Relevance to Thin-Film Devices: A Tutorial Review. *Adv. Mater.*, 21:2741, 2009.
- [109] W. Tress, A. Petrich, M. Hummert, M. Hein, K. Leo, and M. Riede. Imbalanced mobilities causing S-shaped IV curves in planar heterojunction organic solar cells. *Appl. Phys. Lett.*, 98:063301, 2011.
- [110] L. Tzabari and N. Tessler. Shockley–Read–Hall recombination in P3HT:PCBM solar cells as observed under ultralow light intensities. *J. Appl. Phys.*, 109:064501, 2011.
- [111] C. Uhrich, R. Schueppel, A. Petrich, M. Pfeiffer, K. Leo, E. Brier, P. Kilickiran, and P. Baeuerle. Organic Thin–Film Photovoltaic Cells Based on Oligothiophenes with Reduced Bandgap. *Adv. Funct. Mater.*, 17:2991, 2007.
- [112] C. Uhrich, D. Wynands, S. Olthof, M. K. Riede, K. Leo, S. Sonntag, B. Maennig, and M. Pfeiffer. Origin of open circuit voltage in planar and bulk heterojunction organic thin–film photovoltaics depending on doped transport layers. *J. Appl. Phys.*, 104:043107, 2008.

-
- [113] K. Vandewal, A. Gadisa, W. D. Oosterbaan, S. Bertho, F. Banishoeib, I. V. Severen, L. Lutsen, T. J. Cleij, D. Vanderzande, and J. V. Manca. The Relation Between Open-Circuit Voltage and the Onset of Photocurrent Generation by Charge-Transfer Absorption in Polymer : Fullerene Bulk Heterojunction Solar Cells. *Adv. Funct. Mater.*, 18:2064, 2008.
- [114] K. Vandewal, K. Tvingstedt, A. Gadisa, O. Inganäs, and J. V. Manca. Relating the open-circuit voltage to interface molecular properties of donor:acceptor bulk heterojunction solar cells. *Phys. Rev. B*, 81:125204, 2010.
- [115] E. von Hauff, J. Parisi, and V. Dyakonov. Investigations of the effects of tempering and composition dependence on charge carrier field effect mobilities in polymer and fullerene films and blends. *J. Appl. Phys.*, 100:043702, 2006.
- [116] A. Wagenpfahl, C. Deibel, and V. Dyakonov. Organic Solar Cell Efficiencies under the Aspect of Reduced Surface Recombination Velocities. *IEEE J. Sel. Top. Quantum Electron.*, 16:1759, 2010.
- [117] A. Wagenpfahl, D. Rauh, M. Binder, C. Deibel, and V. Dyakonov. S-shaped current-voltage characteristics of organic solar devices. *Phys. Rev. B*, 82:115306, 2010.
- [118] C. C. Wu, C. I. Wu, J. C. Sturm, and A. Kahn. Surface modification of indium tin oxide by plasma treatment: An effective method to improve the efficiency, brightness, and reliability of organic light emitting devices. *Appl. Phys. Lett.*, 70:1348, 1997.
- [119] G. Zhao, Y. He, and Y. Li. 6.5% Efficiency of Polymer Solar Cells Based on poly(3-hexylthiophene) and Indene-C₆₀ Bisadduct by Device Optimization . *Adv. Mater.*, 22:4355, 2011.

A. List of Abbreviations

Abbreviation	Description
AFM	atomic force microscope
Al	aluminium
AM	air mass
BHJ	bulk heterojunction solar cell
bisPC ₆₁ BM	bis[6,6]-phenyl C61 butyric acid methyl ester
C	carbon
Ca	calcium
CB	conduction band
CE	charge extraction
CIGS	copper indium gallium selenide
CIS	copper indium selenide
CO ₂	carbon dioxide
Cr	chromium
CT	charge transfer
Cu	copper
DA	donor-acceptor
DOS	density of states
DSSC	dye sensitized solar cells
EL	electroluminescence
EQE	external quantum efficiency
FET	field effect transistor
GDM	Gaussian disorder model
H ₂ O	water
HCL	hydrochloric acid
He	helium
HNO ₃	nitric acid
HOMO	highest occupied molecular orbital
HTL	hole transport layer
HTR	high temperature regime

A. List of Abbreviations

Abbreviation	Description
HQ	high quality
ICBA	indene-C60 bisadduct
ITO	indium tin oxide
IV	current–voltage
LED	light emitting diode
LTR	low temperature regime
LUMO	lowest unoccupied molecular orbital
MDMO-PPV	poly(2-methoxy-5-(3',7'-dimethyloctyloxy)-1,4-phenylenevinylene)
MIM	metal–insulator–metal
mpp	maximum power point
MTR	multiple trapping and release
N	nitrogen
Na	sodium
O	oxygen
OPV	organic photovoltaics
OSC	organic solar cell
P3HT	poly(3-hexylthiophene-2,5-diyl)
PBDTTPD	poly(di(2-ethylhexyloxy)benzo[1,2-b:4,5-b \bar{O}]dithiophene-co-octylthieno[3,4-c]pyrrole-4,6-dione)
PC ₆₁ BM	[6,6]-phenyl C61 butyric acid methyl ester
PC ₇₁ BM	[6,6]-phenyl C71 butyric acid methyl ester
PCDTBT	poly[[9-(1-octylonyl)-9H-carbazole-2,7-diyl]-2,5-thiophenediyl-2,1,3-benzothiadiazole-4,7-diyl-2,5-thiophenediyl]
PEDOT:PSS	poly(3,4-ethylenedioxythiophene):(polystyrenesulfonate)
PGO	Präzisions Glas & Optik GmbH
PL	photoluminescence
PPV	poly(p-phenylenevinylene)
PTB7	poly[[4,8-bis[(2-ethylhexyl)oxy]benzo[1,2-b:4,5-b \bar{O}]dithiophene-2,6-diyl][3-fluoro-2-[(2-ethylhexyl)carbonyl]thieno[3,4-b]thiophenediyl]]
PV	power–voltage
RMS	root mean squared
rpm	rounds per minute
SC	solar cell
SiO ₂	silicon dioxide
SRH	Shockley–Read–Hall
STC	standard testing conditions
TCNQ	7,7,8,8-tetracyanoquinodimethane
TCO	transparent conductive oxide
TSC	thermally stimulated current

Abbreviation	Description
USB	ultrasonic bath
UV	ultraviolet
VB	valence band
XRD	X-ray diffraction

B. List of Symbols

Symbol	Description	Unit
a	exciton binding distance	m
A	active sample area	m ²
α	exponent of charge carrier dependence of mobility	—
$BB_{acceptor}$	band bending of the electrostatic potential in the acceptor	eV
BB_{donor}	band bending of the electrostatic potential in the donor	eV
β	exponent of charge carrier dependence of recombination prefactor	—
c	speed of light in vacuum	m/s
c_n	slope of $d\ln(n/dV_{oc})$	not defined
C	capacitance	F
d	active layer thickness	m
δ	exponent of light intensity dependence of generation rate	
E	energy	eV
E_0	characteristic energy (exponential density of states)	eV
ΔE	activation energy	eV
E_B	exciton binding energy	eV
E_{CT}	energy of the charge transfer state	eV
E_F	Fermi energy	eV
E_g	effective band gap	eV
$E_{g,eff}$	reduced effective band gap due to disorder	eV
$E_{g,eff,d}$	reduced effective band gap due to disorder in a degraded solar cell	eV
$E_{g,eff,nd}$	reduced effective band gap due to disorder in a non degraded solar cell	eV
E_{HOMO}	energy of highest occupied molecular orbital	eV
$E_{HOMO_{donor}}$	energy of highest occupied molecular orbital of the donor	eV
E_{LUMO}	energy of lowest unoccupied molecular orbital	eV
$E_{LUMO_{acceptor}}$	energy of lowest unoccupied molecular orbital of the acceptor	eV
$E_{LUMO_{donor}}$	energy of lowest unoccupied molecular orbital of the donor	eV
E_{tr}	transport energy	eV
$E_{tr,LUMO}$	transport energy in LUMO level	eV

B. List of Symbols

Symbol	Description	Unit
$E_{tr,d}$	transport energy in the HOMO level in a degraded solar cell	eV
$E_{tr,nd}$	transport energy in the HOMO level in a non degraded solar cell	eV
EQE	external quantum efficiency	—
EQE_{EL}	external quantum efficiency of the electroluminescence	—
EQE_{PV}	photovoltaic external quantum efficiency	—
EQE_{rc}	external quantum efficiency of reference solar cell	—
EQE_{tc}	external quantum efficiency of test solar cell	—
ϵ	absolute permittivity	F/m
ϵ_i	energy of initially occupied localized state	eV
ϵ_j	energy of localized target state	eV
ϵ_r	relative dielectric constant	—
η	solar cell efficiency	—
f	factor describing the interaction between donor and acceptor	m^2J^2
F	electric field	V/m
FF	fill factor	—
$g(E)$	density of states distribution	$m^{-3} eV^{-1}$
$g_e(E)$	electron density of states distribution	$m^{-3} eV^{-1}$
$g_h(E)$	hole density of states distribution	$m^{-3} eV^{-1}$
G	generation rate	$m^{-3}s^{-1}$
ΔG	free energy difference of charge separation	eV
γ	Langevin recombination prefactor	m^3/s
γ_0	inverse localization radius (Miller–Abrahams Equation)	m^{-1}
γ_A	modified Langevin recombination prefactor (Adriaenssens <i>et al.</i>)	m^3/s
γ_D	modified Langevin recombination prefactor (Deibel <i>et al.</i>)	m^3/s
γ_K	modified Langevin recombination prefactor (Koster <i>et al.</i>)	m^3/s
h	Planck's constant	Js
I	current	A
I_{LED}	current to drive LED	A
I_{mpp}	current at maximum power point	A
I_{ph}	photocurrent	A
I_{sc}	short circuit current	A
$I_{sc,rc,AM1.5g}$	short circuit current of reference solar cell under AM1.5g spectrum	A
$I_{sc,rc,ss}$	short circuit current of reference solar cell under solar simulator	A
$I_{sc,S1133}$	short circuit current of reference solar cell S1133	A
j	current density	A/m^2
j_0	dark saturation current density	A/m^2
j_{drift}	drift current density	A/m^2
j_{mpp}	current density at maximum power point	A/m^2
j_n	current density	A/m^2

Symbol	Description	Unit
j_{ph}	photocurrent density	A/m ²
$j_{sat,ph}$	saturated photocurrent density	A/m ²
j_{sc}	short circuit current density	A/m ²
$j_{sc,AM1.5g}$	short circuit current density under AM1.5g spectrum	A/m ²
J	surface recombination rate	A/m ²
k	recombination prefactor	not defined
k_B	Boltzmann constant	eV/K
k_d	polaron pair dissociation rate	s ⁻¹
k_f	polaron pair decay rate	s ⁻¹
k_r	recombination rate of free charges to polaron pairs / monomolecular recombination rate	s ⁻¹
k_λ	recombination prefactor	not defined
κ	exponent of light intensity dependence of photocurrent	—
L	active layer thickness	m
L_D	exciton diffusion length	m
λ	wavelength	m
λ_0	reorganization energy (Marcus theory)	eV
$\lambda + 1$	recombination order	—
$\lambda_l + 1$	recombination order, determined from n(t) at longer times	—
$\lambda_G + 1$	recombination order, where the recombination rate was calculated by the generation rate	—
M	mismatch	—
μ	mobility	m ² /Vs
μ_0	mobility of free charge carriers	m ² /Vs
μ_{drift}	drift mobility	m ² /Vs
$\tilde{\mu}$	value proportional to mobility	Am
μ_n	electron mobility	m ² /Vs
μ_p	hole mobility	m ² /Vs
n	charge carrier density / electron density	m ⁻³
n_0	extrapolated charge carrier density for $V_{oc}=0$ V	m ⁻³
n_c	free (conductive) charge carrier / electron density	m ⁻³
n_{dev}	charge carrier density stored in device	m ⁻³
n_{extr}	extracted charge carrier density	m ⁻³
n_i	intrinsic charge carrier density	m ⁻³
n_{id}	ideality factor	—
n_{loss}	charge carrier density lost during extraction	m ⁻³
n_t	trapped charge carrier / electron density	m ⁻³
n_{th}	thermally activated charge carrier density	m ⁻³

B. List of Symbols

Symbol	Description	Unit
N_c	effective density of states	m^{-3}
N_e	density of states of electrons	m^{-3}
N_h	density of states of holes	m^{-3}
$N_{t,e}$	exponential density of states of electrons	m^{-3}
$N_{t,h}$	exponential density of states of holes	m^{-3}
N_t	trap density	m^{-3}
ν_0	attempt-to-escape frequency	s^{-1}
p	hole density	m^{-3}
p_c	free (conductive) hole density	m^{-3}
p_t	trapped hole density	m^{-3}
P	polaron pair dissociation probability	—
P_L	radiant power of incident light	W
P_{max}	maximum electrical power of the solar cell	W
P_x	radiant power of incident light	W
ϕ_n	quasi Fermi level of electrons	eV
ϕ_p	quasi Fermi level of holes	eV
$\Phi_{AM1.5g}$	spectral irradiance of AM1.5g spectrum	$\text{Wm}^{-2}\text{nm}^{-1}$
Φ_{SS}	spectral irradiance of solar simulator	$\text{Wm}^{-2}\text{nm}^{-1}$
Φ_d	effective energy barrier in a degraded solar cell	eV
Φ_{nd}	effective energy barrier in a non degraded solar cell	eV
ϕ_{BB}^T	black body radiation at a temperature T	$\text{Wm}^{-2}\text{s}^{-1}$
Φ_L	radiant power density of incident light	W/m^2
ϕ_n	injection barriers of contacts for electrons	eV
ϕ_p	injection barriers of contacts for holes	eV
q	elementary charge	C
Q_{extr}	extracted charge	C
Q_{plates}	charge stored on plates (capacitor)	C
R	recombination rate	$\text{m}^{-3}\text{s}^{-1}$
R_{ij}	spatial distance between initial and target state	m
R_p	parallel resistance	Ω
R_s	serial resistance	Ω
R_{Voc}	resistance at V_{oc}	Ω
ρ	density of occupied states distribution	$\text{m}^{-3} \text{eV}^{-1}$
S	surface recombination velocity	ms^{-1}
S_n^a	surface recombination velocity of electrons at the anode	ms^{-1}
S_p^a	surface recombination velocity of holes at the anode	ms^{-1}
σ	width of Gaussian density of states	eV
σ_d	width of Gaussian density of states in a degraded solar cell	eV
σ_{nd}	width of Gaussian density of states in a non degraded solar cell	eV

Symbol	Description	Unit
t	time	s
Δt	time intervall	s
t_0	lifetime of free charge carriers until they are trapped	s
t_{end}	specific time (charge extraction)	s
T	temperature	K
τ_0	exciton lifetime	s
v_d	drift velocity	ms^{-1}
V	applied voltage	V
V_{appl}	applied voltage	V
V_{mpp}	voltage at maximum power point	V
V_s	sample volume	m^3
V_{oc}	open circuit voltage	V
ΔV_{oc}	open circuit voltage difference	V
ΔV_{nonrad}	loss in open circuit voltage due non radiative recombination	V
ΔV_{rad}	loss in open circuit voltage due radiative recombination	V
W_{ij}	Miller–Abrahams hopping rate	s^{-1}
x	spatial position	m
ζ	reduction factor (Langevin recombination)	—
∞	infinity	—

C. Acknowledgement

Obwohl eine Dissertation selbstständig verfasst werden muss, ist es dennoch nicht ohne Hilfe verschiedenster Personen möglich, die dahintersteckende Arbeit, die oftmals ein Vielfaches dessen beträgt, was in der tatsächlich abgegeben Schrift zum Vorschein kommt, zu bewältigen. Deshalb ist es mir eine Freude einigen Personen in den folgenden Zeilen meinen Dank auszusprechen.

Zuerst gebührt mein Dank natürlich Prof. Vladimir Dyakonov, der es mir nicht nur ermöglicht hat diese Arbeit überhaupt zu erstellen, sondern mir auch durch seine kritische Auseinandersetzung mit meinen Arbeiten beigebracht hat, vor allem wenn es um Publikationen oder Vorträge ging, wie man den Fokus auf die Präsentation der Arbeit zu legen hat um erfolgreich zu sein.

Bei fachlichen Diskussion ist natürlich Dr. Carsten Deibel zuerst zu nennen, dessen Tür immer offen stand um dabei zu helfen die neuesten Ergebnisse, die einem zu Beginn untypisch erschienen, mit viel Einfallsreichtum zu analysieren und dabei neue Erkenntnisse zu gewinnen. Wie er es geschafft hat, bei so vielen zu betreuenden Doktoranden den Überblick zu behalten, so schnell auf Emails — zu jeder Tages- und Nachtzeit — zu antworten und auch Arbeiten jedweder Art zu korrigieren, ist mir noch immer ein Rätsel. Chapeau Carsten! Auf ähnlich hoher Stufe bezüglich fachlicher Hilfe steht natürlich Dr. Julia Rauh, aber da sie, wie man am Nachnamen erkennen kann, auch noch anderweitig mit mir in Kontakt steht, bekommt sie am Ende noch einen extra Absatz um mit Dank überhäuft zu werden :-).

Am Lehrstuhl gab es natürlich eine lange Liste an Kollegen denen ich danken möchte :

- Meine Diplomanden in chronologischer Reihenfolge: Stefan Geißendörfer, Alexander Förtig und Michael Binder mit denen ich viele nette Stunden im Labor verbracht habe und ich durch die jeweiligen sehr verschiedenen Themengebiete die Möglichkeit hatte mich mit verschiedensten Aspekten der organischen Photovoltaik auseinanderzusetzen.
- Meine Zimmerkollegen Dr. Markus Mingeback, Dr. Andreas Baumann und Volker Lorrmann. Vielen Dank für die vielen Diskussionen, ob fachlich oder nicht, es hat immer Spass mit euch gemacht! Vor allem während Fussball WM bzw. EM, Olympia, Montags nach Bundesliga,...
- Besonderer Dank geht an Alexander Wagenpfahl, meinem Lieblingskoautor und persönlichem Simulant. Wenn es um Simulationen für meine Arbeit ging war er immer bereit den Rechner für mich anzuwerfen bzw. mir zu helfen diese selbst durchzuführen. Auch bei der Diskussion theoretischer Grundlagen war er immer zur Stelle, genauso wie Jens Lorrmann, unser zweiter Simulator.
- Den Kollegen von der photophysikalischen Front, die da wären: Dr. Moritz Liedtke, Andreas Sperlich, Hannes Kraus, Björn Giesecking, Stefan Väth und deren jeweiligen Diplomanten.

C. Acknowledgement

- Den Pfaumis, vor allem dem Cheffe selbst, Prof. Dr. Jens Pflaum, der mir das TCNQ zu Verfügung stellte und auch sonst bei Fragen ein offenes Ohr hatte. Natürlich nicht zu vergessen Nis Hauke Hansen für die XRD Messungen.
- Dr. Volker Drach für weitere XRD Messungen.
- Diep Phan, der guten Seele des Lehrstuhls, die einem sehr viele organisatorische Dinge abgenommen hat.
- Andre Thiem-Riebe für die Hilfe, wenn mal wieder was im Labor geklemmt hat.
- Valentin Baianov für die geduldige und akkurate Konstruktion von komplizierten optischen Schemata.
- Den Damen vom ZAE Sekretariat: Barbara Englert und Ildiko Trantow, für die Unterstützung bei den ZAE spezifischen organisatorischen Dingen des Arbeitslebens.
- Klaus Opwis und der restlichen DEPHOTEX Gang für die tolle Zeit. Wenn auch die wissenschaftlichen Ergebnisse nicht zufriedenstellend waren, so waren wenigstens die inoffiziellen Parts der Projektmeetings unvergesslich.

Neben den vielen fachlichen Kollegen ist natürlich der familiäre Rückhalt nicht zu verachten, wenn es um das Erstellen einer solchen Arbeit geht. Deshalb danke ich meiner Familie, Mama und Papa, meiner Schwester und meinem Bruder mit allen die noch dazugehören. Mit euch konnte man mal richtig abschalten und an etwas anderes als Arbeit denken, was in bestimmten Phasen schwierig war.

Zuallerletzt, wie schon oben angedeutet, möchte ich mich bei meiner lieben Frau bedanken. Privates möchte ich gerne privat lassen, weshalb ich dir an dieser Stelle nur für deine Liebe und die wahnsinnig schöne gemeinsame Zeit danke. Fachlich wird die Liste etwas länger. Für mich warst du immer die erste Ansprechpartnerin wenn meinem Hirn mal wieder irgendwelche Ideen entsprungen sind und hast diese geduldig mit mir diskutiert und mich immer bei deren Umsetzung unterstützt. Natürlich sind auch deine Fähigkeiten als weltbeste und -schnellste Solarzellenkontaktiererin zu nennen. Ohne dich wäre ich bestimmt beim selber Kontaktieren irgendwann durchgedreht. Die Liste könnte ewig weitergehen, wie z.B. geduldige ZuhörerIn beim x.ten Testdurchlauf von Vorträgen, Durchsicht von Schriftstücken, Für all das Danke ich Dir und zu guter letzt auch dafür, dass du mich immer wieder motiviert hast diese Arbeit zu beenden.

List of Publications

Refereed Articles

- A. Baumann, J. Lorrmann, **D. Rauh**, C. Deibel and V. Dyakonov, *A new approach of probing the mobility and lifetime of photogenerated charge carriers in organic solar cells under real operating conditions*, Adv. Mater. 24:4381 (2012)
- **D. Rauh**, C. Deibel and V. Dyakonov, *Charge density dependent nongeminate recombination in organic bulk heterojunction solar cells*, Adv. Funct. Mater. 22:3371 (2012)
- S. Rausch, **D. Rauh**, C. Deibel, S. Vidi, H. P. Ebert *Thin-Film Thermal-Conductivity Measurement on Semi-Conducting Polymer Material Using the 3ω Technique*, Int. J. Thermophys. DOI: 10.1007/s10765-012-1174-4
- J. Gorenflot, A. Sperlich, A. Baumann, **D. Rauh**, A. Vasilev, C. Li, M. Baumgarten, C. Deibel, V. Dyakonov *Detailed study of N,N' -(diisopropylphenyl)-terrylene-3,4:11,12-bis(dicarboximide) as electron acceptor for solar cells application*, Synth. Metals, 161:2669 (2012)
- **D. Rauh**, A. Wagenpfahl, C. Deibel and V. Dyakonov, *Relation of open circuit voltage to charge carrier density in organic bulkheterojunction solar cells*, Appl. Phys. Lett., 98:133301(2011)
- A. Wagenpfahl, **D. Rauh**, M. Binder, C. Deibel, V. Dyakonov, *S-shaped current-voltage characteristics of organic solar devices*, Phys. Rev. B, 82:115306 (2010)
- C. Deibel, D. Mack, J. Gorenflot, A. Schöll, S. Krause, F. Reinert, **D. Rauh**, V. Dyakonov, *Energetics of excited states in the conjugated polymer poly(3-hexylthiophene)*, Phys. Rev. B, 81:085202 (2010)
- J. L. Delgado, E. Espildora, M. Liedtke, A. Sperlich, **D. Rauh**, A. Baumann, C. Deibel, V. Dyakonov, N. Martin, *Fullerene Dimers (C60/C70) for Energy Harvesting*, Chem. Eur. J. 15:13474 (2009)
- R. A. Babunts, N. G. Romanov, D. O. Tolmachev, A. G. Badalyan, V. A. Khramtsov, P. G. Baranov, **D. Rauh**, V. Dyakonov, *Identification of Recombination Centers in Wide Band Gap Crystals and Related Nanostructures from Spin Dependent Tunneling Afterglow*, Phys. Sol. State 51:2437 (2009)
- P. Bouit, **D. Rauh**, S. Neugebauer, J. L. Delgado, E. Di Piazza, S. Rigaut, O. Maury, C. Andraud, V. Dyakonov, N. Martin, *A "Cyanine-Cyanine" salt exhibiting photovoltaic properties*, Org. Lett. 11:4806 (2009)

- A. Foertig, A. Baumann, **D. Rauh**, V. Dyakonov, C. Deibel, *Charge Carrier Concentration and Temperature Dependent Recombination in Polymer-Fullerene Solar Cells*, Appl. Phys. Lett. 95:052104 (2009)
- M. Hammer, **D. Rauh**, V. Lorrmann, C. Deibel, V. Dyakonov, *Effect of doping- and field-induced Charge Carrier Density on the Electron Transport in nanocrystalline ZnO*, Nanotechnology 19:485701 (2008)
- S. B. Orlinskii, J. Schmidt, P. G. Baranov, V. Lorrmann, I. Riedel, **D. Rauh**, V. Dyakonov, *Identification of shallow Al donors in Al-doped ZnO nanocrystals: EPR and ENDOR spectroscopy*, Phys. Rev. B 77:115334 (2008)

Intellectual Property Right

- **D. Rauh**, A. Baumann, J. Lorrmann, C. Deibel, V. Dyakonov, *Verfahren zur simultanen Bestimmung der Beweglichkeit, Dichte und Lebenszeit photogenerierter Ladungsträger in optisch anregbaren Materialien sowie Vorrichtungen zur Bestimmung derselbigen*.

Contributed Talks

- DPG Frühjahrstagung 2010, Dresden: **D. Rauh**, A. Wagenpfahl C. Deibel and V. Dyakonov, *Relation of open circuit voltage to charge carrier concentration in organic bulk heterojunction solar cells*
- MRS Fall Meeting 2010, Boston: **D. Rauh**, A. Wagenpfahl, C. Deibel and V. Dyakonov, *Relation of open circuit voltage to charge carrier concentration in organic bulk heterojunction solar cells*

Poster Presentations

- DPG Frühjahrstagung 2007, Regensburg: **D. Rauh**, V. Lorrmann, C. Deibel, V. Dyakonov, I. Riedel, *Polymer-Fullerene Bulk-Heterojunction Solar Cells With Additional ZnO:Al Layer*
- DPG Frühjahrstagung 2008, Berlin: **D. Rauh**, V. Lorrmann, M. Hammer, A. Sperlich, M. Liedtke, C. Deibel, I. Riedel, V. Dyakonov, *Development of Al-doped ZnO-nanocrystals for applications in advanced cell concepts of organic photovoltaics*
- DPG Frühjahrstagung 2009, Dresden: **D. Rauh**, S. Geißendörfer, C. Deibel, V. Dyakonov, *Investigation of s-shaped Current-Voltage Characteristics of Organic Bulk Heterojunction Solar Cells*

Lebenslauf

Daniel Rauh

geboren am 13. November 1981 in Werneck
verheiratet

Schulbildung

1988- 1992 Grundschule, Oerlenbach
1992- 2002 Jack-Steinberger-Gymnasium, Bad Kissingen
28.06.2002 Abitur

Studium

10/2002- 12/2007: Physik (Diplom) an der Julius-Maximilians-Universität Würzburg
07.10.2004 Vordiplom
21.12.2007 Diplom
Titel: *Herstellung und Charakterisierung von aluminiumdotierten Zinkoxid-Nanopartikeln*

Promotion

seit 02/2008: Promotion an der Julius-Maximilians-Universität Würzburg
bei Prof. Dr. Vladimir Dyakonov
Titel: *Impact of Charge Carrier Density and Trap States on the Open Circuit Voltage and the Polaron Recombination in Organic Solar Cell*

beruflicher Werdegang

seit 04/2012: Ingenieur Funktionsentwicklung bei Bosch Engineering GmbH

Förderungen

- Förderung durch das Wilhelm und Else Heraeus-Förderprogramm 03/2007, 02/2008, 03/2009, 03/2010

Ehrenwörtliche Erklärung

gemäß § 5 Abs. 2 Ziff. 2 und 5
der Promotionsordnung der
Fakultät für Physik und Astronomie
der Julius-Maximilians-Universität Würzburg

Hiermit erkläre ich ehrenwörtlich, dass ich die Dissertation selbstständig und ohne Hilfe eines Promotionsberaters angefertigt und keine weiteren als die angegebenen Quellen und Hilfsmittel benutzt habe.

Die Dissertation wurde bisher weder vollständig noch teilweise einer anderen Hochschule mit dem Ziel einen akademischen Grad zu erwerben vorgelegt.

Am 21. Dezember 2007 wurde mir von der Julius-Maximilians-Universität Würzburg der akademische Grad "Diplom-Physiker Univ." verliehen. Weitere akademische Grade habe ich weder erworben noch versucht zu erwerben.

Die Dissertation wurde von Prof. Dr. Vladimir Dyakonov betreut.

Würzburg, den 05.02.2013

Daniel Rauh

